DESIGNING AN INTERPLANETARY AUTONOMOUS SPACECRAFT NAVIGATION SYSTEM USING VISIBLE PLANETS

A Dissertation

by

REZA RAYMOND KARIMI

Submitted to the Office of Graduate Studies of
Texas A&M University
in partial fulfillment of the requirements for the degree of

DOCTOR OF PHILOSOPHY

May 2012

Major Subject: Aerospace Engineering

DESIGNING AN INTERPLANETARY AUTONOMOUS SPACECRAFT NAVIGATION SYSTEM USING VISIBLE PLANETS

A Dissertation

by

REZA RAYMOND KARIMI

Submitted to the Office of Graduate Studies of
Texas A&M University
in partial fulfillment of the requirements for the degree of

DOCTOR OF PHILOSOPHY

Approved by:

Chair of Committee,	Daniele Mortari
Committee Members,	John L. Junkins
	Srinivas Rao Vadali
	Johnny E. Hurtado
	Shankar Bhattacharya
Head of Department,	Dimitris Lagoudas

May 2012

Major Subject: Aerospace Engineering

ABSTRACT

Designing an Interplanetary Autonomous
Spacecraft Navigation System Using Visible Planets. (May 2012)
Reza Raymond Karimi, B.S., Tehran Azad University;
M.S., Tarbiat Modares University
Chair of Advisory Committee: Dr. Daniele Mortari

A perfect duality exists between the problem of space-based orbit determination from line-of-sight measurements and the problem of designing an interplanetary autonomous navigation system. Mathematically, these two problems are equivalent. Any method solving the first problem can be used to solve the second one and, vice versa. While the first problem estimates the observed unknown object orbit using the known observer orbit, the second problem does exactly the opposite (e.g. the spacecraft observes a known visible planet). However, in an interplanetary navigation problem, in addition to the measurement noise, the following "perturbations" must be considered: 1) light-time effect due to the finite speed of light and large distances between the observer and planets, and 2) light aberration including special relativistic effect. These two effects require corrections of the initial orbit estimation problems. Because of the duality problem of space-based orbit determination, several new techniques of angles-only Initial Orbit Determination (IOD) are here developed which are capable of using multiple observations and provide higher orbit estimation accuracy and also they are not suffering from some of the limitations associated with the classical and some newly developed methods of initial orbit determination. Using multiple observations make these techniques suitable for the coplanar orbit determination problems which is the case for the spacecraft navigation using visible planets as the solar system planets are all almost coplanar. Four new IOD techniques

were developed and Laplace method was modified. For the autonomous navigation purpose, Extended Kalman Filter (EKF) is employed. The output of the IOD algorithm is then used as the initial condition to extended Kalman filter. The two "perturbations" caused by light-time effect and stellar aberration including special relativistic effect also need to be taken into consideration and corrections should be implemented into the extended Kalman filter scheme for the autonomous spacecraft navigation problem.

To my parents

To Issac Newton

ACKNOWLEDGMENTS

I would like to thank my research advisor, Dr. Daniele Mortari, and my teaching supervisor, Mr. Michael Golla, for being great mentors and friends. I would like to thank Dr. John L. Junkins, Dr. S. Rao Vadali, Dr. Johny E. Hurtado, Dr. Shankar Bhattacharyya, Dr. James Turner, and Dr. Walter Haisler for their help and support. Also I would like to thank my dear friend Johnathan Hebert and his father for their unconditional support.

TABLE OF CONTENTS

CHAPTER Page

CHAPTER Page

LIST OF TABLES

TABLE Page

TABLE Page

LIST OF FIGURES

FIGURE Page

CHAPTER I

INTRODUCTION

In the first section of this chapter, a short review of the history of orbital dynamics is presented. In the second section, the duality between space-based orbit determination problem and interplanetary spacecraft navigation is explained followed by a survey and review of the classical and some modern angles-only initial orbit determination methods. Then, several Initial Orbit Determination (IOD) techniques developed are introduced and at the end of this chapter, two different ways of presenting the results will be described.

A. Orbital Dynamics Background

The ancient Greeks were best known for their contribution to mathematics. Euclid (330-370 B.C.) is credited with being the first to write about conic sections, but his writings were lost. Consequently, Apollonius (287-212 B.C) is credited with the first known treatise on conic sections (225 B.C.) and was the first to name the sections. He probably also introduced *excentric* and *epicycle* theories of orbital motions. Although records from this period are scarce because of fires and destruction over the time, it is commonly thought that that Aristarchus (310-250 B.C.) suggested the Earth revolved around the Sun. Unfortunately, his theory did not gain immediate acceptance because it could not predict the position of Mars and did not accommodate the expected angular separation from different viewing locations. It was almost 1800 years later when Copernicus used some of Aristarchus' results to develop his own heliocentric model. Eratosthenes (275-194 B.C.) was perhaps the first person

---

The journal model is AIAA *Journal of Guidance, Control, and Dynamics*.

to obtain a reasonable estimate of the Earth's radius. He did this using knowledge of the Sun's light rays during the summer solstice in Syene, Egypt.

Hipparchus (161-126 B.C.) developed spherical geometry and taught the Earth was the center of the universe (even though Pythagorous and Aristarchus placed the Sun at the center much earlier). Hipparchus also noticed an increase in the longitude of the stars, [1]. Hipparchus likewise developed the first system of cataloging star magnitudes. The list categorized about 1,000 stars by brightness. Hipparchus also developed theories to describe orbital motion. He made very accurate observations, which presented some problems when trying to describe the orbital motion. Lastly, Claudisu Ptolemaeus (usually called Ptolemy) (100-170 A.D.) published a 13-volume work, called the *Mathematical Collection* or the *Almagest*, which contained his theory of an Earth-centered solar system. He used the results of Hipparchus but was unaware of earlier astronomers' works that declared the Earth was spherical and rotating around the Sun.

The long period of inactivity in the roots of orbital dynamics from the end of ancient times began to change with Nicholas Copernicus (1473-1543). Copernicus was the first scientist to bridge the gap between antiquity and modern times. He worked more than 31 years to resolve the fundamental motions of the solar system, [2]. In many respects, Galileo Galilei (1564-1642) picked up where Copernicus left off. In fact, he adopted the Copernicus' ideas a few years before 1597, even though his famous works were published more than ten years later. The main advantage of his research was his use of the telescope for regular and dedicated scientific research. Galileo's perhaps best known for his support of theories which opposed the religious doctrine of the time. Galileo Galilei served a valuable role in continuing the new thought which was about to take solid shape under Tycho Brahe, Johann Kepler, and Isaac Newton. Scientific change accelerated when Johann Kepler (1571-1630)

an Tycho Brahe (1546-1601) combined forces. In 1594, Kepler accepted a teaching position in Graz. Part of his duties in this position was to compile annual almanacs. Several years and many positions later, Kepler became the imperial court mathematician for Emperor Rudolf II in Prague in 1601. Tycho Brahe had died shortly before, leaving Kepler with all his very precious observational data. This was perfect for Kepler. Unfortunately, providing horoscope for the Emperor was not thrilling work, but it provided income and allowed him to pursue technical interests on the side.

The relatively "large" eccentricity of the Martian orbit attracted Kepler's interest. After many years of work, he published *Astronomia Nova (New Astronomy)* in 1609. This was a huge work containing his first two laws. It is worth mentioning that Kepler completed the paper in 1605 but couldn't print it for four more years. Finally, Kepler published his third law in 1619 as *Harmonics Mundi Libri V* (Harmony of the World). Kepler's third law now receives particular attention in the literature, but all three are important; 1) The orbit of each planet is an ellipse with the Sun at one focus, 2) The line joining the planet to the Sun sweeps out equal areas in equal times, and 3) The square of the period of a planet is proportional to the cube of its mean distance to the Sun.

As remarkable as Kepler's laws were, they did not completely solve planetary motion. They captured the kinematics of motion, but the dynamics of motion remained unsolved until Sir Isaac Newton (1642-1727) unlocked them. Newton published his famous three laws in 1687 (Emmond Halley (1656-1742), the discoverer of Hally's Comet, paid for the printing of the manuscript) as *Philosophia Naturalis Principa Mathematica* or *Principa*. Newton was fascinated by the beauty and precision of Kepler's laws and set about the task of discovering what force law must be existing between bodies in the solar system to be consistent with his laws of motion and Kepler's experimentally

verified laws of planetary motion. From this analysis, Newton discovered the law of universal gravitation, and the analytical solution of Keplerian motion, [3].

B. Duality Between a Space-Based Orbit Determination Problem and Interplanetary Spacecraft Navigation

A perfect Duality (actually an equivalency) exists between the problem of space-based orbit determination from line-of-sight measurements and the problem of designing an interplanetary autonomous navigation system. Mathematically, these two problems are equivalent. Any method solving the first problem can be used to solve the second and, viceversa. While the first problem estimates the observed unknown object orbit using the known observer orbit, the second problem does exactly the opposite (e.g. the spacecraft observes a known visible planet). However, in an interplanetary navigation problem, in addition to the measurement noise, the following "perturbations" must be considered: 1) the light-time effect due to the finite speed of light and large distances between the observer and planets. This effect causes the measured lines-of-sight at time $t = t_0$ (spacecraft time) belong to the position of the observed planet at time $t = t_0 - \delta t$ where δt is the unknown time that takes light to travel from the planet to the spacecraft, and 2) the restricted relativistic light aberration effect. This effect causes the measured lines-of-sight to be compressed towards the direction of the spacecraft velocity vector and the angle between the measured line-of-sight and velocity vector seems smaller than the true angle. These two effects require corrections of the initial orbit estimation problems.

In this work, several new techniques of angles-only initial orbit determination were developed which are capable of using multiple observations resulting in higher orbit estimation accuracy and also bypassing some of the drawbacks associated with

the classical and some newly developed IOD methods. In the following section, a review of the angles-only initial orbit determination methods is presented.

C. Survey on Initial Orbit Determination Methods

Satellite Orbit Determination (OD) can be described as the method of determining the position and velocity (i.e., the state vector, state, or ephemeris) of an orbiting object such as an interplanetary spacecraft or an Earth orbiting satellite. The OD problem is generally described by the computational process (generally solved by applying statistical estimation techniques) of determining the state of a satellite as a function of time using the set of measurements collected onboard the satellite and/or by ground-based tracking stations.

The satellite is indeed influenced by a variety of external forces, including gravity, atmospheric drag, solar radiation pressure, third-body perturbations, Earth tidal effects, and general relativity in addition to satellite internal control actions. The complex description of these forces results in a highly nonlinear set of dynamical equations of motion. Furthermore, the lack of detailed knowledge of the physics of the environment through which the satellite travels limits the accuracy with which the state of the satellite can be determined at any given time. Similarly, observational data are inherently nonlinear with respect to the state of the satellite. The impossibility to find closed form solutions of these nonlinear equations forces to use linearization so that linear estimation techniques can be used to resolve the OD problem. The solution can be obtained over a short orbit arc of less than 1 hr over a long orbit arc approaching many days or longer. Different techniques have also been devised to obtain an accurate solution. The key ideas of these techniques can be applied to a wide variety of OD problems, ranging from near-Earth satellite orbits

to lunar and interplanetary transfer orbits.

As stated above, the state vector of an orbiting satellite is composed of a set of position and velocity components that are usually defined in a inertial reference frame, normally with origin at Earth's center. The term "state vector" is sometimes used interchangeably with the word "state" to describe the satellites location in 3-D space.

The objective of Precise Orbit Determination (POD) is to obtain an accurate orbit estimation that accounts for the dynamical environment in which the motion occurs, including all relevant forces affecting the satellites motion. To initiate this process, a preliminary orbit is estimated using a minimum number of observations. This estimate provides the initial conditions for numerical integration of the nonlinear differential equations of motion to obtain a reference orbit. A differential correction procedure is then used to iteratively correct the reference orbit and refine the final orbit solution. An improved orbit is thus obtained by using many observations or observational data sets along with an accurate physics-based model describing the dynamical environment. POD orbits are those that best satisfy all available observations and require the ultimate in observational accuracy, [4].

Probably Hipparchus (190 B.C. − 120 B.C.) can be considered as the first one who did work on orbit determination. He is known to have been a working astronomer at least from 162 to 127 BC, [5]. Hipparchus is considered the greatest ancient astronomical observer and, by some, the greatest overall astronomer of antiquity. He was the first whose quantitative and accurate models for the motion of the Sun and Moon survive. For this he certainly made use of the observations and perhaps the mathematical techniques accumulated over centuries by the Chaldeans from Babylonia. With his solar and lunar theories and his trigonometry, he may have been the first to develop a reliable method to predict solar eclipses. In the modern ages, one

of the first works on the development of orbit determination methods were carried out by Laplace [6] and Gauss [7], [8] about two centuries ago. Their techniques were based upon three angles-only observations. Indeed the first attempts to develop the orbit determination techniques were for the applications of comets,asteroids, planets, and all other natural celestial bodies. The technique developed by the astronomer Paul Herget [10], [11] in late 1930's early 1940's was capable of using multiple observations. With the advent of the Space age, more computer-based algorithms with iterative nature were developed among which the Double-r iteration technique by Escobal [12] and more recently a new approach by Gooding [13], which are both angles-only methods, could be mentioned. In this the following, some classical and rather newly developed angles-only initial orbit determination methods are briefly reviewed.

1. Laplace

Laplace's method of orbit determination was first proposed in the *Memoires de l'Academie Royal des Sciences de Paris* in 1780 [6]. The method was originally developed for planets and comets and yields poor results for near-earth orbiting objects. The algorithm uses a span of measured lines-of-sight vectors and estimates the middle range (eventually satellite position vector) and velocity. The technique needs at least three measured directions, but with more data available, the first and second derivatives of the quantities involved in the algorithm can be approximated with a higher accuracy. Laplace started with taking the fist and second derivatives of the geometry of an orbit determination problem, $\mathbf{r} = \mathbf{R} + \rho\,\hat{\boldsymbol{\rho}}$, where $\mathbf{r}$ and $\mathbf{R}$ are the unknown position vector of the observed orbiting object and known position vector of the observer respectively

$$\dot{\mathbf{r}} = \dot{\rho}\hat{\boldsymbol{\rho}} + \rho\dot{\hat{\boldsymbol{\rho}}} + \dot{\mathbf{R}} \tag{1.1}$$

and

$$\ddot{\mathbf{r}} = \ddot{\rho}\hat{\boldsymbol{\rho}} + 2\dot{\rho}\dot{\hat{\boldsymbol{\rho}}} + \rho\ddot{\hat{\boldsymbol{\rho}}} + \ddot{\mathbf{R}} \tag{1.2}$$

The first and second derivatives of the observer position vector $\mathbf{R}$ and measured line-of-sight $\hat{\boldsymbol{\rho}}$ are known, and the second derivative of the spacecraft position vector $\mathbf{r}$ is replaced by the two-body Keplerian motion equation. The unknown range ρ and its derivatives can be determined through the following set of equations

$$\left[\begin{array}{ccc} \hat{\boldsymbol{\rho}} & 2\dot{\hat{\boldsymbol{\rho}}} & \ddot{\hat{\boldsymbol{\rho}}} + \dfrac{\mu}{r^3}\hat{\boldsymbol{\rho}} \end{array} \right]_{3\times 3} \left\{ \begin{array}{c} \ddot{\rho} \\ \dot{\rho} \\ \rho \end{array} \right\}_{3\times 1} = -\left\{ \ddot{\mathbf{R}} + \frac{\mu}{r^3}\mathbf{R} \right\}_{3\times 1} \tag{1.3}$$

For more details on Laplace's method, see Chapter 2.

2. Gauss

The Gauss IOD method was developed by Carl Friedrich Gauss, a German mathematician, in 1809. The method has been developed based on lines-of-sight measurements and requires three observations. Gauss' method receives mixed reviews from the astrodynamic community. The opinions range from little concern because the method works best for interplanetary studies, to feeling that it is not very accurate for near-Earth orbit determination. Long [9] suggests that it works best when the angular separation between observation is less than 60°. The method performs remarkably well when the data is separated by 10° or less.

The success of Gauss' method also depends on the method used to determine the

Lagrange f and g functions. In general, Guass' algorithm is a rather robust technique to determine a spacecraft position with angles-only measurements, [3]. The Gauss method takes advantage of the fact that the orbit motion is planar and, therefore, each position vector $\mathbf{r}$ can be expressed in terms of a linear combination of the other position vectors as

$$a_1\mathbf{r}_1 + a_2\mathbf{r}_2 + a_3\mathbf{r}_3 = 0 \tag{1.4}$$

or

$$\mathbf{r}_2 = c_2\mathbf{r}_1 + d_2\mathbf{r}_3 \tag{1.5}$$

and since all these three position vectors should satisfy the two-body Keplerian motion, and also position vectors $\mathbf{r}_1$ and $\mathbf{r}_3$ can be related to $\mathbf{r}_2$ through f and g functions, the coefficients c_2 and d_2 can be determined in terms of f and g. The original Gauss' method of initial orbit determination uses three lines of dight. The detailed procedure of the technique will be discussed in Chapter 3.

Gauss' method was refined by Gibbs in 1888, [14] and [15]. Gauss included terms up to t^2 in the expressions for f and g functions, while Gibbs showed how to include terms up to t^4. Moulton investigated the radius of convergence of the involved series expansion in 1903, [16].

3. Gibbs

Gibbs method uses three position vectors to determine the orbit,[17]. Solving Gibbs relies on knowing the Gauss formulation. Indeed, the first few steps are actually a variant of the original Gauss method. The Gibbs problem is formed supposing we know three non-zero coplanar position vectors which represent three time-sequential

vectors of a satellite in its orbit. These assumptions are needed for a solution. The"non-zero" constraint simply prevents divided-by-zero operation. The sequential requirement is very important because we consider a sequence of vectors while forming the solution and take several cross products based on the given order. Changing from a sequential order will give erroneous results. Finally, we require the vectors to be coplanar. This procedure is basically vector analysis. The overall procedure is to find a constant (the middle velocity vector) which is common between the given vectors. Considering the coplanar position vectors $\mathbf{r}_1$, $\mathbf{r}_2$, and $\mathbf{r}_3$ and defining the vectors $\mathbf{D}$, $\mathbf{N}$, and $\mathbf{S}$ as

$$\begin{cases} \mathbf{D} = \mathbf{r_1} \times \mathbf{r_2} + \mathbf{r_2} \times \mathbf{r_3} + \mathbf{r_3} \times \mathbf{r_1} \\ \mathbf{N} = \mathbf{r_1}(\mathbf{r_2} \times \mathbf{r_3}) + \mathbf{r_2}(\mathbf{r_3} \times \mathbf{r_1}) + \mathbf{r_3}(\mathbf{r_1} \times \mathbf{r_2}) \\ \mathbf{S} = \mathbf{r_1}(\mathbf{r_2} - \mathbf{r_3}) + \mathbf{r_2}(\mathbf{r_3} - \mathbf{r_1}) + \mathbf{r_3}(\mathbf{r_1} - \mathbf{r_2}) \end{cases} \tag{1.6}$$

then, according to Gibbs, the middle velocity vector is determined as

$$\mathbf{v}_2 = \frac{L_g}{r_2}\mathbf{B} + \mathbf{L_g}\mathbf{S} \tag{1.7}$$

where $L_g \equiv \sqrt{\frac{\mu}{ND}}$ and $\mathbf{B} \equiv \mathbf{D} \times \mathbf{r_2}$. Once the middle velocity is known, the orbital elements can be obtained using $\mathbf{r}_2$ and $\mathbf{v}_2$. The angular-separation values are of interest because the method is based on geometry. Small angles will cause numerical instability and may yield incorrect results. The method is robust and works well with angles as close as 1°, but it quickly loses efficiency for angles between the measurements smaller than 1°, [3]. The Herrick-Gibbs method bypasses this drawback and does not suffer from closely spaced observations.

4. Herrick-Gibbs

The immediate question arising from the Gibbs method is how to overcome the problem associated with the case when the observations are closely spaced (less than 1°). In fact, a set of measured data of spacecraft contains hundreds of observations that are very close together. For those occasions where the position vectors are very closely spaced, answers from the Gibbs method are unreliable. One solution is the Herrick-Gibbs method, [18] which tries to find the middle velocity vector given three sequential position vectors $\mathbf{r}_1$, $\mathbf{r}_2$, and $\mathbf{r}_3$ and their observation times t_1, t_2, and t_3. Herrick-Gibbs is just a variation of the Gibbs method. The main idea uses a Taylor's series expansion to obtain an expression for the middle velocity vector. Because this method is approximate, the Herrick-Gibbs method is not as robust as the Gibbs method, and has a more limited application. To begin the procedure, the position vector is expanded using a Taylor's series about the middle time, t_2. In general, the form of the Taylor series is

$$\mathbf{r}(t) = \mathbf{r}_2 + [\frac{d\mathbf{r}}{dt}]_{t_2}(t-t_2) + \frac{1}{2!}[\frac{d^2\mathbf{r}}{dt^2}]_{t_2}(t-t_2)^2 + \frac{1}{3!}[\frac{d^3\mathbf{r}}{dt^3}]_{t_2}(t-t_2)^3 + \cdots + \frac{1}{N!}[\frac{d^N\mathbf{r}}{dt^N}]_{t_2}(t-t_2)^N \tag{1.8}$$

Now, use this form for the position vectors, $\mathbf{r}_1$, $\mathbf{r}_3$, and simply the notation for the time difference as $\Delta t_{ij} = t_i - t_j$, we have

$$\begin{cases} \mathbf{r}_1 = \mathbf{r}_2 + \dfrac{d\mathbf{r}}{dt}|_{t_2}\Delta t_{12} + \dfrac{1}{2!}\dfrac{d^2\mathbf{r}}{dt^2}|_{t_2}\Delta t_{12}^2 + \dfrac{1}{3!}\dfrac{d^3\mathbf{r}}{dt^3}|_{t_2}\Delta t_{12}^3 + \cdots + \dfrac{1}{N!}\dfrac{d^N\mathbf{r}}{dt^N}|_{t_2}\Delta t_{12}^N \\ \mathbf{r}_3 = \mathbf{r}_2 + \dfrac{d\mathbf{r}}{dt}|_{t_2}\Delta t_{32} + \dfrac{1}{2!}\dfrac{d^2\mathbf{r}}{dt^2}|_{t_2}\Delta t_{32}^2 + \dfrac{1}{3!}\dfrac{d^3\mathbf{r}}{dt^3}|_{t_2}\Delta t_{32}^3 + \cdots + \dfrac{1}{N!}\dfrac{d^N\mathbf{r}}{dt^N}|_{t_2}\Delta t_{32}^N \end{cases} \tag{1.9}$$

The goal is to find the middle velocity. By ignoring all terms higher than fourth

order, the Herrick-Gibbs method gives the expression for the $\mathbf{v}_2$ as

$$\mathbf{v}_2 = -\Delta t_{32}\left(\frac{1}{\Delta t_{21}\Delta t_{31}} + \frac{\mu}{12r_1^3}\right)\mathbf{r}_1 + (\Delta t_{32} - \Delta t_{21})\left(\frac{1}{\Delta t_{21}\Delta t_{32}} + \frac{\mu}{12r_2^3}\right)\mathbf{r}_2 + \Delta t_{21}\left(\frac{1}{\Delta t_{32}\Delta t_{31}} + \frac{\mu}{12r_3^3}\right)\mathbf{r}_3 \quad (1.10)$$

and the orbital elements can be computed using the set $\mathbf{r}_2$ and $\mathbf{v}_2$. For more details on the algorithm development, see [3]. Because Gibbs performs well with widely spaces data, whereas Herrick-Gibbs works better with closely spaces observations, an approximate cross-point between 1° and 5° can be defined. Below 1°, Herrick-Gibbs is superior and above 5°, Gibbs is superior.

5. Double r-iteration

Escobal [12] developed an interesting angles-only initial orbit determination method that uses a combination of numerical and dynamical techniques. The algorithm is more efficient for observations which are far apart, something that Gauss' technique does not do well. In Double r-iteration technique, there are four main steps to arrive at a solution.

1) The first step bounds the guesses from the available information.

2) The second step, is the main idea of the technique Double r-iteration. The subsequent iterations use the second portion to determine intermediate guesses, so it is important to have a modular routine.

3) The third section begins the formal iterative process. It tries to align the times with the estimated values of the orbits.

4) Finally, a type of differential correction determines the answer.

This algorithm uses three observations at times t_1, t_2, and t_3. Considering the

corresponding known observer site position vectors $\mathbf{R}_1$, $\mathbf{R}_2$, $\mathbf{R}_3$ and measured lines-of-sight $\hat{\boldsymbol{\rho}}_1$, $\hat{\boldsymbol{\rho}}_2$, $\hat{\boldsymbol{\rho}}_3$, and initial guess for the first two unknown ranges (ρ_1 and ρ_2), the space craft guessed position vectors can be determined as

$$\mathbf{r}_i = \mathbf{R}_i + \rho_i \, \hat{\boldsymbol{\rho}}_i, \qquad i = 1, 2 \tag{1.11}$$

and the third unknown range ρ_3

$$\begin{cases} \hat{\mathbf{w}} = \dfrac{\mathbf{r}_1 \times \mathbf{r}_2}{|\mathbf{r}_1||\mathbf{r}_2|} \\ \\ \rho_3 = \dfrac{-\mathbf{R}_3 \cdot \hat{\mathbf{w}}}{\hat{\boldsymbol{\rho}}_3 \cdot \hat{\mathbf{w}}} \end{cases} \tag{1.12}$$

The main idea behind the double r-iteration technique is to minimize the residuals

$$\begin{cases} \xi_1 = \tau_1 - \dfrac{\Delta M_{12}}{n} \\ \\ \xi_2 = \tau_3 - \dfrac{\Delta M_{32}}{n} \end{cases} \tag{1.13}$$

where $\tau_1 = t_1 - t_2$, $\tau_3 = t_3 - t_2$, M is mean anomaly ($\Delta M_{ij} = M_i - M_j$), and n is mean motion. The rest of the procedure is as the following

$$\begin{cases} \dfrac{\partial \xi_1}{\partial r_1} = \dfrac{\xi_1(r_1 + \Delta r_1, r_2) - \xi_1(r_1, r_2)}{\Delta r_1} \\ \\ \dfrac{\partial \xi_2}{\partial r_1} = \dfrac{\xi_2(r_1 + \Delta r_1, r_2) - \xi_2(r_1, r_2)}{\Delta r_1} \end{cases} \tag{1.14}$$

and

$$\begin{cases} \dfrac{\partial \xi_1}{\partial r_2} = \dfrac{\xi_1(r_1, r_2 + \Delta r_2) - \xi_1(r_1, r_2)}{\Delta r_2} \\ \\ \dfrac{\partial \xi_2}{\partial r_2} = \dfrac{\xi_2(r_1, r_2 + \Delta r_2) - \xi_2(r_1, r_2)}{\Delta r_2} \end{cases} \tag{1.15}$$

where $\Delta r_1 = \epsilon r_1$ and $\Delta r_2 = \epsilon r_2$ with $\epsilon \ll 1$. Corrections for r_1 and r_2 are

$$\Delta = \frac{\partial \xi_1}{\partial r_1}\frac{\partial \xi_2}{\partial r_2} - \frac{\partial \xi_2}{\partial r_1}\frac{\partial \xi_1}{\partial r_2} \tag{1.16}$$

and

$$\begin{cases} \Delta_1 = \dfrac{\partial \xi_2}{\partial r_2}\xi_1 - \dfrac{\partial \xi_1}{\partial r_2}\xi_2 \\ \\ \Delta_2 = \dfrac{\partial \xi_1}{\partial r_1}\xi_2 - \dfrac{\partial \xi_2}{\partial r_1}\xi_1 \end{cases} \tag{1.17}$$

and the update is computed as

$$\begin{cases} \Delta r_1 = -\dfrac{\Delta_1}{\Delta} \\ \\ \Delta r_1 = -\dfrac{\Delta_2}{\Delta} \end{cases} \tag{1.18}$$

This differential correction ($r_1 = r_1 + \Delta r_1$ and $r_2 = r_2 + \Delta r_2$)continues until convergence occurs. The middle range velocity $\mathbf{v}_2$ is obtained using f and g functions

$$\mathbf{v}_2 = \frac{\mathbf{r}_3 - f\mathbf{r}_2}{g} \tag{1.19}$$

and

$$\begin{cases} f = 1 - \dfrac{a}{r_2}(1 - cos(\Delta E_{32})) \\ g = \tau_3 - \sqrt{\dfrac{a^3}{\mu}}(\Delta E_{32} - sin(\Delta E_{32})) \end{cases} \tag{1.20}$$

where E is the Eccentric anomaly ($\Delta E_{ij} = E_i - E_j$) and a is the semi-major axis. For more details on this, see [3].

6. Gooding

A brief review of the original Gooding method of initial orbit determination is presented here (full details may be found in [13]). At three times, $t_j, \quad j = 1, 2, 3$, measurements are made from three sites defined by the position vectors, $\mathbf{R}_j$. The measurements are unit vectors $\hat{\boldsymbol{\rho}}_j$ which are line-of-sight (i.e., direction) vectors from the site to the orbiting spacecraft. The vectors $\hat{\boldsymbol{\rho}}_j$ are easily obtained from an optical source on Earth. The vector r_j denotes the position of the spacecraft and the unknown range, ρ_j allows us to write the geometry of the problem at time t_j

$$\rho_j \hat{\boldsymbol{\rho}}_j = \mathbf{r}_j - \mathbf{R}_j, \quad j = 1, 2, 3 \tag{1.21}$$

The algorithm computes the spacecraft position at t_2 derived from assumed positions at t_1 and t_3. Lamberts problem [19] is solved with the given times and assumed positions to determine the position at t_2. Gooding chose to use the Newton-Raphson procedure for correcting the assumed values of ρ_1 and ρ_2. The procedure for two variables follows:

$$\begin{Bmatrix} \delta x \\ \delta y \end{Bmatrix} \begin{bmatrix} f_x & f_y \\ g_x & g_y \end{bmatrix}^{-1} = \begin{Bmatrix} f \\ g \end{Bmatrix} \tag{1.22}$$

where f and g are Lagrange coefficients and δx and δy are the corrections for the current estimates of a pair of roots of the equations

$$f(x, y) = g(x, y) = 0 \tag{1.23}$$

Gooding method assumes that $g = 0$ already, allowing Eq. (1.22) to be reduced to

$$\delta x = -D^{-1} f g_y, \quad \delta y = D^{-1} f g_x \tag{1.24}$$

where D is the determinant of the derivative matrix. As the partial derivatives f and g are obtained by truncating a Taylor series, a small error is introduced into the process. This also means that starting values too far from the solution either take a large number of iterations in order to converge or do not converge. Assuming the derivative matrix D is well conditioned, then the convergence is quadratic. It should also be noted that for a given initial guess of the range, the Gooding Algorithm is deterministic. Pseudo-code for Goodings algorithm is given in Table I.

Table I. Pseudo-code for Gooding Algorithm

1	Given values are $\mathbf{R}_j$, t_j , and $\hat{\boldsymbol{\rho}}_j$, for $j = 1, 2, 3$
2	Assume a value for ρ_1 and ρ_3
3	**while** Not Maximum Iterations or Tolerance Reached *do*
4	Generate an estimated orbit by solving Lambert problem using $\mathbf{r}_1$, $\mathbf{r}_3$, and $t_3 - t_1$
5	Compute the error in the position measurement of the spacecraft at t_2
6	Iterate ρ_1 and ρ_3 using the Newton-Raphson procedure
7	**end while**

This method yields the trivial solution of zero for space-based IOD scenarios and needs initial guess close to the truth. Recently, Henderson and Mortari modified the Gooding method (N-Gooding) and made it capable of using multiple observations and enhanced its performance for space-based scenarios, [20].

7. Other IOD Methods

Since the first modern initial orbit determination technique developed by Laplace in 1780, several different IOD algorithms have been proposed with the hope to either bypass the drawbacks of the previous methods or enhance the accuracy of the orbit determination problems. Between 1816 and 1818, Mossotti [21] developed a method which is based on four observations. The technique proposed by Shefer [22] uses four observations. Apart from the methods briefly reviewed in the previous section, the following IOD methods can be mentioned: Paul Herget [10], [11] a Polish Astronomer, developed a technique for planets and comets orbit determination capable of using multiple observations. It works well with short arcs. In 1976, Taff [23] developed a technique based on the conservation of angular momentum and orbit energy for every instant of time. The algorithm by Baker and Jacoby can handle coplanar cases with no singularity, [24]. Also Neutsch proposed a simple method of IOD capable of using more than three observations, [25]. The technique by Kristensen (2009) [26] uses a least square scheme of multiple observations for an initial orbit determination problem.

8. Proposed IOD Algorithms

The available classical and some of the modern angles-only initial orbit determination techniques suffer from some limitations which make them unsuitable for the problem of space-based orbit determination specifically in the application of spacecraft navigation. One of the main drawbacks associated with the majority of these methods is that they show singularities for coplanar orbit determination problems (coplanar is the case in which the observed object lines-of-sight lie on the object orbit plane) while the planets have near to coplanar orbits compared to the Earth's orbit plane,

for instance, Venus', Mars', and Jupiter's orbit inclination angles are 3.39°, 1.85°, and 1.30° respectively. Another issue which make most of the available methods not practical for the spacecraft navigation problem is the rather low estimation accuracy they yield. To bypass these disadvantages, some new angles-only initial orbit determination techniques were developed. These methods were named ML_n [27], J_n [28],[29], L_n [29], P_n [30], and V_n [31]. The first letter of the name of the method refers to the idea based on which the algorithm has been developed and the index n refers to the number of observations the method is using for orbit determination. ML_n: Modified Laplace, J_n and L_n: based on position vectors coplanarity, Jacobian and Least-square in the heart of the algorithms, P_n: based on Prescribed orbits, and V_n: based on Variation of orbital error (e.g.,P_8 refers to the IOD method based on prescribed orbits using eight observations). These techniques will be fully descried in Chapters 2 through 5 respectively.

D. Result Presentation

The results of the initial orbit determination methods are presented in two ways:

1) position and velocity relative percentage error defined as

$$\begin{cases} r_{error}\% = 100 * \dfrac{|\mathbf{r}_{true} - \mathbf{r}_{est}|}{|\mathbf{r}_{true}|} \\ \\ v_{error}\% = 100 * \dfrac{|\mathbf{v}_{true} - \mathbf{v}_{est}|}{|\mathbf{v}_{true}|} \end{cases} \tag{1.25}$$

2) orbit shape and orientation error. In the following subsection, a review of such result error presentation is given.

1. Orbit Error

Let us consider the problem of describing the error between two different orbits, for instance, the error between the true orbit, characterized by the orbital elements $[a_t, e_t, \Omega_t, \omega_t, i_t, \varphi_t]$ and the estimated orbit, characterized by $[a_e, e_e, \Omega_e, \omega_e, i_e, \varphi_e]$, where the six elements are, respectively, the semi-major axis, eccentricity, right ascension of the ascending node, argument of perigee, inclination, and true anomaly. The orbital parameters identifying the orbit in space can be suitably split in two independent sets. One set consisting of Ω, $\omega + \varphi$, and i, that identify the orientation of a rotating orbital reference frame $[\hat{\boldsymbol{r}}, \quad \hat{\boldsymbol{t}}, \quad \hat{\boldsymbol{h}}]$ with respect to the inertial reference frame. The axes of this orbital frame are identified by the radius direction $\hat{\boldsymbol{r}}$, the direction of the angular momentum $\hat{\boldsymbol{h}}$, and the third axis to form a right-handed frame $\hat{\boldsymbol{t}} = \hat{\boldsymbol{h}} \times \hat{\boldsymbol{r}}$. Therefore, the transformation matrix, C_{OI}, moving from inertial to the orbital reference frames can be written as

$$C_{OI} = R_3(\omega + \varphi)\, R_1(i)\, R_3(\Omega) = \Big[\, \hat{\boldsymbol{r}}, \quad \hat{\boldsymbol{h}} \times \hat{\boldsymbol{r}}, \quad \hat{\boldsymbol{h}} \,\Big]^{\mathrm{T}} \tag{1.26}$$

where R_1 and R_2 are the rotation matrices about the $\hat{\boldsymbol{x}}$ and $\hat{\boldsymbol{z}}$ coordinate axes, respectively.

Orientation Error. This error is identified by an angle δ that can be computed by the following relationship using the true, C_t, and the estimated, C_e, transformation matrices

$$\cos\delta = \frac{1}{2}\,\left[\mathrm{tr}(C_t C_e^{\mathrm{T}}) - 1\right] \tag{1.27}$$

From a mathematical point of view δ represents the principal angle of the corrective attitude matrix, $C_t C_e^{\mathrm{T}}$, between the two attitudes matrices, C_t and C_e. Specific error information can be easily derived from the orbit orientation error. These can be, a) the distance between estimated and true radii $|\mathbf{r}_t - \mathbf{r}_e|$ to capture the ability

to estimate the spacecraft position, and b) the angle between estimated and true angular momentum directions, $\hat{\boldsymbol{h}}_t$ and $\hat{\boldsymbol{h}}_e$, to capture the ability to estimate the orbit plane orientation.

Shape Error. The orbit shape is identified using the semi-major and semi-minor axes because they are (dimensionally) consistent parameters. Using these two orbit elements, the shape of an orbit can be identified as a point in the a-b plane. Thus the orbit shape error can be simply described by the distance d from estimated and true points in the a-b plane

$$d = \sqrt{(a_t - a_e)^2 + (b_t - b_e)^2} \tag{1.28}$$

For more details on orbit error, see [32].

E. Noise Simulation

The known input information fed into a typical angles-only initial orbit determination method are the known position of the observer or known position of the observed object(for the spacecraft navigation problem) $\mathbf{R}$ and also the measured lines-of-sight $\hat{\boldsymbol{\rho}}$. The lines-of-sight are measured by a Star Trek either at a ground-based observer site or on board spacecraft for space-based IOD scenarios. Since no perfect and flawless camera exists, so the measured data are off from the ideal measurements by some angle. This angle is basically the standard deviation $\sigma_{\hat{\boldsymbol{\rho}}}$ of the noise involved in the measurements. To simulate this noise, the simulated ideal measurements $\hat{\boldsymbol{\rho}}_{ideal}$ should be corrupted. To this end, the ideal line-of-sight is rotated about a random axis by the angle $\phi = \sigma_{\hat{\boldsymbol{\rho}}}$

$$\hat{\boldsymbol{\rho}}_{corrupted} = \Re(\boldsymbol{n}, \phi)\hat{\boldsymbol{\rho}}_{ideal} \tag{1.29}$$

where $\Re(\boldsymbol{n}, \phi)$ is a rotation matrix, $\boldsymbol{n}$ is a random unit vector as the principal axis of rotation, and ϕ is the principal angle of rotation which is equal to the standard deviation of the a mean-zero Gaussian noise. The rotation matrix $\Re$ in terms of principal axis and principal angle is given as

$$\Re(\boldsymbol{n}, \phi) = (\cos\phi + (1 - \cos\phi)\boldsymbol{n}\boldsymbol{n}^T - \sin\phi[\tilde{\boldsymbol{n}}]) \tag{1.30}$$

where $\tilde{\boldsymbol{n}}$ is defined as $\begin{pmatrix} 0 & -n_3 & n_2 \\ n_3 & 0 & -n_1 \\ -n_2 & n_1 & 0 \end{pmatrix}$.

CHAPTER II

MODIFIED LAPLACE INITIAL ORBIT DETERMINATION METHOD

In this section, the modifications made to the angles-only Laplace method of initial orbit determination are presented.

A. Introduction

Laplace's method of orbit determination was first proposed in the *Memoires de l'Academie Royal des Sciences de Paris* in 1780 [6]. The method was originally developed for planets and comets and yields poor results for near-earth orbiting objects. The algorithm uses a span of measured lines-of-sight vectors and estimates the middle range (eventually satellite position vector) and velocity. The technique needs at least three measured directions, but with more data available, the first and second derivatives of the quantities involved in the algorithm can be approximated with a higher accuracy. In this work, efforts have been made to eliminate some of the drawbacks and limitations associated with Laplace's method and also make is suitable for near-earth satellites. As one of the main steps of the algorithms, an eighth order polynomial needs to solved so its proper root can be used for the next iteration as the middle range gets corrected. Through the first modification, the need for the polynomial root solving is completely eliminated and also the trivial initial guess of zero can be used instead which helps the operator significantly when dealing with different problems of orbit determination of different natures. Some IOD methods like Gooding [13] and Double-r iteration [12] need very close and close initial guesses to the true values respectively. As mentioned above, the method estimates the middle range (or position vector) of a bunch of data. In each system of equations solved through Laplace's technique (say three equations corresponding with three observa-

tions for now) to obtain the middle range, the first and second time derivatives of the second range are also determined. The first time derivative is useful as it can be used for determining the estimated velocity vector when trying to find the orbital elements. But the second time derivative of the range is useless for our purpose and just is a burden in the solving process. The idea of the second modification (which will eventually lead to the singularity removal for the coplanar cases) is based on removing the second time derivative (and also the first time derivative) from the set of equations and replacing them by approximated expressions in terms of the unknown ranges. One way to do this is using the Lagrange's interpolation formula. So, we are dealing with a system of equation containing all unknown ranges. The set of equations now can be solved for all ranges at the same time while the original Laplace's method is able to obtain the ranges once at the time. One advantage of this range time derivatives removal is when dealing with coplanar IOD scenarios. In Laplace's original algorithm, for a coplanar case, the set of equations collapses to two while we have three unknown parameters namely range, range first and second derivatives, so singularity occurs. In the third modification, a minimum number of observations (four) is required. So we can construct two sets of equations. Applying the range derivatives removal procedure mentioned previously and combining those two sets, we can construct a set of equations of four while we have four unknown parameters namely ranges one through four. So the system of equation will not show singularity any more as for the coplanar case, each set of equation collapses into two algebraic equations and we have a total of four equations which is sufficient to determine the four unknown. Note that even multiple data can be used and would result in higher accuracy. To have a more accurate approximations of the first and second derivatives of the quantities involved in the algorithm, the measured data need to be as close apart as possible for a certain number of data. On the other hand, since we have

noise involved in the measurements, data being so closely apart would be affected more by the noise than being further apart, so this is a trade-off which needs to be taken into consideration. In the next section, the modifications made to Laplace's method will be discussed in more details. At the end, some different scenarios will be studied for validation.

B. Laplace Original Method

As seen in Chapter 1, the Laplace original algorithm is trying to solve for the unknown middle range ρ and its first and second derivatives through the following equation

$$\left[\begin{array}{ccc} \hat{\rho}_2 & 2\dot{\hat{\rho}}_2 & \ddot{\hat{\rho}}_2 + \frac{\mu}{r_2^3}\hat{\rho}_2 \end{array}\right]_{3\times 3} \left\{\begin{array}{c} \ddot{\rho}_2 \\ \dot{\rho}_2 \\ \rho_2 \end{array}\right\}_{3\times 1} = -\left\{\begin{array}{c} \ddot{\mathbf{R}}_2 + \frac{\mu}{r_2^3}\mathbf{R}_2 \end{array}\right\}_{3\times 1} \tag{2.1}$$

For for more details see [3],[12] and [33]. In the heart of the algorithm, an eighth order polynomial in terms of r_2^3 needs to be solved for each iteration as the middle range gets corrected. This is a computational burden which will be discussed in the next section along with the modifications made to the Laplace original method of initial orbit determination.

C. Modifications

In this section, the three improvements made to the original Laplace's algorithm are presented. Consider Eq. (2.1) through which the range (here middle range) and its derivatives can be estimated. Of all these three quantities, the range maybe the only one of interest. So the other two $\dot{\rho}$ and $\ddot{\rho}$ may not be of great important to us (sometime $\dot{\rho}$ is needed for velocity calculations). Imagine for some reason, we would

like to estimate all three ranges namely ρ_1,ρ_2, and ρ_3 together with just one time solving Eq. (2.1) To this end, the first and second range time derivatives can be approximated using Lagrange interpolation functions as

$$\begin{cases} \dot{\rho}_2 = \dot{l}_1(t_2)\rho_1 + \dot{l}_2(t_2)\rho_2 + \dot{l}_3(t_2)\rho_3 \\ \ddot{\rho}_2 = \ddot{l}_1(t_2)\rho_1 + \ddot{l}_2(t_2)\rho_2 + \ddot{l}_3(t_2)\rho_3 \end{cases} \tag{2.2}$$

Now substituting Eq. (2.1) in Eq. (2.2) and rearranging

$$\begin{bmatrix} A_{11} & A_{12} & A_{13} \end{bmatrix}_{3\times 3} \begin{Bmatrix} \rho_1 \\ \rho_2 \\ \rho_3 \end{Bmatrix}_{3\times 1} = -\left\{ \ddot{\mathbf{R}}_2 + \frac{\mu}{r_2^3}\mathbf{R}_2 \right\}_{3\times 1} \tag{2.3}$$

where

$$\begin{cases} A_{11} = \ddot{l}_1(t_2)\hat{\rho}_2 + 2\dot{l}_1(t_2)\dot{\hat{\rho}}_2 \\ A_{12} = \ddot{l}_2(t_2)\hat{\rho}_2 + 2\dot{l}_2(t_2)\dot{\hat{\rho}}_2 + (\ddot{\hat{\rho}}_2 + \frac{\mu}{r_2^3}\hat{\rho}_2) \\ A_{13} = \ddot{l}_3(t_2)\hat{\rho}_2 + 2\dot{l}_3(t_2)\dot{\hat{\rho}}_2 \end{cases} \tag{2.4}$$

The time derivatives of $\hat{\rho}$, $\dot{\hat{\rho}}$ and $\ddot{\hat{\rho}}$, can be computed using Lagrange interpolation functions. Equation (2.3) can be put in the following compact form

$$[A]_{3\times 3} \begin{Bmatrix} \rho_1 \\ \rho_2 \\ \rho_3 \end{Bmatrix}_{3\times 1} = [B]_{3\times 1} \tag{2.5}$$

where B is the right-hand side of (2.3). Finally solving for unknown ranges

$$\left\{ \begin{array}{c} \rho_1 \\ \rho_2 \\ \rho_3 \end{array} \right\}_{3\times 1} = [A]^{-1}_{3\times 3}[B]_{3\times 1} \tag{2.6}$$

Equation (2.6) yields all three ranges together. Also note that the term r_2^3 appears in both matrices A and B, so no closed-form form solution is available and the unknown ranges need to be obtained through an iterative procedure. As mentioned earlier, in the Laplace original algorithm, an eight order polynomial in terms of r_2 needs to be solved and fed back to the set of equations which is a computational burden. To bypass this drawback, we simply replaced r_2 by the equation defining the geometry of the problem. In the next section, we will see that this modification yields results comparable to those of the original Laplace method. Also, the initial guess of zero can be used for all the unknown ranges. In the case of non- coplanar orbits (line-of-sights not lying on the satellite orbit plane), matrix A is invertible, but in case of coplanar (line-of-sights are on the satellite orbit plane), Eq. (2.5) collapses into two while we have three unknown, as a result, matrix A is not full rank and singularity occurs. The next modification discusses this issue.

When dealing with coplanar cases, at least one more observation is needed to avoid singularity. Assume we have four observations, so two sets of equations each looking like Eq. (2.5) can be constructed. Since each set contains two scaler equations, so the total of four equations would be sufficient to solve for the four unknown ranges. After combining the two sets, we have

$$\begin{bmatrix} A_{11} & A_{12} & A_{13} & 0_{3\times1} \\ 0_{3\times1} & A_{22} & A_{23} & A_{24} \end{bmatrix}_{6\times4} \begin{Bmatrix} \rho_1 \\ \rho_2 \\ \rho_3 \\ \rho_4 \end{Bmatrix}_{4\times1} = - \begin{Bmatrix} \ddot{\mathbf{R}}_2 + \frac{\mu}{r_2^3}\mathbf{R}_2 \\ \ddot{\mathbf{R}}_3 + \frac{\mu}{r_3^3}\mathbf{R}_3 \end{Bmatrix}_{6\times1} \tag{2.7}$$

where

$$\begin{cases} A_{11} = \ddot{l}_1(t_2)\hat{\rho}_2 + 2\dot{l}_1(t_2)\dot{\hat{\rho}}_2 \\ A_{12} = \ddot{l}_2(t_2)\hat{\rho}_2 + 2\dot{l}_2(t_2)\dot{\hat{\rho}}_2 + (\ddot{\hat{\rho}}_2 + \frac{\mu}{r_2^3}\hat{\rho}_2) \\ A_{13} = \ddot{l}_3(t_2)\hat{\rho}_2 + 2\dot{l}_3(t_2)\dot{\hat{\rho}}_2 \\ ..... \\ A_{22} = \ddot{l}_1(t_3)\hat{\rho}_3 + 2\dot{l}_1(t_3)\dot{\hat{\rho}}_3 \\ A_{23} = \ddot{l}_2(t_3)\hat{\rho}_3 + 2\dot{l}_2(t_3)\dot{\hat{\rho}}_3 + (\ddot{\hat{\rho}}_3 + \frac{\mu}{r_3^3}\hat{\rho}_3) \\ A_{24} = \ddot{l}_3(t_3)\hat{\rho}_3 + 2\dot{l}_3(t_3)\dot{\hat{\rho}}_3 \end{cases} \tag{2.8}$$

or in a compact form

$$[A]_{6\times4} \begin{Bmatrix} \rho_1 \\ \rho_2 \\ \rho_3 \\ \rho_4 \end{Bmatrix}_{4\times1} = [B]_{6\times1} \tag{2.9}$$

and finally

$$\begin{Bmatrix} \rho_1 \\ \rho_2 \\ \rho_3 \\ \rho_4 \end{Bmatrix}_{4\times1} = ([A^T][W][A])^{-1}_{4\times4}[A^T]_{4\times6}[W][B]_{6\times1} \tag{2.10}$$

where W is a weight matrix. Note that even in the case of coplanar, A^TA is full rank and hence invertible. In case of multiple observations, Eq. (2.9) can be generalized and written in the following form

$$\begin{bmatrix} A_{11} & A_{12} & A_{13} & 0_{3\times1} & ... & 0_{3\times1} \\ 0_{3\times1} & A_{22} & A_{23} & A_{24} & ... & 0_{3\times1} \\ \vdots & \vdots & \vdots & \vdots & ... & \vdots \\ 0_{3\times1} & 0_{3\times1} & ... & A_{(n-2)(n-2)} & A_{(n-2)(n-1)} & A_{(n-2)(n)} \end{bmatrix} \begin{Bmatrix} \rho_1 \\ \rho_2 \\ \vdots \\ \rho_n \end{Bmatrix} = - \begin{Bmatrix} \ddot{\mathbf{R}}_2 + \frac{\mu}{r_2^3}\mathbf{R}_2 \\ \ddot{\mathbf{R}}_3 + \frac{\mu}{r_3^3}\mathbf{R}_3 \\ \vdots \\ \ddot{\mathbf{R}}_{n-1} + \frac{\mu}{r_{n-1}^3}\mathbf{R}_{n-1} \end{Bmatrix} \tag{2.11}$$

and then solution for the unknown ranges

$$\begin{Bmatrix} \rho_1 \\ \rho_2 \\ \vdots \\ \rho_n \end{Bmatrix}_{n\times1} = ([A^T][W][A])^{-1}_{n\times n}[A^T]_{n\times3(n-2)}[W][B]_{3(n-2)\times1} \tag{2.12}$$

where W is a weight matrix. Using more observations than three, not only fixes the singularity issue, but enhances the accuracy of the estimated satellite position and

velocity vector.

D. Selected Test Scenarios and Results

The validation and effectiveness of the developed modifications were tested through several different scenarios. All the observations were made from a ground-based site located at a point of zero longitude and zero latitude for the sake of simplicity. To simulate the real data, the ideal measured data were corrupted with Gaussian noise with standard deviation of $3\sigma = 10arcsec$. The estimated error are presented in terms of orbit shape and orbit orientation. In the following subsection, the orbit shape and orbit orientation error is briefly introduced.

1. Non-coplanar Scenarios

To test the performance of the modified and original algorithms, a Monte Carlo analysis was conducted using 2326 different scenarios. A random orbit generator was used for the purpose. The orbits have eccentricity ranging from 0 to 0.2 and inclination angle from 5° to 90°. The coplanar scenarios were not included in this first part of the analysis as the original Laplace (with three observations) shows singularity for coplanar cases. For each scenario, the orbital elements were calculated using the original and modified Laplace algorithms and then the results were compared both qualitatively and quantitatively. To have a better feeling of the performances of the different algorithms used, we collected the estimated a and b with relative percentage error up to 1% (defined as $100 \times |true - estimated|/true$) and Φ up to 1°. Out of 2326 scenarios, the original Laplace, and modified Laplace with 3,4,5, and 6 observations yielded 194, 294, 410, 533, and 585 occurrences respectively. Table II presents the results of this analysis.

Table II. Non-Coplanar Monte Carlo Analysis for 2326 LEO Scenarios ($3\sigma = 10$" and $\Delta t = 10$s)

Laplace	*Original*	$n = 3$	$n = 4$	$n = 5$	$n = 6$
Occurrences	194	294	410	533	585
Percentage (%)	8.4	12.6	17.6	22.9	25.2

As can be seen, with more number of observations used, more scenarios fall into the specified error zone ($a_{error} < \%1, b_{error} < \%1, \Phi < 1^{\circ}$). For example, the performance of the modified Laplace with number of observations $n = 6$ gets three times better than that of the original Laplace. Apart from this qualitative analysis, we also were interested in testing some specific scenarios as quantitative comparison. So, one random case was considered. The orbital elements of this scenario is presented in Table III.

Table III. Orbital Elements for a Single Random Scenario: Non-coplanar

Scenario	a	e	i	Ω	ω	φ
	km	[-]	(deg)	(deg)	(deg)	(deg)
Non-coplanar	7,800.0	0.1	45	345	15	0

Tables IV presents the semi-major axis and semi-minor axis relative percentage errors, attitude error matrix principal angle, and CPU time. As can be seen, as the number of observations increases, the accuracy of the estimated orbit shape and orientation improves with no significant change in the CPU time. Note how the results improve from Laplace original to Laplace with $n = 6$ for both orbit shape and orientation errors. The original Laplace yields poor results for the near-earth orbits, but as it can be seen, the modified Laplace can successfully be used for the LEO orbit determination problems.

Table IV. Performance Comparison of Original and Modified Laplace for One Single Non-coplanar Scenario ($3\sigma = 10$" and $\Delta t = 10$s)

Algorithms (*Laplace*)	$a_{error}(\%)$	$b_{error}(\%)$	Φ (deg)	Elapsed Time (s)
Original	0.72	0.68	14.8	0.014
n=3	0.56	0.53	35	0.011
n=4	0.2	0.19	0.03	0.011
n=5	0.06	0.059	0.028	0.012
n=6	0.018	0.015	0.027	0.013

2. Coplanar Scenarios

As mentioned in the forgoing, the original Laplace method shows singularity when dealing with coplanar cases (line-of-sights are lying on the satellite orbit plane). To bypass this drawback, at least one more observation needs to be added to the set of equations. To test the performance of the developed modified algorithm, a Monte-Carlo analysis was conducted for 2212 coplanar cases. A random orbit generator was used for the purpose. The orbits have the semi-major axis ranging from 6768.324km to 9621.290km and eccentricity ranging from 0 to 0.2. Again, we collected the estimated a and b with relative percentage error up to 1% and the angular momentum vector error θup to 1° as the specified error zone. Note that since for the coplanar cases, the Right Ascension Ascending Node Ω is indefinable, so the orbit orientation error criterion used for the non-coplanar cases can not be used for coplanar scenarios. So instead, the angle between the true and estimated angular momentum vectors θ was used as the indication of the orbit orientation error. The noise with $3\sigma = 10$" and time interval of $\Delta t = 15$s were used for the analysis. Out of 2212 scenarios, the modified Laplace with 4,5, and 6 observations yielded 153, 341,

and 482 occurrences respectively. This shows that as the number of observations increase, the estimation accuracy improves. Table V presents a summary of this Monte Carlo analysis.

Table V. Coplanar Monte Carlo Analysis for 2212 LEO Scenarios (3σ = 10" and Δt = 10s)

Laplace	$n = 4$	$n = 5$	$n = 6$
Occurrences	153	341	482
Percentage (%)	6.9	15.4	21.8

Table VI presents the orbit elements of a single scenario and Table VII presents the results using the modified Laplace using number of observations 4, 5, and 6. The angle between the true and estimated angular momentum vectors θ was used as the orbit orientation error criterion.

Table VI. Orbital Elements for a Single Random Scenario: Coplanar

Scenario	a	e	i	Ω	ω	φ
	km	[-]	(deg)	(deg)	(deg)	(deg)
Coplanar	7,602.35	0.034	0	0	2.45	0

Table VII. Performance Comparison of the Modified Laplace for One Single Coplanar Scenario (3σ = 10" and Δt = 10s)

Algorithms (*Laplace*)	a_{error}(%)	b_{error}(%)	θ (deg)	Elapsed Time (s)
n=4	2.17	1.57	0.0038	0.012
n=5	0.54	0.06	0.0037	0.012
n=6	0.027	0.0095	0.0037	0.013

As can be seen, the CPU time and orientation error remain almost the same whereas the orbit shape error improves significantly.

E. Conclusion

Three modifications were made to the Original Laplace method of initial orbit determination and successfully tested. The first modification eliminates the need for solving an eighth order polynomial in the original Laplace algorithm. As the second modification, the unknown ranges can be estimated all together while the original method offers just one unknown range at a time. In the third modification, the Laplace method was generalized to multiple observations which makes it suitable for dealing with the coplanar cases as the original Laplace shows singularity for coplanar orbit determination problems. Two Monte Carlo Analysis were performed for both coplanar and non-coplanar scenarios. The modified Laplace algorithm showed much better results compared to those of the original Laplace whereas the CPU time remained almost the same. The error presented in this work are in terms of orbit error which contains both orbit shape and orbit orientation errors. The time interval between the measurements was considered $\Delta t = 15$s with the measurement noise of $3\sigma = 10$". As the time interval increases, the measurements are less affected by the noise, but in turn, the approximated quantities lose accuracy, and as the time interval decreases, the approximation would be more accurate, but the measurements are more affected by the noise. So, there is an optimal time interval with respect to the level of the noise involved in the measurements. The original Laplace yields poor results for LEO orbit determination problems, whereas the modified algorithm showed reasonable results for the near-earth orbits. The Lagrange interpolation polynomials were used for the approximation purposes which may not be the best way to do so.

The least square technique and using some other sort of functions can be tried as an alternative for the Lagrange interpolation functions.

CHAPTER III

INITIAL ORBIT DETERMINATION USING MULTIPLE OBSERVATIONS

In this chapter, two new angles-only initial orbit determination techniques are presented.

A. Introduction

With the advent of the space age, more computer-based algorithms with iterative nature were developed among which the Double r-iteration technique by Escobal [12] and, more recently, the new approach by Gooding [13], which are both angles-only methods, can be mentioned. Basically, in the Double r-iteration method, the mean anomaly and the mean motion are computed based on the estimated ranges (initial guess) and then the residuals defined as the difference between the real time interval (between the measured observations) and estimated time interval (mean anomaly divided by mean motion) are tried to be minimized with respect to the unknown range. The solution is achieved when the residuals become smaller than some prescribed tolerance. Laplace's doesn't exhibit acceptable performance for near-Earth satellites and only yields good results on the middle range (the second range out of three observations). Gauss' method offers good results on all three computed ranges and is more accurate for near-Earth satellites than Laplace's, obtaining its best accuracy when the measured data are less than 10° apart [3]. Gauss's and Laplace's methods exhibit singularity on coplanar orbit determination problems, namely, when the observed line-of-sight vectors all lie on the observer's orbital plane. The Double r-iteration method is based on the iterative improvement of estimates for the first and last ranges. This method is, unlike Gauss', effective for large spreads in the observations, but suffers from some limitations such as very limited initial guess

converging region and is less stable when dealing with real data corrupted by noise (as compared to the techniques proposed here). Gooding method yields multiple solutions including the all zero-range trivial solution on space-based orbit estimation problems (e.i., satellite tracking satellite). Another drawback of the Gooding method is that the initial guess should be close enough to the true values which results in failure when too noisy data are used. The presented technique yields an acceptable robustness with respect to the noise levels and initial guess. The methods using three angles-only observations typically become more complex if they are to be modified for multiple observations, whereas the complexity of the proposed techniques does increase with the number of observations. The algorithm presented in this chapter relies on the fact that, for unperturbed Keplerian orbits, all position vectors lie on the same (orbital) plane and uses the Lagrangian coefficients, f and g, similarly to Gauss' method. For this reason, the proposed technique is compared to the classic methods of Gauss' as they have been constructed on the same foundation and compared with the Double r-iteration, as they both are iterative techniques.

The four particular features of the presented method are:

1. capable of using multiple observations;
2. does not show singularity for coplanar angles-only orbit determination problems;
3. does not converge to the trivial solution for space-based applications, and
4. exhibits more robustness to the initial guess with a larger region of convergence.

In the following section, the formulation development for three and multiple observations is introduced. Then, the subsequent section deals with the performance of the presented method. Finally, four scenarios will be considered to test the perfor-

mance and to validate the proposed method. In particular, the observed lines-of-sight directions are corrupted with Gaussian noise to simulate real observations.

B. Formulation Development

Let us consider n measured line-of-sight unit-vectors, $\hat{\boldsymbol{\rho}}_k$, observed at times $t_1, t_2, \ldots, t_n$, respectively. Let $\mathbf{R}_k$ be the observer known position vectors, ρ_k the spacecraft unknown ranges, and $\mathbf{r}_k$ the spacecraft unknown position vectors. These vectors satisfy the n identities

$$\mathbf{r}_k = \mathbf{R}_k + \rho_k \, \hat{\boldsymbol{\rho}}_k, \qquad k = 1, 2, \ldots, n \tag{3.1}$$

Since all the spacecraft position vectors lie on the same orbital plane, we can always express one vector as a linear combination of the other two as,

$$\mathbf{r}_k = c_k \, \mathbf{r}_{k-1} + d_k \, \mathbf{r}_{k+1}, \qquad k = 2, 3, \ldots, n-1 \tag{3.2}$$

The coefficients c_k and d_k are obtained by expressing the vectors $\mathbf{r}_{k-1}$ and $\mathbf{r}_{k+1}$ in terms of position and velocity vectors at time t_k, $\mathbf{r}_k$ and $\mathbf{v}_k$. This is done using the Lagrange coefficients, f and g, as in the following

$$\begin{cases} \mathbf{r}_{k-1} = f_{k-1} \, \mathbf{r}_k + g_{k-1} \, \mathbf{v}_k \\ \mathbf{r}_{k+1} = f_{k+1} \, \mathbf{r}_k + g_{k+1} \, \mathbf{v}_k \end{cases} \tag{3.3}$$

Equation (3.3) allows us to eliminate the vector $\mathbf{v}_k$. This gives us a relationship between the vectors $\mathbf{r}_{k-1}$, $\mathbf{r}_k$, and $\mathbf{r}_{k+1}$. By comparing this equation with Eq. (3.2), we obtain an expression for the coefficients c_k and d_k

$$c_k = \frac{g_{k+1}}{f_{k-1} \, g_{k+1} - f_{k+1} \, g_{k-1}} \qquad \text{and} \qquad d_k = -\frac{g_{k-1}}{f_{k-1} \, g_{k+1} - f_{k+1} \, g_{k-1}} \tag{3.4}$$

Therefore, Eq. (3.2) can be written as

$$\mathbf{r}_k = \frac{g_{k+1}}{f_{k-1}\, g_{k+1} - f_{k+1}\, g_{k-1}}\, \mathbf{r}_{k-1} - \frac{g_{k-1}}{f_{k-1}\, g_{k+1} - f_{k+1}\, g_{k-1}}\, \mathbf{r}_{k+1} \tag{3.5}$$

Also by eliminating $\mathbf{r}_k$ in Eq. (3.3), the velocity $\mathbf{v}_k$ can be written as

$$\mathbf{v}_k = -\frac{f_{k+1}}{f_{k-1}\, g_{k+1} - f_{k+1}\, g_{k-1}}\, \mathbf{r}_{k-1} + \frac{f_{k-1}}{f_{k-1}\, g_{k+1} - f_{k+1}\, g_{k-1}}\, \mathbf{r}_{k+1} \tag{3.6}$$

Lagrange coefficients f_k and g_k can be expanded in series of time difference $\triangle t_k = t_k - t_{k-1}$. The coefficients series expansions up to fourth order are [34]

$$\begin{cases} f_{k-1} \approx 1 - \dfrac{\mu}{2r_k^3}\triangle t_k^2 - \dfrac{\mu(\mathbf{r}_k\cdot\mathbf{v}_k)}{2r_k^5}\triangle t_k^3 + \\ \qquad\qquad + \dfrac{\mu}{24}\left[-2\dfrac{\mu}{r_k^6} + 3\dfrac{v_k^2}{r_k^5} - 15\dfrac{(\mathbf{r}_k\cdot\mathbf{v}_k)^2}{r_k^7}\right]\triangle t_k^4 \\ f_{k+1} \approx 1 - \dfrac{\mu}{2r_k^3}\triangle t_{k+1}^2 + \dfrac{\mu(\mathbf{r}_k\cdot\mathbf{v}_k)}{2r_k^5}\triangle t_{k+1}^3 + \\ \qquad\qquad + \dfrac{\mu}{24}\left[-2\dfrac{\mu}{r_k^6} + 3\dfrac{v_k^2}{r_k^5} - 15\dfrac{(\mathbf{r}_k\cdot\mathbf{v}_k)^2}{r_k^7}\right]\triangle t_{k+1}^4 \\ g_{k-1} \approx -\triangle t_k + \dfrac{\mu}{6\,r_k^3}\triangle t_k^3 + \dfrac{\mu\,(\mathbf{r}_k\cdot\mathbf{v}_k)}{4\,r_k^5}\triangle t_k^4 \\ g_{k+1} \approx \triangle t_{k+1} - \dfrac{\mu}{6\,r_k^3}\triangle t_{k+1}^3 + \dfrac{\mu\,(\mathbf{r}_k\cdot\mathbf{v}_k)}{4\,r_k^5}\triangle t_{k+1}^4 \end{cases} \tag{3.7}$$

where $\mu = 398,600.44\ \mathrm{km}^3/\mathrm{s}^2$ is the Earth gravitational parameter.

1. Numerical Solution

First we develop the procedure for $n = 3$ measurements and then we will extend it to multiple observations. For small time intervals $\triangle t_k$ (small with respect to the orbital period), the coefficients f and g can be well approximated using the first two terms

of the series expansions, only. This yields [34] to the approximated expressions

$$\begin{cases} c_k \approx \dfrac{\triangle t_{k+1}}{\triangle t_k + \triangle t_{k+1}} \left[1 + \mu \dfrac{(\triangle t_k + \triangle t_{k+1})^2 - \triangle t_{k+1}^2}{6\, r_k^3}\right] \\ \\ d_k \approx \dfrac{\triangle t_k}{\triangle t_k + \triangle t_{k+1}} \left[1 + \mu \dfrac{(\triangle t_k + \triangle t_{k+1})^2 - \triangle t_k^2}{6\, r_k^3}\right] \end{cases} \tag{3.8}$$

where $k = 2, \ldots, n-1$ and for equally spaced measured times ($\triangle t = \text{const}$)

$$c_k = d_k = \frac{1}{2}\left(1 + \frac{\mu}{2\, r_k^3}\, \triangle t^2\right) \tag{3.9}$$

Using the expressions obtained for c_k and d_k from Eq. (3.9), we can rewrite Eq. (3.2) in a scalar form. For three lines-of-sight, $\hat{\boldsymbol{\rho}}_1$, $\hat{\boldsymbol{\rho}}_2$, and $\hat{\boldsymbol{\rho}}_3$, we obtain a set of three algebraic equations in terms of the unknown ranges. This allows us to introduce the residuals $\psi_j(\rho_1, \rho_2, \rho_3),\ j = 1, 2, 3$, as

$$\begin{cases} \psi_1 = c_2(\mathbf{R}_{1,x} + \rho_1\, \hat{\boldsymbol{\rho}}_{1,x}) + d_2(\mathbf{R}_{3,x} + \rho_3\, \hat{\boldsymbol{\rho}}_{3,x}) - (\mathbf{R}_{2,x} + \rho_2\, \hat{\boldsymbol{\rho}}_{2,x}) \\ \psi_2 = c_2(\mathbf{R}_{1,y} + \rho_1\, \hat{\boldsymbol{\rho}}_{1,y}) + d_2(\mathbf{R}_{3,y} + \rho_3\, \hat{\boldsymbol{\rho}}_{3,y}) - (\mathbf{R}_{2,y} + \rho_2\, \hat{\boldsymbol{\rho}}_{2,y}) \\ \psi_3 = c_2(\mathbf{R}_{1,z} + \rho_1\, \hat{\boldsymbol{\rho}}_{1,z}) + d_2(\mathbf{R}_{3,z} + \rho_3\, \hat{\boldsymbol{\rho}}_{3,z}) - (\mathbf{R}_{2,z} + \rho_2\, \hat{\boldsymbol{\rho}}_{2,z}) \end{cases} \tag{3.10}$$

Hence, the searched solution must satisfy

$$\psi_j(\rho_1^*,\, \rho_2^*,\, \rho_3^*) = 0, \qquad j = 1, 2, 3. \tag{3.11}$$

Let us now write the Taylor's series expansion of Eq. (3.10) up to the 2^{nd} order

$$\psi_{i+1} \approx \psi_i + J_i\, \triangle\rho_i + \frac{1}{2}\, \triangle\rho_i^{\mathrm{T}} H_i\, \triangle\rho_i \tag{3.12}$$

where

$$J_i = \begin{bmatrix} \frac{\partial \psi_{1i}}{\partial \rho_1} & \frac{\partial \psi_{1i}}{\partial \rho_2} & \frac{\partial \psi_{1i}}{\partial \rho_3} \\ \frac{\partial \psi_{2i}}{\partial \rho_1} & \frac{\partial \psi_{2i}}{\partial \rho_2} & \frac{\partial \psi_{2i}}{\partial \rho_3} \\ \frac{\partial \psi_{3i}}{\partial \rho_1} & \frac{\partial \psi_{3i}}{\partial \rho_2} & \frac{\partial \psi_{3i}}{\partial \rho_3} \end{bmatrix} \quad \text{and} \quad H_i = \begin{bmatrix} \frac{\partial^2 \psi_i}{\partial \rho_1^2} & \frac{\partial^2 \psi_i}{\partial \rho_1 \partial \rho_2} & \frac{\partial^2 \psi_i}{\partial \rho_1 \partial \rho_3} \\ \frac{\partial^2 \psi_i}{\partial \rho_2 \partial \rho_1} & \frac{\partial^2 \psi_i}{\partial \rho_2^2} & \frac{\partial^2 \psi_i}{\partial \rho_2 \partial \rho_3} \\ \frac{\partial^2 \psi_i}{\partial \rho_3 \partial \rho_1} & \frac{\partial^2 \psi_i}{\partial \rho_3 \partial \rho_2} & \frac{\partial^2 \psi_i}{\partial \rho_3^2} \end{bmatrix} \tag{3.13}$$

are the Jacobian matrix and the Hessian tensor, respectively. The iterative solution for ρ is [35]

$$\rho_{i+1} = \rho_i - J_i^{-1} \left[\psi_i + \frac{1}{2} \left(J_i^{-1} \psi_i \right)^{\mathrm{T}} H_i \left(J_i^{-1} \psi_i \right) \right] \tag{3.14}$$

Once the ranges have been computed, the orbital elements are evaluated in terms of Cartesian coordinates as radius and velocity at mid-point. The initial and final radii, $\mathbf{r}_1$ and $\mathbf{r}_3$, are evaluated using Eq. (3.1) while radius and velocity at mid-point, $\mathbf{r}_2$ and $\mathbf{v}_2$, are evaluated using Eq. (3.5) and Eq. (3.6), respectively. Alternative approach is to use Lambert solver with $\mathbf{r}_1$, $\mathbf{r}_3$, and $\Delta t = t_3 - t_1$.

Having the Hessian matrix involved in the series expansion does not enhance the accuracy of the estimation mainly because of the approximations made in the heart of the algorithm. The numerical simulations demonstrated that the linear expansion (Jacobian only) is sufficient to guarantee the convergence for a wide initial guess region. More importantly, the linear approach has the important advantage of being substantially faster.

This claim is validated by numerical results presented in Scenario I of Section 3, in which the linear model (Jacobian only) was adopted for simulation. Also, using more terms of the Lagrange coefficients makes it less cost-effective as it will be shown in Section 3 as the noise involved in the measured data, even having exact values of f and g, has no effect on the accuracy of most cases. For the orbit determination problems in which the exact values of f and g are effective, another technique (L_n) will be presented, based on a least-squares scheme. In conclusion, for this numerical

approach, only the first two terms of Taylor's series expansion and approximated Lagrange coefficients are adopted. This numerical procedure will be referred to as J_n throughout this paper, where "J" stands for "Jacobian" and the subscript, n, indicates the number of observations. The algorithm through which the components of the Jacobian matrix were constructed is provided in Appendix A.

When the observer position vectors ($\mathbf{R}_1$, $\mathbf{R}_2$, $\mathbf{R}_3$) and the measured lines-of-sight directions ($\hat{\boldsymbol{\rho}}_1$, $\hat{\boldsymbol{\rho}}_2$, $\hat{\boldsymbol{\rho}}_3$) all lie on the satellite orbit plane, the co-planarity condition given in Eq. (3.2) collapses into two equations (the third equation becomes zero as the coordinate perpendicular to the orbit plane vanishes). In this case we have three unknowns (ρ_1, ρ_2, and ρ_3) and two equations. This is the case referred to as singularity case. To obtain the solution, a fourth observation is required with which two co-planarity conditions can be constructed. Now since each co-planarity condition collapses into two equations for the coplanar case, we obtain a total of four equations which is sufficient to solve for the four unknown ranges, ρ_1, ρ_2, ρ_3, and ρ_4.

2. Extension to Multiple Observations

In the case of n observations ($n > 3$) more than one coplanarity condition can be written. For n observations we have

$$\begin{cases} \mathbf{r}_2 & = & c_2\,\mathbf{r}_1 + d_2\,\mathbf{r}_3 \\ \mathbf{r}_3 & = & c_3\,\mathbf{r}_2 + d_3\,\mathbf{r}_4 \\ & \vdots & \\ \mathbf{r}_{n-1} & = & c_{n-1}\,\mathbf{r}_{n-2} + d_{n-1}\,\mathbf{r}_n \end{cases} \tag{3.15}$$

By substituting Eq. (3.1) in Eq. (3.15), a set of $3(n-2)$ algebraic equations

$$\begin{cases} \psi_1 & = & c_2(\mathbf{R}_{1,x} + \rho_1\,\hat{\boldsymbol{\rho}}_{1,x}) + d_2(\mathbf{R}_{3,x} + \rho_3\,\hat{\boldsymbol{\rho}}_{3,x}) - (\mathbf{R}_{2,x} + \rho_2\,\hat{\boldsymbol{\rho}}_{2,x}) \\ & \vdots & \\ \psi_{3(n-2)} & = & c_{n-1}(\mathbf{R}_{n-2,z} + \rho_{n-2}\,\hat{\boldsymbol{\rho}}_{n-2,z}) + d_{n-1}(\mathbf{R}_{n,z} + \rho_n\,\hat{\boldsymbol{\rho}}_{n,z}) + \\ & & -(\mathbf{R}_{n-1,z} + \rho_{n-1}\,\hat{\boldsymbol{\rho}}_{n-1,z}) \end{cases} \tag{3.16}$$

is obtained. This set of equation can be written in the compact form

$$\psi_j(\rho_k^*) = 0, \qquad j = 1, 2, \ldots, 3(n-2), \qquad k = 1, 2, \ldots, n. \tag{3.17}$$

In general, the Jacobian is a $3(n-2) \times n$ matrix and not necessarily square, so Eq. (3.14) becomes (no Hessian involved)

$$\rho_{i+1} = \rho_i - (J_i^{\mathrm{T}}\, W\, J_i)^{-1}\, J_i^{\mathrm{T}} W \psi_i \tag{3.18}$$

where W is a weight matrix. The Jacobian J is built as shown in Appendix A. This technique, called "J_n", requires building the Jacobian. In the contrary, the technique presented in the next section does not require constructing the Jacobian or computing any sort of higher derivatives.

3. Least-Squares Solution

The coplanarity conditions can written in the matrix form, $M\,\rho = \xi$, where ρ and ξ are $n \times 1$ and $3(n-2) \times 1$ vectors respectively and M is a $3(n-2) \times n$ matrix. For any set of ranges, ρ_k, we can write $(n-2)$ vectorial identities

$$c_k\,\rho_{k-1}\,\hat{\boldsymbol{\rho}}_{k-1} - \rho_k\,\hat{\boldsymbol{\rho}}_k + d_k\,\rho_{k+1}\,\hat{\boldsymbol{\rho}}_{k+1} = \mathbf{R}_k - (c_k\,\mathbf{R}_{k-1} + d_k\,\mathbf{R}_{k+1}) \tag{3.19}$$

where $k = 2, 3, \ldots, n-1$. Setting $\xi_k = \mathbf{R}_k - c_k\,\mathbf{R}_{k-1} - d_k\,\mathbf{R}_{k+1}$, we can rewrite the $(n-2)$ equations given in Eq. (3.19) in the compact matrix form, $M\,\rho = \xi$, where

$$\begin{bmatrix} c_2\hat{\rho}_1 & -\hat{\rho}_2 & d_2\hat{\rho}_3 & \mathbf{0} & \mathbf{0} & \cdots & \mathbf{0} \\ \mathbf{0} & c_3\hat{\rho}_2 & -\hat{\rho}_3 & d_3\hat{\rho}_4 & \mathbf{0} & \cdots & \mathbf{0} \\ \mathbf{0} & \mathbf{0} & c_4\hat{\rho}_3 & -\hat{\rho}_4 & d_4\hat{\rho}_5 & \cdots & \mathbf{0} \\ \vdots & \vdots & \vdots & \vdots & \vdots & \ddots & \vdots \\ \mathbf{0} & \mathbf{0} & \mathbf{0} & \mathbf{0} & \mathbf{0} & \cdots & d_{n-1}\hat{\rho}_n \end{bmatrix} \begin{Bmatrix} \rho_1 \\ \rho_2 \\ \rho_3 \\ \vdots \\ \rho_n \end{Bmatrix} = \begin{Bmatrix} \xi_2 \\ \xi_3 \\ \xi_4 \\ \vdots \\ \xi_{n-1} \end{Bmatrix} \tag{3.20}$$

where $\mathbf{0}$ identifies a 3×1 vector of zeroes. The least-squares solution of Eq. (3.20) is

$$\rho = \left(M^{\mathrm{T}}\,W M\right)^{-1}\,M^{\mathrm{T}}\,W\xi \tag{3.21}$$

Once the range vector, ρ, has been computed, the orbital elements are then evaluated using Lambert solver with the most orthogonal estimated radii using Eq. (3.1). For short-arc observations, these are usually the first and the last ones.

Although this procedure is iterative, the initial guess of all ranges set to zero works efficiently for almost all cases. This technique does not require using approximated (truncated) values of the Lagrange coefficients, so the exact values of f and g can be used. This least-squares algorithm will be referred to as L_n throughout this paper where "L" stands for Least-squares and the index n is the number of observations. In the examples we have used the Taylor's series expansion of the Lagrange coefficients up to the fourth order.

4. Gauss-exact

The accuracy of the original Gauss method (approximate Lagrange coefficients) can be enhanced by using the exact values of the coefficients. Reference [36] explains how this can be achieved using the exact values of the coefficients f and g and Universal

Kepler's Equation. A brief review of the procedure will be explained here for the sake of completeness. The exact values of the Lagrange coefficients can be written in terms of the universal anomaly, χ, as

$$\begin{cases} f = 1 - \dfrac{\chi^2}{r_0} C(\alpha\,\chi^2) \\ g = \Delta t - \dfrac{1}{\sqrt{\mu}}\,\chi^3\, S(\alpha\,\chi^2) \end{cases} \tag{3.22}$$

where C and S are Stumpff functions and defined as

$$\begin{cases} S(\alpha\chi^2) = \dfrac{\sqrt{\alpha\chi^2} - \sin\sqrt{\alpha\chi^2}}{(\sqrt{\alpha\chi^2})^3} \\ C(\alpha\chi^2) = \dfrac{1 - \cos\sqrt{\alpha\chi^2}}{\alpha\chi^2} \end{cases} \tag{3.23}$$

and r_0 is the magnitude of the initial position vector. The quantity α is defined as $\alpha = \frac{2}{r_0} - \frac{v_0^2}{\mu}$ where v_0 is the magnitude of the initial velocity vector.The Universal Kepler's Equation in terms of universal anomaly

$$\sqrt{\mu}\Delta t = \frac{r_0 v_{r0}}{\sqrt{\mu}}\chi^2 C(\alpha\chi^2) + (1 - \alpha r_0)\chi^3 S(\alpha\chi^2) + r_0\chi \tag{3.24}$$

here v_{r0} is the magnitude of the tangential component of the velocity vector. The solution of Eq. (3.24), χ, then will be plugged back into Eq. (3.22) to obtain the exact values of f and g.

C. Simulations and Results

Four different scenarios were used for testing and validation. In all cases, the measurements were made from a ground tracking site located at a zero longitude and zero latitude for the sake of simplicity. The results from the developed techniques were compared with those of Gauss, Double r-iteration, and improved Gauss which is referred to as Gauss-exact here. The accuracy of the original Gauss method (using

approximated Lagrange coefficients) can be enhanced by using the exact values of the coefficients. Reference [3] (Algorithm 5.6) explains how this can be achieved using the exact values of the coefficients f and g and universal Kepler's equation. To simulate the true measurements, the ideal data were corrupted with Gaussian noise with standard deviation of $\sigma = 5''$. The ideal measured lines-of-sight were simulated through the following procedure:

(a) Orbital elements of a typical low earth orbit (LEO) were selected. The orbital elements selection was made consistent with the observation site selection so that the observed satellite is actually in view.

(b) The initial position and velocity vectors are then obtained using the orbital elements selected from the previous step.

(c) The satellite initial position and velocity vectors (initial condition) are then propagated using the Keplerian two-body problem to obtain subsequent observations, $\mathbf{r}_k, \quad k = 1, 2, \ldots, n$, which are the ideal position vectors.

(d) Since we know where the ground observer is located, the $\mathbf{R}_k$ vectors are already known.

(e) The ideal measured lines-of-sight $\hat{\boldsymbol{\rho}}_k$, are then obtained using Eq. (3.1).

The initial satellite real position and velocity vectors of each scenario can be found in Table VI. The observer position vector is the same for all scenarios. The initial position vector of the ground tracking site is $\mathbf{R}_1 = \{6,378.137, \quad 0, \quad 0\}^{\mathrm{T}}$ km. Using these data, the real (ideal) lines-of-sight vectors can be calculated following item (e), mentioned above. The estimated error presented in all four scenarios is in terms of relative position percentage error defined as error $(\%) = 100\,(|\mathbf{r}_{est} -$

$\mathbf{r}_{true}|)/|\mathbf{r}_{true}|$. Finally, the errors provided in the Tables and Figures are obtained by averaging the estimated error of each observation.

1. **Scenario I:** *Tracking equatorial LEO satellite (coplanar case).* The first test is dedicated to compare the performance of the presented technique for a coplanar case. Comparisons were made with respect to Gauss' method as it is (along with Laplace's) not capable of handling the coplanar case problem. In this scenario, where the measured directions are lying on the satellite orbital plane, the coplanarity condition, Eq. (3.2), collapses into two algebraic equations. Since, each coplanarity condition involves three unknown ranges (ρ_1, ρ_2, ρ_3) in order to obtain the sufficient number of equations, one more observation is needed. This leads to two coplanarity conditions and a set of four algebraic equations with four unknown ranges. For this specific case, the satellite orbital plane is assumed to be lying on the Earth equatorial plane.

   The time intervals between the observations was chosen $\triangle t = 50$ s. Table VIII presents the results of our technique versus those of Gauss' and Double r-iteration. Table VIII provides the results obtained using J_n and L_n methods for $n > 3$ observations.

   As it can be seen from Table VIII the number of observation of five is optimal as, for this specific problem, no accuracy improvement has been experienced with more observations.

   Scenario I was run twice with linear and quadratic theories using 4 observations. With Hessian term involved, we obtained error (%) = 0.0197 and error (%) = 0.02 without it. The small increase of accuracy does not fully justify the substantial complexity increase due to Hessian evaluation.

2. **Scenario II:** *Tracking a* 45° *LEO satellite (inclined case).* In this case, the

Table VIII. Tracking Equatorial LEO Satellite (Coplanar Case)

Approach	Observations	Position error (%)	Iterations	Elapsed time (s)
Gauss	3	singular	non-iterative	N/A
Gauss-exact	3	singular	5	N/A
Double-r	3	diverged	1	N/A
J_4	4	0.02	2	0.0082
J_5	5	0.016	2	0.0083
J_6	6	0.016	2	0.0084
L_4	4	0.017	7	0.028
L_5	5	0.011	7	0.03
L_6	6	0.011	7	0.032

orbit has a 45° inclination, and three observations would be sufficient to obtain the solution. The time interval between the observations was $\triangle t = 50$ s. Table IX shows the results for $n = 3$ as well as for multiple observations using J_n and L_n methods.

Table IX. Tracking a 45 deg. LEO Satellite (Inclined Case)

Approach	Observations	Position error (%)	Iterations	Elapsed time (s)
Gauss	3	0.06	non-iterative	0.036
Gauss-exact	3	0.06	5	0.05
Double-r	3	0.06	3	0.035
J_3	3	0.06	2	0.007
J_4	4	0.035	2	0.0084
J_5	5	0.030	2	0.0084
J_6	6	0.030	2	0.0086
L_3	3	0.06	7	0.026
L_4	4	0.030	10	0.03
L_5	5	0.023	10	0.032
L_6	6	0.020	10	0.034

3. **Scenario III:** *Tracking a polar LEO satellite (orthogonal case).* In this case, a polar orbit was considered using the same time interval between measurements. Results are provided in Table X.

Table X. Tracking a Polar LEO Satellite (Orthogonal Case)

Approach	Observations	Position error (%)	Iterations	Elapsed time (s)
Gauss	3	0.18	non-iterative	0.035
Gauss-exact	3	0.18	5	0.05
Double-r	3	0.18	3	0.036
J_3	3	0.18	2	0.007
J_4	4	0.086	2	0.0083
J_5	5	0.07	2	0.0083
J_6	6	0.058	2	0.0087
L_3	3	0.18	10	0.027
L_4	4	0.083	12	0.031
L_5	5	0.06	15	0.035
L_6	6	0.052	16	0.04

4. **Scenario IV:** *Tracking an asteroid (hyperbolic case).* In this case, an astroid flying by the Earth on a hyperbolic orbit was considered with $\triangle t = 50$ s to be consistent with the other three previous scenarios. Results are presented in Table XI. The methods of J_n and L_n were run using multiple observations again for results accuracy enhancement.

   The technique J_n yields the same accuracy level over a wide range of initial guess, from almost 0.5 to 10 times of the true solution. The technique L_n

Table XI. Tracking an Asteroid on Hyperbolic Orbit

Approach	Observations	Position error (%)	Iterations	Elapsed time (s)
Gauss	3	0.021	non-iterative	0.026
Gauss-exact	3	0.021	5	0.1
Double-r	3	0.021	5	0.052
J_3	3	0.021	2	0.007
J_4	4	0.019	2	0.008
J_5	5	0.017	2	0.0082
J_6	6	0.018	2	0.0084
L_3	3	0.021	7	0.026
L_4	4	0.018	7	0.03
L_5	5	0.014	7	0.032
L_6	6	0.014	7	0.034

can work with almost every initial guess whereas the Double r-iteration is so sensitive to the initial guess with very smaller initial guess convergence region as compared to the proposed techniques.

Tables XII and XIII present the orbital elements of the four scenarios and initial real position and velocity vectors respectively.

1. Sensitivity Analysis

This section demonstrates that the orbit estimation accuracy mainly depends on noise level, time intervals between measurements, and the specific selection of orbital elements. Also different observations combinations were tried to see how the accuracy of the results would be affected. To quantify the contribution of these parameters to

Table XII. Orbital Elements

Scenario	a	e	i	Ω	ω	ν
	km	[-]	(deg)	(deg)	(deg)	(deg)
I	7,780.0	0.1	0	0	0	0
II	7,800.0	0.1	45	345	15	0
III	7,800.0	0.1	90	345	15	0
IV	-14,738.0	1.45	45	358	354	7

Table XIII. Initial Real Position and Velocity Vectors

Scenario	x	y	z	V_x	V_y	V_z
	km	km	km	km/s	km/s	km/s
I	7,002	0.0	0.0	0	7.9132	0
II	6,882.26672	-514.02760	1,284.74917	-0.5787	5.7434	5.3979
III	6,549.74917	-1,755.0	1,816.90970	-1.9757	0.5294	7.6338
IV	6,659.28394	-150.28970	82.20751	0.9623	8.5237	8.5521

the accuracy, the sensitivity analysis is performed around a base scenario. Scenario II was selected as the case study. The effect of the noise on the results accuracy is obtained by varying the noise level from zero to $5''$ (1σ). Figure 1 shows the satellite relative position error (as defined in the previous section) as a function of noise. The axes are in log-log scale.

Figure 1 shows, for very low noisy data, that the Double r-iteration, Gauss-exact, and L_n yield excellent accuracies, while Gauss and J_n do not. This is due to the approximations made in the Lagrange coefficients in Eq. (3.9). This figure shows that, for the noise level greater than $\sigma = 2''$, the five different methods provide the same levels of accuracy. Since J_n has the smallest running time and also the

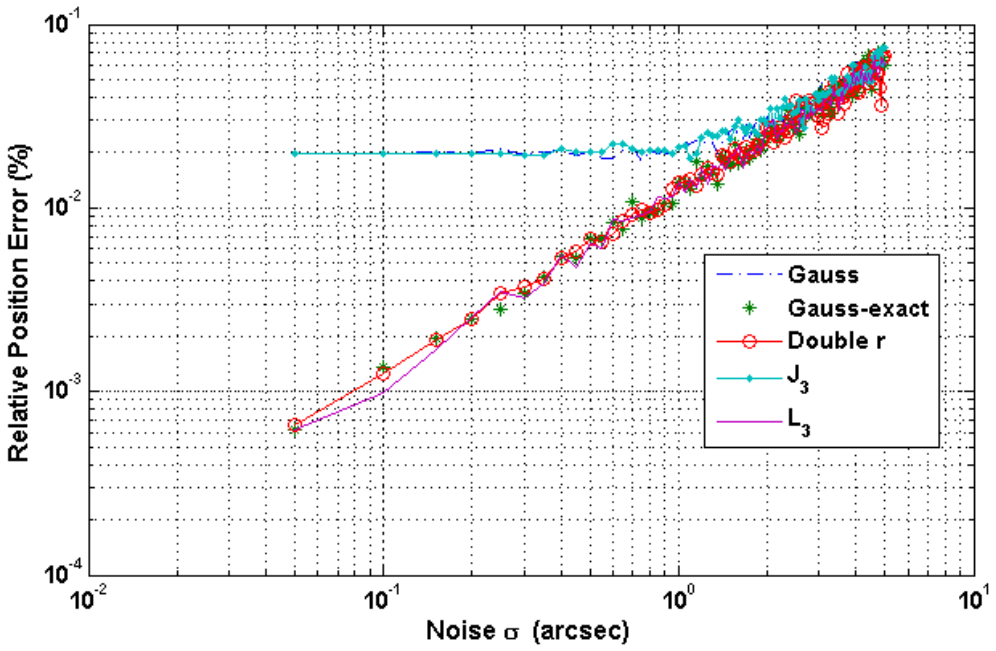

Fig. 1. Scenario II:Relative Position Percentage Error vs. Noise ($\triangle t = 50$ s)

running time almost remains the same regardless of the number of observations J_n can be considered the most cost-effective approach. In fact, the computation of the exact values of the Lagrange coefficients becomes worthless when higher levels of noise are considered. To avoid this drawback, an increase in the time interval can be considered. This reduces the noise effect on the accuracy. However, increasing $\triangle t$ has technical limitations. For instance, since the tracking site field-of-view is limited, all measurements should be made within some specific time range.

To see the effect of the time interval Δt on the accuracy of the results, Scenario II was solved again for the time intervals varying from 20 s to 120 s. In this case, the noise level was considered $\sigma = 5''$. Figure 2 shows that increasing the time interval has caused an accuracy improvement in all five schemes up to $\Delta t = 60$ s. But for the time intervals larger than almost 60 s, the performance of J_n and Gauss drop as the Lagrange coefficients used in these two methods are approximated. Since Gauss-

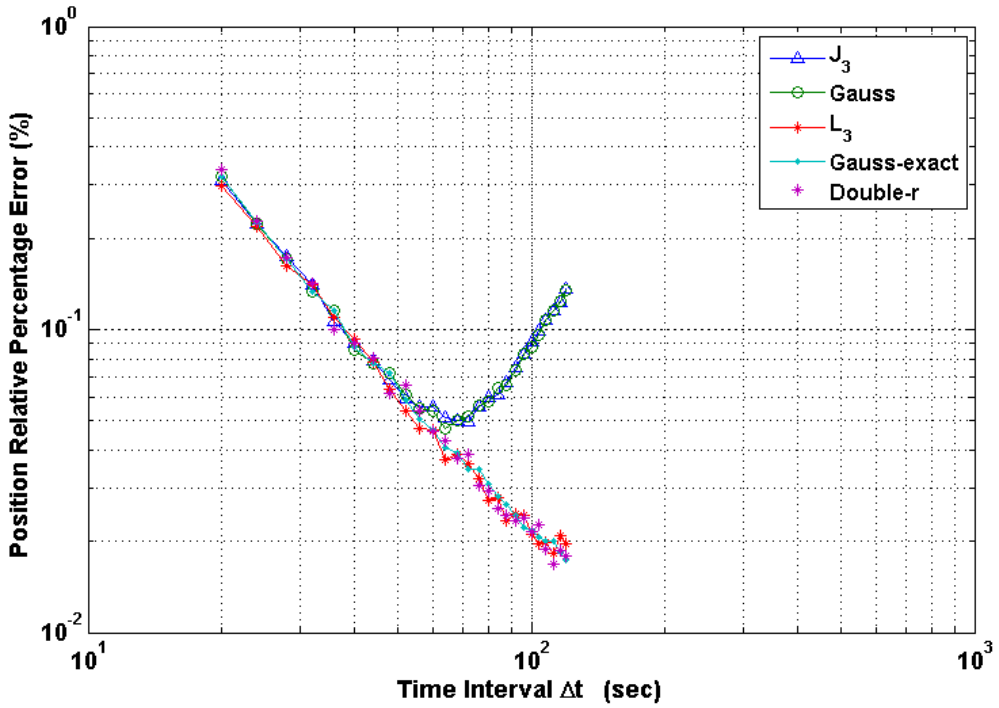

Fig. 2. Scenario II:Relative Position Percentage Error vs. Time Interval $\triangle t$ ($\sigma = 5''$)

exact and L_n use almost the exact values of f and g, the accuracy gets better as the time interval increases. The number of observations used for this case was three. Also to see how the estimated position error would be improved with more number of observations, L_n was run with $n = 4, 5$, and 6. Figure 3 shows the performance of L_n versus those of Gauss-exact and Double r-iteration. The technique L_n seems to be the most suitable one as it can take care of multiple observations for higher accuracy with almost the same running time as Double r-iteration and Gauss-exact. Another factor affecting the results accuracy is the orbital elements. The technique adopted for these tests was J_n. Figure 4 shows how the estimated position error changes versus the eccentricity, semi-major axis, and true anomaly, respectively. In this part of the sensitivity analysis, the time interval, $\Delta t = 50$ s, remains constant. In the first plot of Fig. 4, the eccentricity was changed from zero to 0.25 while the

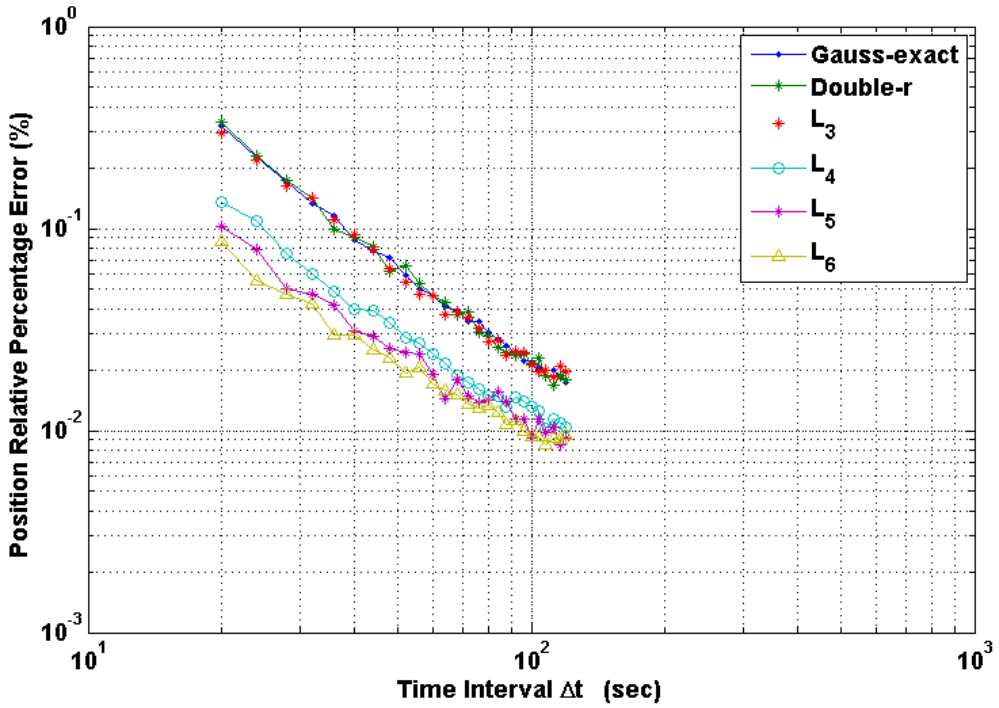

Fig. 3. Scenario II:Performance of L_n vs Double r-iteration and Gauss-exact vs. Time Interval $\triangle t$ ($\sigma = 5''$)

other five orbital elements were kept constant. As it can be seen, the accuracy of the estimated orbit varies versus the orbit eccentricity. The semi-major axis was then changed from 7,500 km to 10,000 km. The results accuracy is given in the middle plot of Fig. 4. At last, the true anomaly was changed from 355° to 5° and the results can be seen in the bottom plot of Fig. 4. In all three plots, the right ascension ($\Omega = 345°$), argument of perigee ($\omega = 15°$), and inclination ($i = 45°$) remained constant. Note that the error behavior shown in Fig. 4 may differ case by case.

Also two more combinations (rather than the original one) of the observations were tested to see how the accuracy of the results would change. For the purpose, 5 observations were considered out of which three coplanarity conditions could be written. The original combination is 123, 234, and 345 referred to as Set I here.

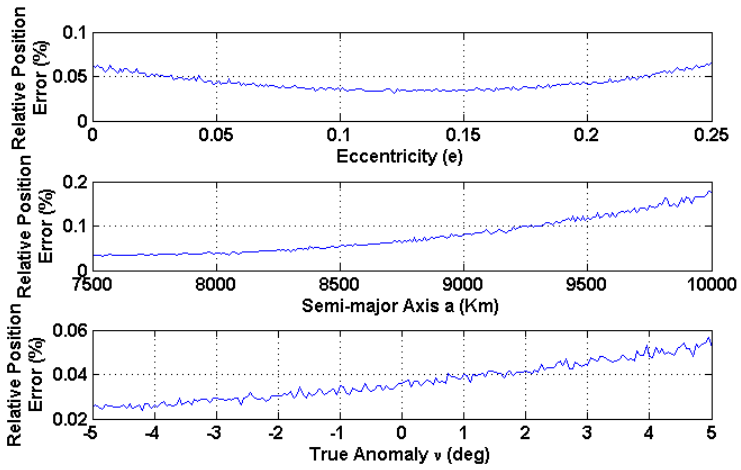

Fig. 4. Scenario II: Relative Position Percentage Error Sensitivity to Orbital Elements. Top: Eccentricity, Middle: Semi-major Axis, Bottom: True Anomaly. ($\Omega = 345°,\ \omega = 15°,\ i = 45°$), ($\Delta t = 50$ s, using J_n)

Two more combinations are: Set II (125,235,245) and Set III (124,135,245). Figure 5 shows all three sets of data exhibit almost same performance over a wide range of time intervals.

2. Results Bias

Scenario II was selected for the bias test with three observations and $\triangle t = 50$ s. While evaluating the performance of the orbit determination methods used in this paper, the results of Gauss and J_n were found biased whereas Gauss-exact, Double r-iteration, and L_n were not. Gauss and J_n are biased because they use approximated Lagrange coefficients. Figure 6 and 7 show the histograms of the error provided by J_n and L_n, respectively. To construct these histograms, the orbit determination problem was run 2,000 times using L_n and J_n. To simulate the true measurements, the ideal data were corrupted with noise ($\sigma = 5''$) and the respective relative position error was recorded. Then, the error was plotted versus the number of occurrences for

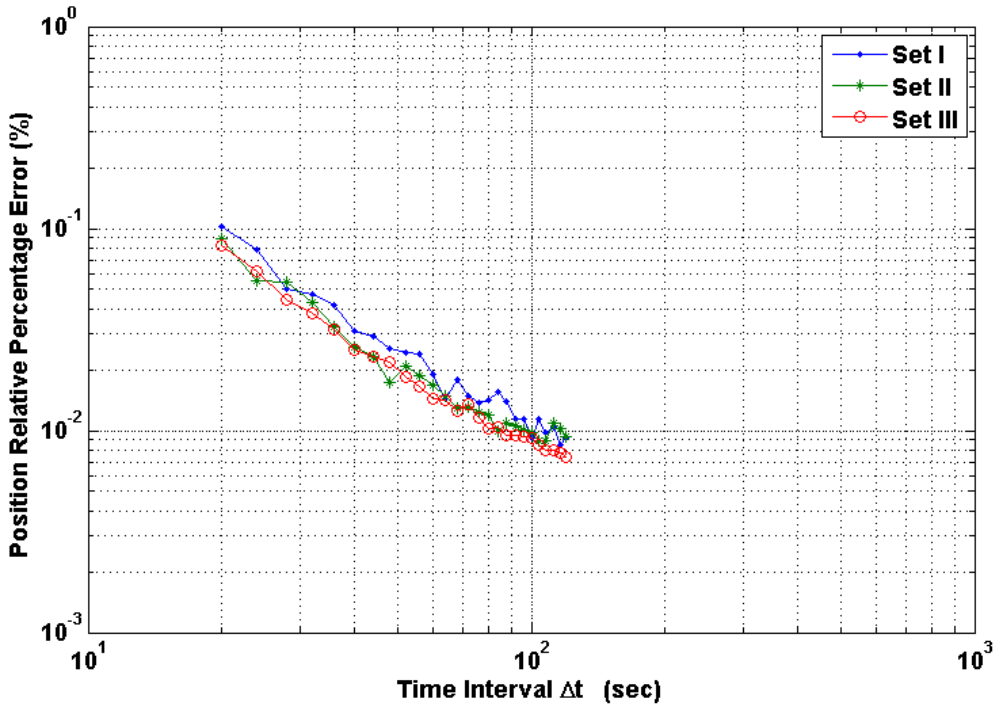

Fig. 5. Scenario II: Relative Position Percentage Error of Different Observations Combinations vs. Interval $\triangle t$ ($\sigma = 5''$)

each amount of error. As it can be seen in Fig. 6, the mean value of the estimated errors using J_n is about 0.01% (off-set from zero) whereas that of L_n is zero which is because of using the exact (or very close to exact) values of f and g functions in L_n. The estimated error presented in the histograms is in terms of relative position percentage error defined as error (%) $= 100\,(|\mathbf{r}_{est}| - |\mathbf{r}_{true}|)/|\mathbf{r}_{true}|$. Note that this definition is slightly different from the one defined in the beginning of this section. The reason is also to show negative errors when plotting the histograms.

For all the above simulations, the time interval between the measurements was considered constant and the number of observations was chosen manually by the operator. The algorithm developed in [37] explains how an optimal combination of N_{obs} and Δt can be achieved.

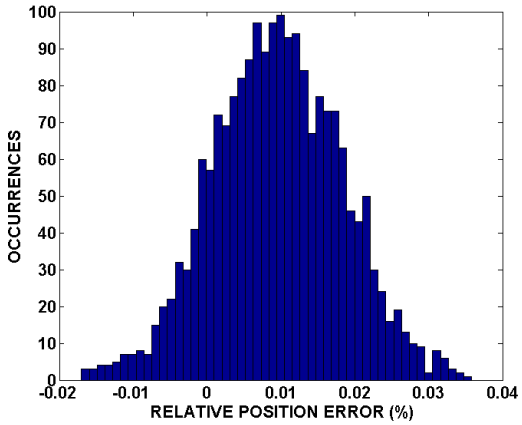

Fig. 6. Error Histogram of J_3

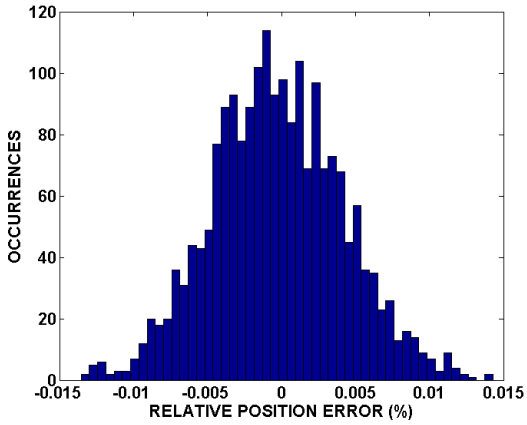

Fig. 7. Error Histogram of L_3

D. Conclusions

Two novel techniques, J_n and L_n, for orbit determination based on multiple angles-only observations are presented and tested. Both algorithms are built using Lagrange coefficients, as Gauss'. These algorithms do not present singularity in the coplanar case, as Gauss' and Laplace's methods. In addition, they are more accurate than these two classical methods as well as Double r-iteration. Finally, the code complexity of these methods is invariant with respect to the number of measurements.

Four scenarios were considered for validation. In the coplanar case (Scenario I), Gauss' and Double r- iteration methods could not succeed as the first one showed singularity and the second one diverged. In Scenario II (inclined orbit and non-coplanar) all five methods provided the same accuracy level with 3 observations, whereas J_n and L_n were able to use more observations (i.e., 4, 5, and 6) providing better results. Identical situations were experienced for the polar and hyperbolic orbits scenarios, III and IV, respectively.

The reason why all the methods provide the same accuracy is because the high level of noise as compared to the time intervals between the measurements, makes

the calculation of the exact values of the Lagrange functions worthless. For this reason J_n can be seen as the most cost-effective method as it has the least running time, almost independent from the number of observations. By increasing the time intervals, having the exact values of the Lagrange coefficients makes the method more accurate. For this reason the L_n technique becomes the most suitable.

In general, when the noise level is lower than $\sigma = 2''$, Double r-iteration, Gauss-exact, and L_n give great accurate results, but as the noise level increases, the estimated position errors become as accurate as those of J_n and Gauss. Increasing the number of observations improves the accuracy. However, the accuracy increase becomes smaller and smaller until it tends to a limit. The orbital elements as well play a role in the accuracy of the estimated satellite position vectors. For the specific scenario used in the sensitivity analysis section, the error decreased as the eccentricity increased up to a certain point; then the error started growing. In particular, the error decreased as the semi-major axis and true anomaly increased. These behaviors are case-depended. Also three different combinations of observations were tried and all three yielded almost the same accuracy for a wide range of time intervals. Finally, this study has shown that the results from J_n is biased as it uses approximate Lagrange coefficients. In the contrary, L_n exhibits no biased results. In conclusion, for each specific orbit determination problem there is an optimum number of observations and time interval for any noise level.

CHAPTER IV

INITIAL ORBIT DETERMINATION USING PRESCRIBED ORBITS

In this chapter, a new angles-only initial orbit determination technique based on prescribed orbits is presented.

A. Introduction

The initial orbit determination method using multiple observations developed so far have been able to handle many of the ground and space based orbit determination problems for both near earth and long distance objects including coplanar cases. These two techniques are so robust with respect to the initial guess selection and rarely go unstable because of that. The only drawback associated with these two algorithms is that as the number of observations and/or time intervals between the measured directions increase, the accuracy does not get any better and in some cases, it even drops. The IOD method by Paul Herget [10], [11] is also capable of using multiple observations basically suitable for the comets, meteors, and planets and suitable for short arcs. The presented technique was developed in an effort to be able to handle all the orbit determination scenarios as much as possible with a higher accuracy compared to the available orbit determination methods, bypassing the drawbacks and keeping the advantages . The presented technique is also able to deal with one of the most challenging IOD problems, a co-planar case as the classic methods of Gauss and Laplace, and Double-r iteration show singularity and instability when used for coplanar cases. In this technique, an assumed solution is forced to satisfy both the geometry of the problem and also the Keplerian two-body problem equation. For the sake of this work, a polynomial was used. In the next section, the algorithm will be explained in details. Two ways to present the

results and performance of the current method compared to those of previous ones are considered. The error in terms of shape and orientation of the estimated orbit and error in terms of estimated position vector. Monte Carlo analysis was performed along with three specific LEO satellite scenarios. The results show the developed technique is dominant over the classis and recently developed IOD methods by the authors from every aspect.

B. Algorithm Development

The main idea of this technique is to assume a solution to the Keplerian two-body problem (no need to solve it and obtain the exact solution) and also enforce the approximated solution to satisfy the geometry of the problem. The approximated solution could be a polynomial or any other function best describing that part of orbit under determination. The algorithm is first developed with a 3-rd order polynomial to describe the methodology, but the results will be generated using a 5-th order polynomial. A 5-th order polynomial was accurate enough to handle almost all the scenarios. The geometry of a typical orbit determination problem with n observations can be written as

$$\mathbf{r}_i = \mathbf{R}_i + \rho_i \, \hat{\boldsymbol{\rho}}_i, \qquad i = 1, 2, \cdots, n \tag{4.1}$$

where r_i and R_i are the i-th spacecraft and tracking site position vectors respectively. The unknown range ρ_i is the one to be determined and $\hat{\rho}_i$ is the measured direction (a unit vector) of the spacecraft. The trajectory of an orbiting object should satisfy

the two-body problem. Let us now assume an approximated solution in the form of

$$\begin{cases} x(t) = p_x(t) \\ y(t) = p_y(t) \\ z(t) = p_z(t) \end{cases} \tag{4.2}$$

and by considering a 3-rd order polynomial, we have

$$\begin{cases} p_x(t) = a_1 + a_2 t + a_3 t^2 + a_4 t^3 \\ p_y(t) = b_1 + b_2 t + b_3 t^2 + b_4 t^3 \\ p_z(t) = c_1 + c_2 t + c_3 t^2 + c_4 t^3 \end{cases} \tag{4.3}$$

The approximated solution $p(t)$ should also be able to satisfy the geometry Eq.(4.1) so we have

$$\begin{cases} p_x(t_i) \cong R_i^x + \rho_i^x \, \hat{\rho}_i^x \\ p_y(t_i) \cong R_i^y + \rho_i^y \, \hat{\rho}_i^y, \qquad i = 1, 2, \cdots, n \\ p_z(t_i) \cong R_i^z + \rho_i^z \, \hat{\rho}_i^z \end{cases} \tag{4.4}$$

where t_i is the i^{th} measured time. By taking the left hand side of Eq.(4.4) to the right, we can define the residuals as

$$\begin{cases} \phi_{xi} = -p_x(t_i) + (R_i^x + \rho_i^x \, \hat{\rho}_i^x) \\ \phi_{yi} = -p_y(t_i) + (R_i^y + \rho_i^y \, \hat{\rho}_i^y), \qquad i = 1, 2, \cdots, n \\ \phi_{zi} = -p_z(t_i) + (R_i^z + \rho_i^z \, \hat{\rho}_i^z) \end{cases} \tag{4.5}$$

and

$$\begin{cases} \Phi_x = \dfrac{1}{2} \displaystyle\sum_{i=1}^{n} \phi_{xi}^2 \\ \Phi_y = \dfrac{1}{2} \displaystyle\sum_{i=1}^{n} \phi_{yi}^2, \qquad i = 1, 2, \cdots, n \\ \Phi_z = \dfrac{1}{2} \displaystyle\sum_{i=1}^{n} \phi_{zi}^2 \end{cases} \tag{4.6}$$

To have the best fit, the residuals ϕ_x, ϕ_y, and ϕ_z should be minimum with respect

to the polynomial coefficients a_k, b_k, and c_k, $k = 1, 2, 3, 4$. So by applying the least square scheme, the coefficients can be determined in terms of the unknown ranges as

$$\begin{cases} \{a\} = T^{-1}[\sum_{i=1}^{n}(R_i^x + \rho_i^x\,\hat{\rho}_i^x) & \sum_{i=1}^{n}(R_i^x + \rho_i^x\,\hat{\rho}_i^x)t_i & \ldots & \sum_{i=1}^{n}(R_i^x + \rho_i^x\,\hat{\rho}_i^x)t_i^3]^{\mathrm{T}} \\ \{b\} = T^{-1}[\sum_{i=1}^{n}(R_i^y + \rho_i^y\,\hat{\rho}_i^y) & \sum_{i=1}^{n}(R_i^y + \rho_i^y\,\hat{\rho}_i^y)t_i & \ldots & \sum_{i=1}^{n}(R_i^y + \rho_i^y\,\hat{\rho}_i^y)t_i^3]^{\mathrm{T}} \\ \{c\} = T^{-1}[\sum_{i=1}^{n}(R_i^z + \rho_i^z\,\hat{\rho}_i^z) & \sum_{i=1}^{n}(R_i^z + \rho_i^z\,\hat{\rho}_i^z)t_i & \ldots & \sum_{i=1}^{n}(R_i^z + \rho_i^z\,\hat{\rho}_i^z)t_i^3]^{\mathrm{T}} \end{cases} \tag{4.7}$$

where $\{a\} = \{a_1 \quad a_2 \quad a_3 \quad a_4\}^{\mathrm{T}}$, $\{b\} = \{b_1 \quad b_2 \quad b_3 \quad b_4\}^{\mathrm{T}}$, $\{c\} = \{c_1 \quad c_2 \quad c_3 \quad c_4\}^{\mathrm{T}}$, and T is 3×3 matrix

$$T = \begin{bmatrix} n & \sum_{i=1}^{n} t_i & \ldots & \sum_{i=1}^{n} t_i^3 \\ \sum_{i=1}^{n} t_i & \sum_{i=1}^{n} t_i^2 & \ldots & \sum_{i=1}^{n} t_i^4 \\ \ldots & \ldots & \ldots & \ldots \\ \sum_{i=1}^{n} t_i^3 & \sum_{i=1}^{n} t_i^4 & \ldots & \sum_{i=1}^{n} t_i^6 \end{bmatrix} \tag{4.8}$$

Up to now, the polynomial coefficients have been eliminated and we have them in terms of the unknown ρ_i . The next step towards completing the algorithm is enforce the assumed solution to satisfy the Keplerian two-body problem as the following

$$\begin{cases} \ddot{p}_x(t_i) \cong -\dfrac{\mu p_x(t_i)}{[p_x(t_i)^2 + p_y(t_i)^2 + p_z(t_i)^2]^{3/2}} \\ \ddot{p}_y(t_i) \cong -\dfrac{\mu p_y(t_i)}{[p_x(t_i)^2 + p_y(t_i)^2 + p_z(t_i)^2]^{3/2}}, \quad i = 1, 2, \cdots, n \\ \ddot{p}_z(t_i) \cong -\dfrac{\mu p_z(t_i)}{[p_x(t_i)^2 + p_y(t_i)^2 + p_z(t_i)^2]^{3/2}} \end{cases} \tag{4.9}$$

or in the residual form

$$\begin{cases} \psi_{xi} = \ddot{p}_x(t_i) + \dfrac{\mu p_x(t_i)}{[p_x(t_i)^2 + p_y(t_i)^2 + p_z(t_i)^2]^{3/2}} \\ \psi_{yi} = \ddot{p}_y(t_i) + \dfrac{\mu p_y(t_i)}{[p_x(t_i)^2 + p_y(t_i)^2 + p_z(t_i)^2]^{3/2}}, \quad i = 1, 2, \cdots, n \\ \psi_{zi} = \ddot{p}_z(t_i) + \dfrac{\mu p_z(t_i)}{[p_x(t_i)^2 + p_y(t_i)^2 + p_z(t_i)^2]^{3/2}} \end{cases} \tag{4.10}$$

We now define the residual vector as $\Psi = [\psi_{xi}|\psi_{yi}|\psi_{zi}]^T, \quad i = 1, 2, ..., n$. Let us now

write Ψ in terms of the Taylor's series expansion up to the 2-nd order, so we have

$$\psi_{k+1} \cong \psi_k + \triangle\rho_k^{\mathrm{T}}[\frac{\partial\Psi}{\partial\rho}]_k + \frac{1}{2}\triangle\rho_k^{\mathrm{T}}[\frac{\partial^2\Psi}{\partial\rho^2}]_k \triangle\rho_k \tag{4.11}$$

which yields to the iterative solution

$$\rho_{k+1} = \rho_k - J_k^{-1}\left[\psi_k + \frac{1}{2}\left(J_k^{-1}\psi_k\right)^{\mathrm{T}} H_k \left(J_k^{-1}\psi_k\right)\right] \tag{4.12}$$

or up to the 1-st order

$$\rho_{k+1} = \rho_k - \left(J_k^{\mathrm{T}} W J_k\right)^{-1} J_k^{\mathrm{T}} W \psi_k, \quad k = 1, 2, ..., n \tag{4.13}$$

where W is a weight matrix.

C. Example Problems and Results

The performance of the proposed technique was tried to compare with those of J_n and L_n and the classical method of Gauss. As mentioned in the forgoing, the estimated error will be expressed in terms of both orbit shape and attitude. Two cases were considered for validation, coplanar and non-coplanar. The observer was considered at a point with longitude and latitude of zero for the sake of simplicity and all cases are ground-based. A random orbit generator was employed to produced different for obits for the analysis. To simulate the real world data, the ideal measured lines-of-sights were corrupted with Gaussian noise at the level of $3\sigma = 10''$. The number of observations used was $N_{obs} = 7$ with two different time intervals, $\Delta t = 50$ s and $\Delta t = 80$ s. We refer to our new technique as P_n (Prescribed Orbits). The index n denotes the number of observations, so, for instance, P_7 means the Prescribed Orbits method using seven observations. A 5-th order polynomial was used in the proposed algorithm for the sake of this study.

1. *LEO Satellite: coplanar orbits* In this case, the Monte Carlo analysis was performed using 2182 different coplanar scenarios with the eccentricity ranging from 0 to 0.2. The minimum and maximum semi-major axis are 6743.334 km and 9602.719 km respectively. The number of observations of seven with two different time intervals $\Delta t = 50$s and $\Delta t = 80$s were considered for this case. Since Gauss' method shows singularity for coplanar cases, so the three methods of P_7, J_n, and L_n were used for this analysis. The results are presented in terms of orbit shape error d and the angle between the angular momentum vectors θ. Figures 8 through 10 show the histograms of the orbit shape error d and angular momentum vector error θ using P_n, J_n, and L_n for $\Delta t = 50$ s respectively. Figures 11 through 13 are the same plots as the first three, but for $\Delta = 80$s. As can be seen, all three methods yielded very good orbit shape and orientation estimations. The current technique showed much better estimation of the orbit shape as the time interval Δt increased , whereas J_n and L_n exhibited more accurate orientation estimation (in the order of 0.001 deg) as the time interval increases. The orientation error offered by P_n is in the order of 0.01 deg.

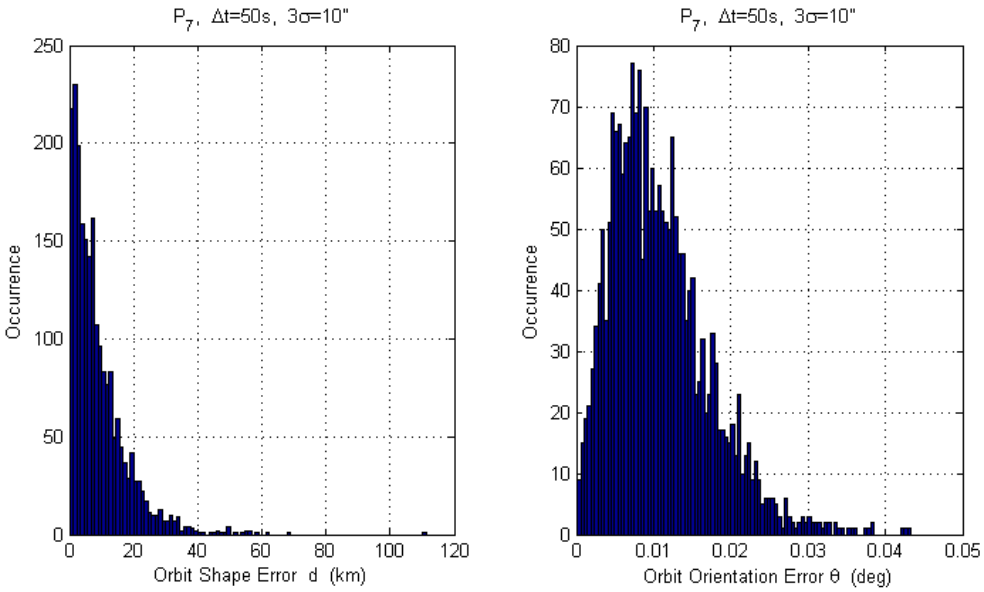

Fig. 8. Orbit Shape and Orientation (Angular momentum) Error Using P_7, Scenarios=2182

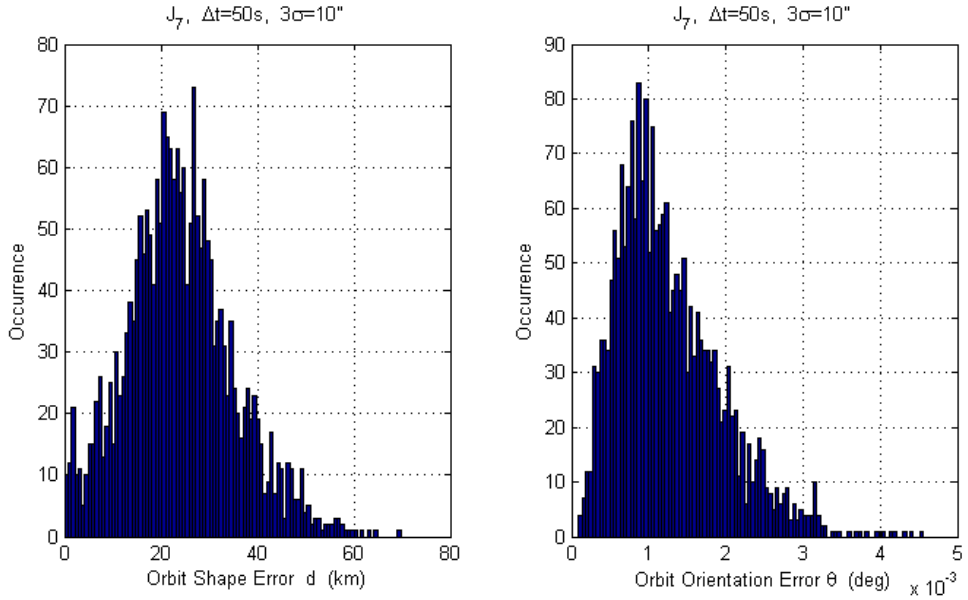

Fig. 9. Orbit Shape and Orientation (Angular Momentum) Error Using J_7, Scenarios=2182

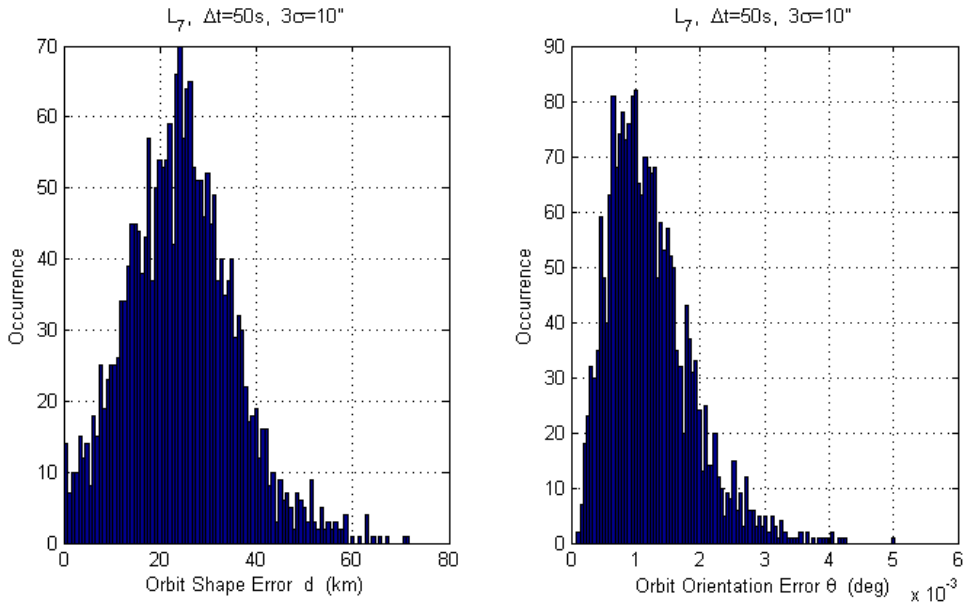

Fig. 10. Orbit Shape and Orientation (Angular Momentum) Error Using L_7, Scenarios=2182

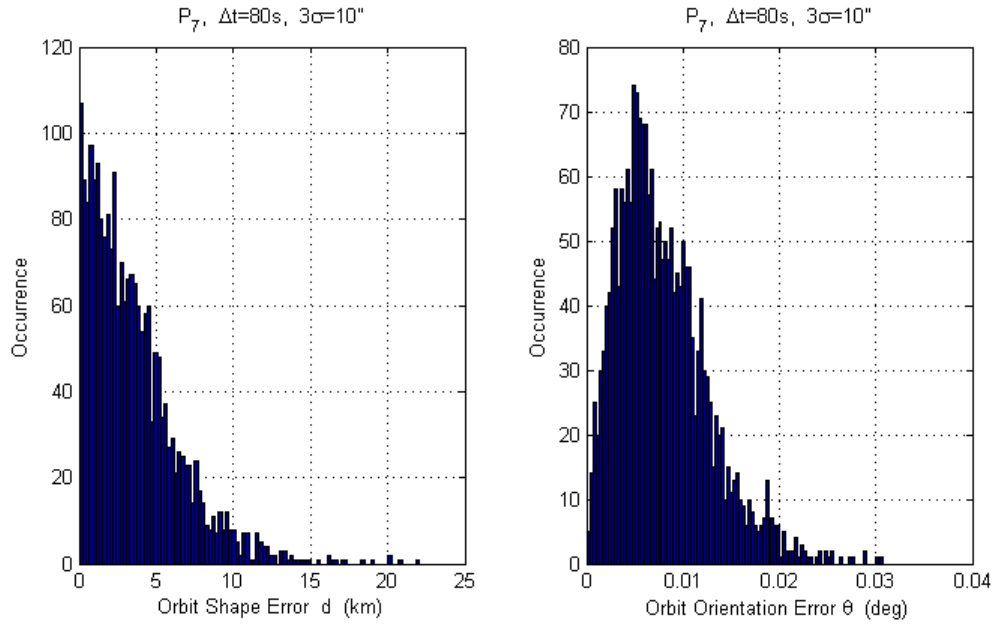

Fig. 11. Orbit Shape and Orientation (Angular Momentum) Error Using P_7, Scenarios=2182

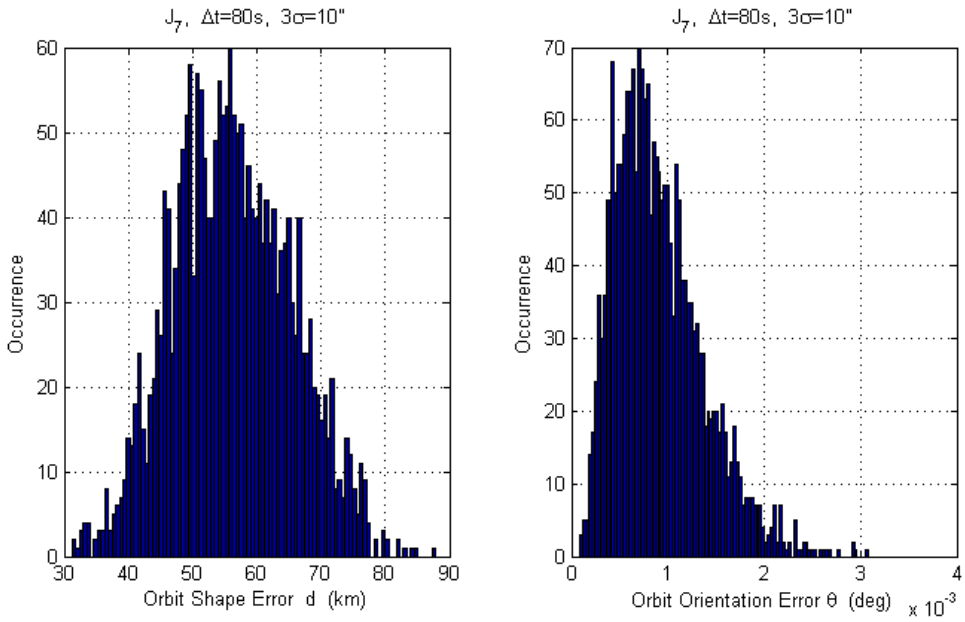

Fig. 12. Orbit Shape and Orientation (Angular Momentum) Error Using J_7, Scenarios=2182

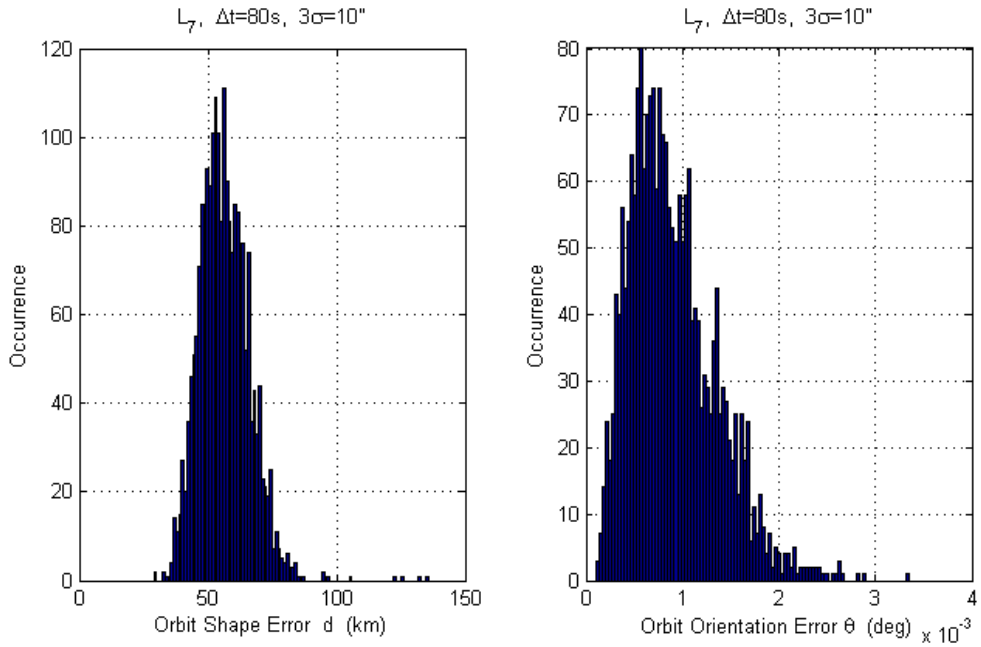

Fig. 13. Orbit Shape and Orientation (Angular Momentum) Error Using L_7,Scenarios=2182

2. *LEO Satellite: non-coplanar orbits* In this case, the Monte Carlo analysis was performed using 2336 different non-coplanar scenarios with the eccentricity ranging from 0 to 0.2 and inclination from 5° to 90°. The minimum and maximum semi-major axis are 6732.241 km and 9634.102 km respectively. The number of observations of seven with two different time intervals $\Delta t = 50$s and $\Delta t = 80$s were considered for this case. The methods P_n,L_n do not require any specific initial guess and basically can operate with any values(P_n shows extreme robustness with respect to initial guess and L_n algorithm can be initiated with the value of zero for a fair number of scenarios) and *Gauss* does not have an iterative nature. Hereby; these three *not required initial guess* IOD methods were used for the non-coplanar scenarios. Results are presented in terms of orbit shape and attitude *phi* error. Figures 14 through 16 depict the histograms of the orbit shape error d and attitude error ϕ using P_n, L_n, and *Gauss* for $\Delta t = 50$s respectively. Figures 17 through 19 are the same plots as the first three, but for $\Delta = 80$s. As can be seen, P_n has the highest accuracy in the orbit shape and attitude estimation. P_n shows more concentration of attitude error towards the point of zero degree for larger time interval ($\Delta t = 80$s), while L_n and *Gauss* become more distributed from zero to 0.5°. The histogram of the attitude error ϕ was plotted up to 0.5°. For $\Delta t = 50$s, the scenarios of 2147, 2214, and 1974 (out of 2336) were used by P_n, L_n, and *Gauss* respectively and for $\Delta t = 80$s, the scenarios are 2201, 1939, and 1813 (out of 2336). The best and worst orbit shape estimation belong to P_7 and *Gauss* ($\Delta t = 80$s) respectively.

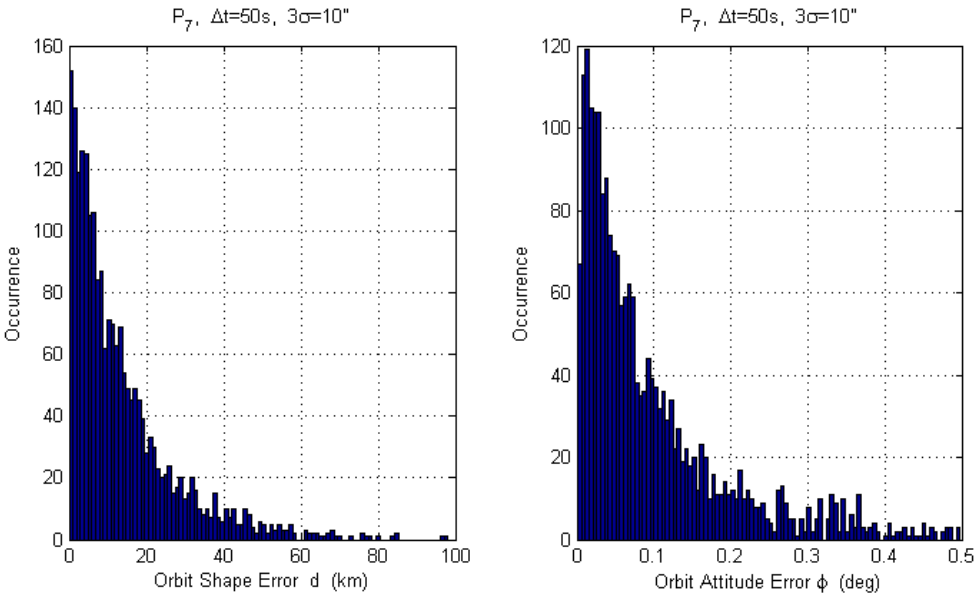

Fig. 14. Orbit Shape and Attitude Error Using P_7, Scenarios=2147 out of 2336

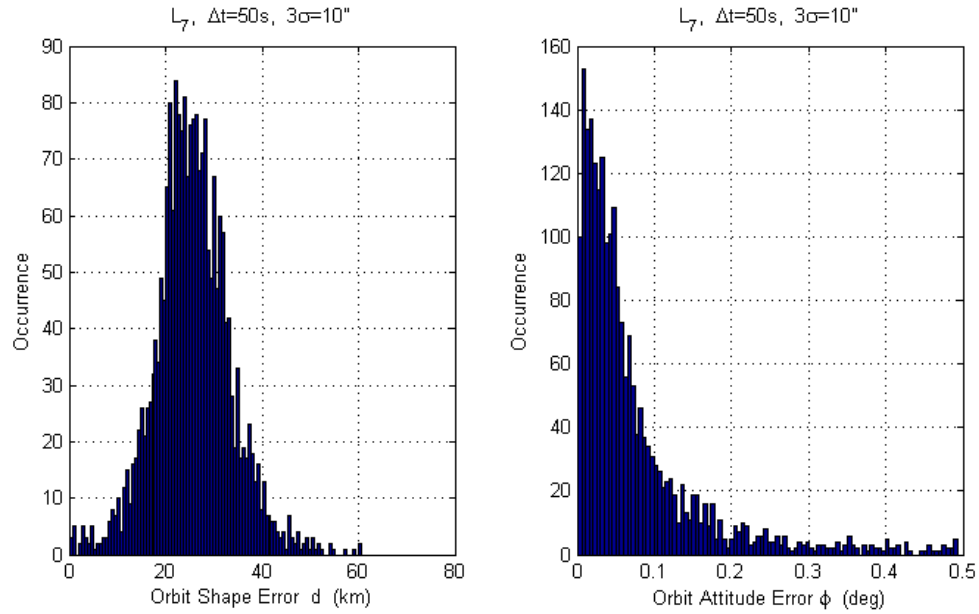

Fig. 15. Orbit Shape and Attitude Error Using L_7, Scenarios=2214 out of 2336

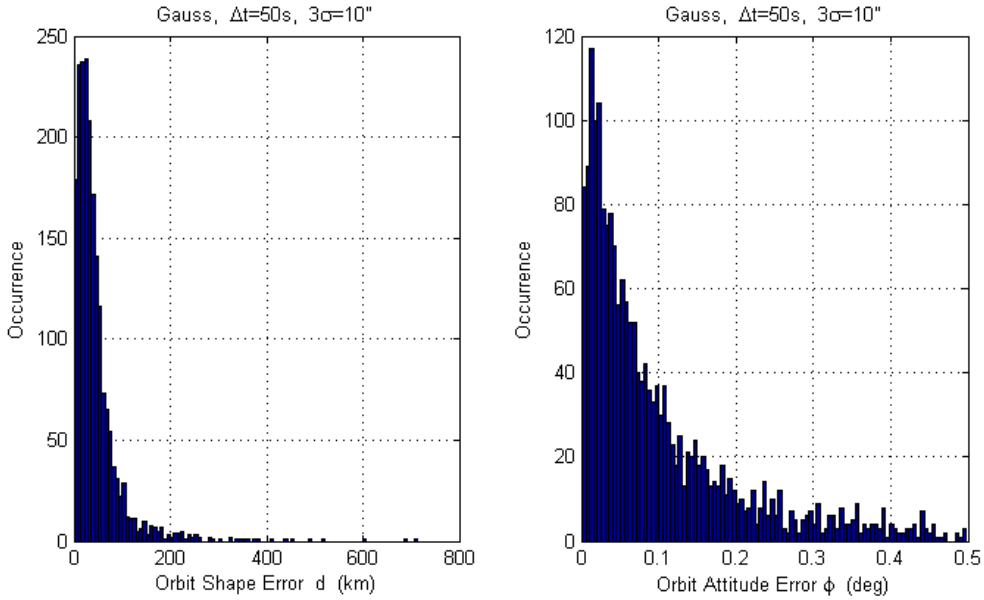

Fig. 16. Orbit Shape and Attitude Error Using Gauss Method, Scenarios=1974 out of 2336

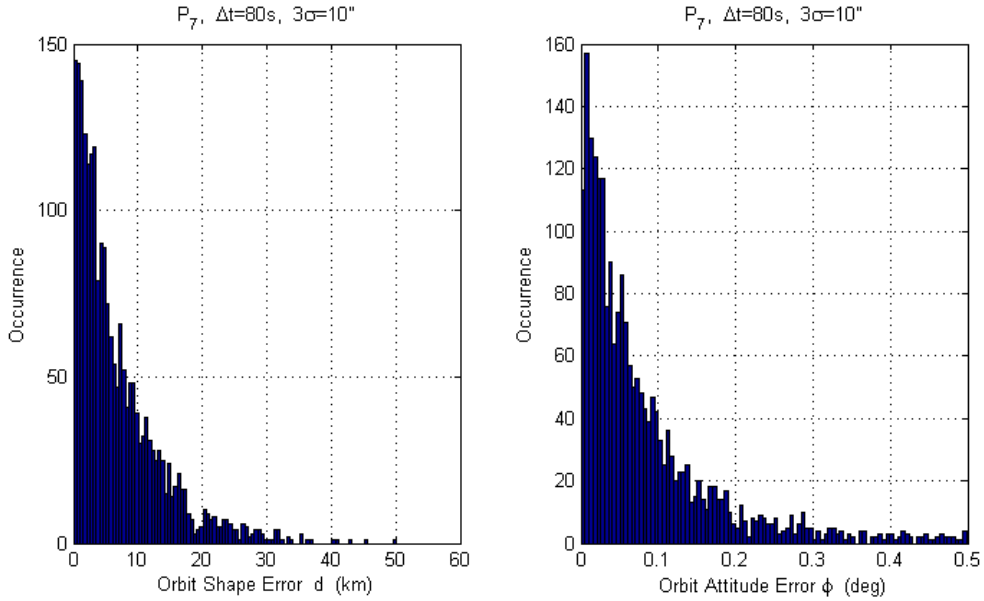

Fig. 17. Orbit Shape and Attitude Error Using P_7, Scenarios=2201 out of 2336

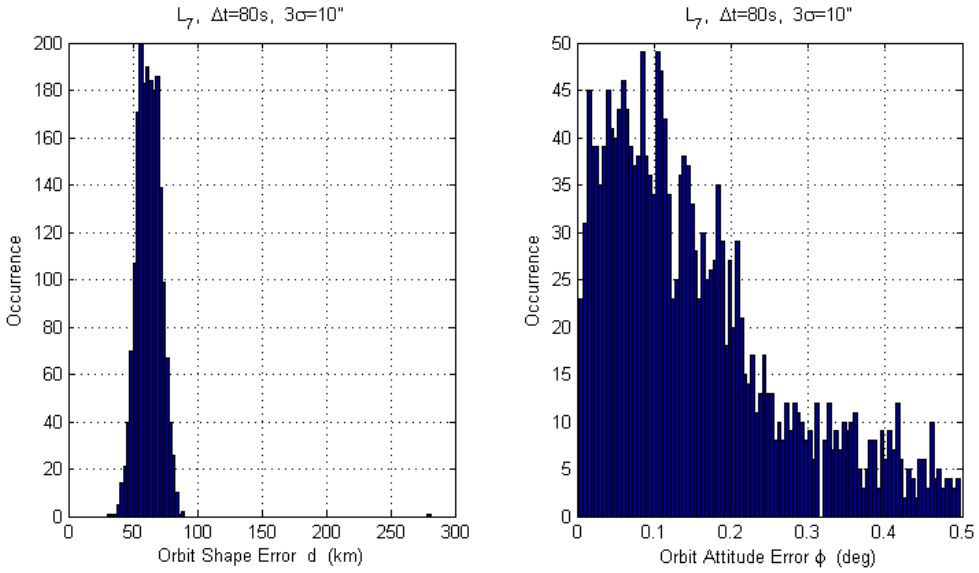

Fig. 18. Orbit Shape and Attitude Error Using L_7, Scenarios=1939 out of 2336

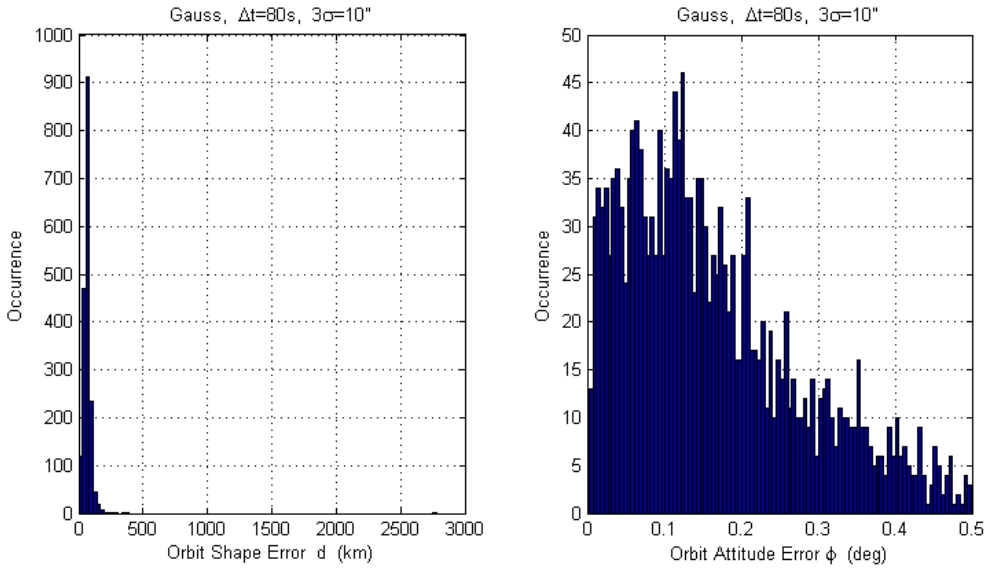

Fig. 19. Orbit Shape and Attitude Error Using Gauss Method, Scenarios=1813 out of 2336

D. Conclusion

A novel technique of IOD based on a prescribed orbit was successfully developed and tested. The method uses an assumed approximated solution as the solution to the Keplerian two-body problem. This solution also needs to satisfy the geometry of the problem. So combining these two facts construct the foundation of the propose technique. Any function which can represent the behavior of an orbit can be used, but as the first phase of the work and for the sake of simplicity, a 5-th order polynomial was used and showed promising performance. The performance of the developed technique was tested versus those of J_n and L_n and classical IOD method of Gauss. The estimated errors were presented in two ways: 1) orbit shape and 2) orbit attitude. Also two different cases namely coplanar and non-coplanar were considered. The Monte Carlo simulations were performed for 2182 and 2336 different coplanar and non-coplanar scenarios respectively. The results showed the superiority of proposed technique over *Gauss*, J_n and L_n. The methods P_n, J_n, and L_n use multiple observations and are sensitive to the combinations of the number of observations and time interval, while these two parameters were kept constant during the Monte Carlo simulation. P_n demonstrated that it was able to bypass the drawbacks associated with Gauss, J_n and L_n. Gauss's shows singularity for coplanar cases and all three yield less accuracy when the time interval Δt increases, whereas P_n exhibited higher accuracy with larger time intervals. P_7 and Gauss ($\Delta t = 80$s) presented the best and worst orbit shape and attitude estimation respectively.

CHAPTER V

INITIAL ORBIT DETERMINATION BASED ON VARIATION OF ORBITAL ERROR

A novel technique of angles-only initial initial orbit determination based on variations of orbital error is presented for the case of Keplerian orbit.

A. Introduction

Several angles-only initial orbit determination techniques have been developed and modified in this current work. The main attempt was to determine the unknown spacecraft ranges leading to spacecraft position and velocity vectors and, consequently, orbital elements estimation. The classical and newly developed angles-only IOD method are following almost the same trend and they all try to estimate position and velocity vectors. The initial orbit determination methods of Gauss and Laplace , Herget , Double r-iteration , and Gooding all fall into in this category. The proposed technique takes advantage of the fact that the parameters defining the orbit shape and orientation are constant at any time. Therefore, the basis of the new algorithm is that the residual of (difference between) the estimated orbit shape and orientation for different measurements (line-of-sights) at different times should be minimum with respect to the unknown ranges. Once the set of the algebraic equations is solved, the orbital elements along with the spacecraft position and velocity vectors are determined all together. This method is also capable of using multiple observations and can handle the co-planar orbit determination scenarios, cases in which the measured line-of-sights lie on the spacecraft orbit plane. To validate the proposed algorithm, Monte Carlo analysis were performed for some specific cases. The estimation accuracy is quantified by shape and orientation orbit errors and also the position and

velocity relative percentage error. In the next section, the methodology of the new orbit estimator is presented. At the end, quantitative and qualitative analysis are performed for validation and the results from the new technique will be compared to those of Laplace and Gauss methods of initial orbit determination. Since the time intervals between subsequent measurements are small with respect to the orbital period, all the mentioned methods, included the one presented in this paper, consider the orbit to estimate unperturbed, that is, Keplerian.

B. Methodology

Let us consider the geometry of a typical angle-only orbit determination problem defined by the following equation

$$\mathbf{r}_k = \mathbf{R}_k + \rho_k \, \hat{\boldsymbol{\rho}}_k, \qquad k = 1, 2, \cdots, n, \tag{5.1}$$

where $\mathbf{R}_k$ are the observer known position vectors, ρ_k the spacecraft unknown ranges, $\hat{\boldsymbol{\rho}}_k$ the line-of-sight unit-vectors (directions) measured at time t_1, t_2, $\cdots$, t_n, and $\mathbf{r}_k$ are the spacecraft unknown position vectors. The main idea of the algorithm is based on minimizing the orbit shape and orientation error. In the following subsection, the orbit error and the methodology based upon which the new technique was developed will be discussed. The algorithm first is described with three line-of-sights and then will be generalized to multiple observations.

1. Orbit Error

Let us consider the problem of describing the error between two different orbits, for instance, the error between the true orbit, characterized by the orbital elements $[a_t, e_t, \Omega_t, \omega_t, i_t, \varphi_t]$ and the estimated orbit, characterized by $[a_e, e_e, \Omega_e, \omega_e, i_e, \varphi_e]$,

where the six elements are, respectively, the semi-major axis, eccentricity, right ascension of the ascending node, argument of perigee, inclination, and true anomaly. The orbital parameters identifying the orbit in space can be suitably split in two independent sets. One set consisting of Ω, $\omega + \varphi$, and i, that identify the orientation of a rotating orbital reference frame $[\hat{\boldsymbol{r}}, \quad \hat{\boldsymbol{t}}, \quad \hat{\boldsymbol{h}}]$ with respect to the inertial reference frame. The axes of this orbital frame are identified by the radius direction $\hat{\boldsymbol{r}}$, the direction of the angular momentum $\hat{\boldsymbol{h}}$, and the third axis to form a right-handed frame $\hat{\boldsymbol{t}} = \hat{\boldsymbol{h}} \times \hat{\boldsymbol{r}}$. Therefore, the transformation matrix, C_{OI}, moving from inertial to the orbital reference frames can be written as

$$C_{OI} = R_3(\omega + \varphi)\, R_1(i)\, R_3(\Omega) = \left[\hat{\boldsymbol{r}}, \quad \hat{\boldsymbol{h}} \times \hat{\boldsymbol{r}}, \quad \hat{\boldsymbol{h}}\right]^{\mathrm{T}} \tag{5.2}$$

where R_1 and R_2 are the rotation matrices about the $\hat{\boldsymbol{x}}$ and $\hat{\boldsymbol{z}}$ coordinate axes, respectively.

Orientation Error. This error is identified by an angle δ that can be computed by the following relationship using the true, C_t, and the estimated, C_e, transformation matrices

$$\cos\delta = \frac{1}{2}\left[\mathrm{tr}(C_t C_e^{\mathrm{T}}) - 1\right] \tag{5.3}$$

From a mathematical point of view δ represents the principal angle of the corrective attitude matrix, $C_t C_e^{\mathrm{T}}$, between the two attitudes matrices, C_t and C_e. Specific error information can be easily derived from the orbit orientation error. These can be, a) the distance between estimated and true radii $|\mathbf{r}_t - \mathbf{r}_e|$ to capture the ability to estimate the spacecraft position, and b) the angle between estimated and true angular momentum directions, $\hat{\boldsymbol{h}}_t$ and $\hat{\boldsymbol{h}}_e$, to capture the ability to estimate the orbit plane orientation.

Shape Error. The orbit shape is identified using the semi-major and semi-minor

axes because they are (dimensionally) consistent parameters. Using these two orbit elements, the shape of an orbit can be identified as a point in the a-b plane. Thus the orbit shape error can be simply described by the distance d from estimated and true points in the a-b plane

$$d = \sqrt{(a_t - a_e)^2 + (b_t - b_e)^2} \tag{5.4}$$

Figure 20 shows how to combine shape and orientation errors into a single descriptor, the *orbit error*, which can be represented as a complex number. In fact, the error associated with the estimated orbit shape and attitude can be expressed as a point on the complex plane where the perpendicular distance between the point and a circle with a constant radius (d^*, whose value can be set as the expectation of the orbit semi-major axis) represents the shape error and the angle between the complex point direction and the real axis represents the attitude error. For more details on the orbit error, see [32].

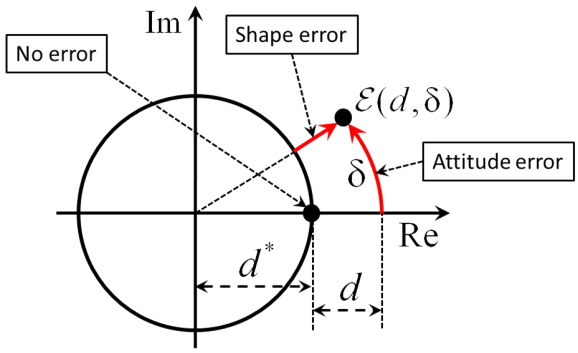

Fig. 20. Orbit Error Definition as a Complex Number

The orbital elements are all functions of the position and velocity vector, so and before constructing the residuals based on orbit shape and orientation error, expressions for position and velocity vectors should be available. These vectors are

simply given using the Lagrange interpolation polynomials. For the position vector we have

$$\mathbf{r}(t) = \ell_1(t)\,\mathbf{r}_1 + \ell_2(t)\,\mathbf{r}_2 + \ell_3(t)\,\mathbf{r}_3 \tag{5.5}$$

where the $\ell_i(t)$ coefficients are the Lagrange interpolation polynomials

$$\ell_i(t) = \prod_{k \neq i} \frac{t - t_k}{t_i - t_k}, \qquad i = 1, 2, \cdots, 3 \tag{5.6}$$

while for the velocity vector we have

$$\mathbf{v}(t) = \dot{\mathbf{r}}(t) = \dot{\ell}_1(t)\,\mathbf{r}_1 + \dot{\ell}_2(t)\,\mathbf{r}_2 + \dot{\ell}_3(t)\,\mathbf{r}_3 \tag{5.7}$$

Equations (5.5) and (5.7) provide position and velocity vectors in terms of the unknown ranges ρ_k, $k = 1, 2, 3$.

a. Residuals Based on Orbit Orientation Error.

The orbit orientation at the mid-range $t = t_2$ (out of three observations) can now be defined as

$$\begin{cases} \cos\delta_{21} = \dfrac{1}{2}\,[\mathrm{tr}(C_{21}^{\mathrm{T}} C_2) - 1] \\ \cos\delta_{23} = \dfrac{1}{2}\,[\mathrm{tr}(C_{23}^{\mathrm{T}} C_2) - 1] \end{cases} \tag{5.8}$$

where C_2 is the orbit orientation at $t = t_2$, C_{21} and C_{23} are the orbit orientations at t_2 obtained by propagating and back-propagating to t_2 from times t_1 and t_3, respectively. The angles δ_{21} and δ_{23} are the orientation errors. Let us know rewrite the orientation matrices in terms of position and angular momentum vectors as in Eq. (5.9)

$$\begin{cases} C_{21} = \left[\hat{\boldsymbol{r}}_{21}, \quad \hat{\boldsymbol{h}}_{21} \times \hat{\boldsymbol{r}}_{21}, \quad \hat{\boldsymbol{h}}_{21}\right]^{\mathrm{T}} \\ C_{23} = \left[\hat{\boldsymbol{r}}_{23}, \quad \hat{\boldsymbol{h}}_{23} \times \hat{\boldsymbol{r}}_{23}, \quad \hat{\boldsymbol{h}}_{23}\right]^{\mathrm{T}} \\ C_{2} = \left[\hat{\boldsymbol{r}}_{2}, \quad \hat{\boldsymbol{h}}_{2} \times \hat{\boldsymbol{r}}_{2}, \quad \hat{\boldsymbol{h}}_{2}\right]^{\mathrm{T}} \end{cases} \tag{5.9}$$

where $\hat{\boldsymbol{r}}_{21}$ and $\hat{\boldsymbol{r}}_{23}$ are the position vector directions propagated and back-propagated to t_2 from t_1 and t_3, respectively. We know that the orientation error angles (δ_{21} and δ_{23}) ideally should be zero resulting in the left hand side of Eq. (5.8) to be one; hence

$$\begin{cases} \mathrm{tr}(C_{21}^{\mathrm{T}} C_2) = 3 \\ \mathrm{tr}(C_{21}^{\mathrm{T}} C_2) = 3 \end{cases} \tag{5.10}$$

Let us now expand Eq. (5.10) in terms of the components of the orientation matrices C_2, C_{21}, and C_{23}, so we have

$$\begin{cases} \hat{\boldsymbol{r}}_{21} \cdot \hat{\boldsymbol{r}}_2 + \hat{\boldsymbol{t}}_{21} \cdot \hat{\boldsymbol{t}}_2 + \hat{\boldsymbol{h}}_{21} \cdot \hat{\boldsymbol{h}}_2 = 3 \\ \hat{\boldsymbol{r}}_{23} \cdot \hat{\boldsymbol{r}}_2 + \hat{\boldsymbol{t}}_{23} \cdot \hat{\boldsymbol{t}}_2 + \hat{\boldsymbol{h}}_{23} \cdot \hat{\boldsymbol{h}}_2 = 3 \end{cases} \tag{5.11}$$

Equation (5.10) implies that to have the minimum orbit orientation error, the value of each term in the parenthesis should be equal to one which makes perfect sense as the error in minimum when $\hat{\boldsymbol{r}}_{21}$, $\hat{\boldsymbol{r}}_{23}$, $\hat{\boldsymbol{h}}_{21}$, and $\hat{\boldsymbol{h}}_{23}$ directions are pointing, respectively, to the $\hat{\boldsymbol{r}}_2$, $\hat{\boldsymbol{r}}_2$, $\hat{\boldsymbol{h}}_2$, and $\hat{\boldsymbol{h}}_2$ directions. The terms involving $\hat{\boldsymbol{t}}$ are redundant as $\hat{\boldsymbol{t}}$ is achieved from the cross product of $\hat{\boldsymbol{h}}$ and $\hat{\boldsymbol{r}}$. So, now the residual associated with the orbit orientation error can be constructed as

$$\begin{cases} \boldsymbol{\psi}_r = \sigma_r^{-1}(\mathbf{r}_{21} - \mathbf{r}_2) \\ \boldsymbol{\psi}_h = \sigma_h^{-1}(\mathbf{h}_{21} - \mathbf{h}_2) \end{cases} \tag{5.12}$$

or as another set of the residual

$$\begin{cases} \boldsymbol{\psi}_r = \sigma_r^{-1}(\mathbf{r}_{23} - \mathbf{r}_2) \\ \boldsymbol{\psi}_h = \sigma_h^{-1}(\mathbf{h}_{23} - \mathbf{h}_2) \end{cases} \tag{5.13}$$

The expressions for $\mathbf{r}_{21}$ and $\mathbf{h}_{21}$ in the first residual set (same trend for the second set of residual) are obtained by propagating the initial position and velocity vectors

$t = t_1$ to $t = t_2$ as

$$\begin{cases} \mathbf{r}_{21} = f_1\mathbf{r}_1 + g_1\mathbf{v}_1 \\ \mathbf{h}_{21} = \mathbf{r}_{21} \times \mathbf{v}_{21} = (f_1\mathbf{r}_1 + g_1\mathbf{v}_1) \times (\dot{f}_1\mathbf{r}_1 + \dot{g}_1\mathbf{v}_1) \end{cases} \tag{5.14}$$

where f, g, $\dot{f}$, and $\dot{g}$ are the Lagrange functions and their respective time derivatives. For small time interval between the measurements (with respect to the orbit error), the Lagrange functions are

$$\begin{cases} f_1 \approx 1 - \dfrac{\mu}{2r_1^3}\triangle t^2 \\ g_1 \approx -\triangle t + \dfrac{\mu}{6\,r_1^3}\triangle t^3 \end{cases} \tag{5.15}$$

where Δt is the time interval between the measured line-of-sights and μ is the gravitational constant. The angular momentum $\mathbf{h}_{21}$ can be expanded as

$$\mathbf{h}_{21} = (f_1\dot{g}_1 - \dot{f}_1 g_1)\mathbf{h}_1 \tag{5.16}$$

In a Keplerian's Two-body problem, the term $f_1\dot{g}_1 - \dot{f}_1 g_1$ is equal to one, so $\mathbf{h}_{21}$ becomes $\mathbf{h}_1$. The residual for the orbit orientation error can be expressed in the following form

$$\begin{cases} \boldsymbol{\psi}_r = \sigma_r^{-1}[(f_1\mathbf{r}_1 + g_1\mathbf{v}_1) - \mathbf{r}_2] \\ \boldsymbol{\psi}_h = \sigma_h^{-1}(\mathbf{h}_1 - \mathbf{h}_2) \end{cases} \tag{5.17}$$

Note that the second equation of Eq. (5.17) is simply the conservation of angular momentum.

b. Residuals Based on Orbit Shape Error

The orbit shape error can be defined as in Eq. (5.4) or simply in a residual force as

$$\begin{cases} \psi_a = \sigma_a^{-1}(a_1 - a_2) \\ \psi_e = \sigma_e^{-1}(e_1 - e_2) \end{cases} \tag{5.18}$$

or as another set of residuals

$$\begin{cases} \psi_a = \sigma_a^{-1}(a_3 - a_2) \\ \psi_e = \sigma_e^{-1}(e_3 - e_2) \end{cases} \tag{5.19}$$

Now we can define the whole set of residuals containing both orbit shape and orbit orientation error as

$$\boldsymbol{\psi} = \begin{Bmatrix} \boldsymbol{\psi}_r \\ \boldsymbol{\psi}_h \\ \psi_a \\ \psi_e \end{Bmatrix}_{8\times 1} \tag{5.20}$$

Writing Taylor's series expansion

$$\boldsymbol{\psi}_{j+1} \cong \boldsymbol{\psi}_j + \left[\frac{\partial \boldsymbol{\psi}}{\partial \boldsymbol{\rho}}\right]_j \triangle \boldsymbol{\rho}_j + H.O.T. \tag{5.21}$$

and the optimal solution can be written as

$$\triangle \boldsymbol{\rho}_j = -J_j^{\dagger}\, \boldsymbol{\psi}_j \tag{5.22}$$

where index j denotes the j-th iteration. The solution in the update form

$$\boldsymbol{\rho}_{j+1} = \boldsymbol{\rho}_j - J_j^{\dagger}\, \boldsymbol{\psi}_j \tag{5.23}$$

and since J is not necessarily square, its pseudo inverse $J^{\dagger}$ is obtained using Moore-Penrose rule as

$$J^{\dagger} = (J^{\mathrm{T}} J)^{-1}\, J^{\mathrm{T}} \tag{5.24}$$

which leads to the final update form of

$$\boldsymbol{\rho}_{j+1} = \boldsymbol{\rho}_j - (J_j^{\mathrm{T}} W J_j)^{-1}\, J_j^{\mathrm{T}}\, W \boldsymbol{\psi}_j, \quad j = 1, 2, ..., n \tag{5.25}$$

where W is a weight matrix. This algorithm has iterative nature, so an initial guess

is required to start the process. The iteration is performed until $\Delta\rho_j < \varepsilon$ where ε is some predefined tolerance. Note that residual vector $\boldsymbol{\psi}$ is only a function of the unknown range ρ_j, $j = 1, 2, 3$ as the semi-major axis a, eccentricity e, and angular momentum $\mathbf{h}$ are all functions of position $\mathbf{r}$ and velocity $\mathbf{v}$ vectors and the velocity vector is also can be expressed in terms of the unknown ranges ρ_j, $j = 1, 2, 3$ according to Eq. (5.7). So, the Jacobian J is just a function of ρ_j.

The authors refer to the new technique as V_n where "V" stands for "*variation*" as the method is based on the variation of orbital error and n is the number of observations used for the initial orbit determination (e.g. V_3, uses three observations).

C. Generalizing to Multiple Observations

This technique was originally developed with three observations, but it can easily be generalized to multiple observations for enhanced performance and accuracy. Also, for the coplanar orbit determination scenarios (it is when the measured line-of-sights lie on the orbit plane), the classical and some of the newly developed initial orbit determination methods show singularities. One remedy to bypass this draw back is using one more observation. Consider that we have multiple n observations available. The residuals (both orbit shape and orbit orientation) of each three observations can be put in the form of Eq. (5.24), so for n measurements we have

$$\boldsymbol{\psi} = \left\{\boldsymbol{\psi}_{r_1}^{\mathrm{T}}, \boldsymbol{\psi}_{h_1}^{\mathrm{T}}, \psi_{a_1}, \psi_{e_1}, \boldsymbol{\psi}_{r_2}^{\mathrm{T}}, \boldsymbol{\psi}_{h_2}^{\mathrm{T}}, \psi_{a_2}, \psi_{e_2}, \cdots, \boldsymbol{\psi}_{r_n}^{\mathrm{T}}, \boldsymbol{\psi}_{h_n}^{\mathrm{T}}, \psi_{a_n}, \psi_{e_n}\right\}^{\mathrm{T}} \tag{5.26}$$

where the vector $\boldsymbol{\psi}$ contains $8(n-2)$ elements. The solution, ρ_k, $k = 1, 2, \cdots, n$, should be able to minimize the the residual ψ in Eq. (5.26). The rest of the procedure is identical to that of three observations, Eq. (5.21) through (5.25). Note that the

Jacobian matrix J is defined as

$$J_{8(n-2)\times n} = \left[\frac{\partial \boldsymbol{\psi}_i}{\partial \boldsymbol{\rho}_j}\right], \quad i = 1, 2, \cdots, 8(n-2), \quad j = 1, 2, \cdots, n \tag{5.27}$$

As seen in the forgoing, for three observations derivations, the velocity vectors were approximated using Lagrange Interpolation Polynomials. As the number of observations increases, working with the Lagrange Interpolation polynomials gets more complex and ineffective. To by pass this drawback, the least square scheme was employed for velocity vector approximations which leads to more simplicity and of course more accuracy. To this end, consider that the position vector components (simply x, y, and z) can be approximated using the following N-th polynomials

$$\begin{cases} p_x(t) = a_1 + a_2 t + a_3 t^2 + \cdots + a_{N+1} t^N \\ p_y(t) = b_1 + b_2 t + b_3 t^2 + \cdots + b_{N+1} t^N \\ p_z(t) = c_1 + c_2 t + c_3 t^2 + \cdots + c_{N+1} t^N \end{cases} \tag{5.28}$$

and consequently the velocity vector component can be approximately determined as

$$\begin{cases} V_x(t) = \dot{p}_x = a_2 + a_3 t + a_4 t^2 + \cdots + a_{N+1} t^{N-1} \\ V_y(t) = \dot{p}_y = b_2 + b_3 t + b_4 t^2 + \cdots + b_{N+1} t^{N-1} \\ V_z(t) = \dot{p}_z = c_2 + c_3 t + c_4 t^2 + \cdots + c_{N+1} t^{N-1} \end{cases} \tag{5.29}$$

For more details regarding how to implement the least square to obtain the velocity vectors in terms of the unknown ranges, see [30]. In practice, not the full length residual vector $\boldsymbol{\psi}$ is required to find the optimum solution. As a matter of fact, since as the number of observations increases, the size of the residual vector grows much faster, using the full length vector would result in convergence instability. So using a portion of the residual vector not only yields more robustness and higher accuracy, but less CPU time.

D. Selected Test Scenarios and Results

The validation of the developed technique was tested through several different scenarios. All the observations were made from a ground-based site located at a point of zero longitude and zero latitude for the sake of simplicity. To simulate the real data, the ideal measured data were corrupted with Gaussian noise with standard deviation of $3\sigma = 10''$. To test the performance of the presented algorithms, Monte Carlo analysis was conducted using 441 non-coplanar and 438 coplanar Low Earth Orbit (LEO) different scenarios. A random orbit generator was used for the purpose. For the non-coplanar cases, the orbits have the eccentricity ranging from 0 to 0.2, inclination ranging from 5° to 90°, and semi-major axis ranging from 6,786.352 km to 9,424.253 km. The coplanar scenarios have the eccentricity ranging from 0 to 0.2 and semi-major axis ranging from 6,746.727 km to 9,731.184 km. Qualitative and quantitative analysis was performed to have a better understanding of the performance of the developed algorithm. For the Monte Carlo analysis, three different time intervals were considered for both coplanar (Δt = 60, 80, 100 s) and non-coplanar (Δt = 120, 150, 180 s) cases. For the non-coplanar, the estimated a and b with relative percentage error up to 0.25% (defined as $100 \times |true - estimated|/true$) and δ (principal angle of the corrective matrix-error) up to 0.05° were collected as acceptable performance. For the coplanar, the estimated a and b with relative percentage error up to 0.5% and θ (angle between the angular momentum vectors) up to 0.05° were collected as acceptable performance. The results from V_n were compared to that of the classical methods of Gauss and Laplace. Tables XIV and XV present the results of the Monte Carlo analysis. For the Monte Carlo analysis, the number of occurrences and corresponding percentage meeting the requirements are presented. The method V_n is rather robust with respect to the initial guess as this technique is

iterative and works very well with the initial guess ranging from zero to the values close to the true solution.

Table XIV. Monte Carlo Analysis for 441 Non-coplanar LEO Scenarios ($3\sigma = 10''$), $a_{error} < 0.25\%$, $b_{error} < 0.25\%$, and $\delta < 0.05°$

Algorithm	$\Delta t = 60$ s	$\Delta t = 80$ s	$\Delta t = 100$ s
Laplace	0 (0%)	0 (0%)	0 (0%)
Gauss	110 (24.9%)	19 (4.3%)	7 (1.6%)
V_3	21 (4.8%)	4 (0.9%)2	0 (0%)
V_5	173 (39.2%)	188 (42.6%)	139 (31.5%)
V_7	232 (52.6%)	300 (68%)	165 (37.4%)

Table XV. Monte Carlo Analysis for 438 Coplanar LEO Scenarios ($3\sigma = 10''$), $a_{error} < 0.5\%$, $b_{error} < 0.5\%$, and $\theta < 0.05°$

Algorithm	$\Delta t = 120$ s	$\Delta t = 150$ s	$\Delta t = 180$ s
V_7	158 (36.1%)	286 (65.3%)	265 (60.5%)
V_8	179 (40.9%)	342 (78.1%)	266 (60.7%)

As can be seen, for the non-coplanar cases, Laplace, Gauss, and V_3 were not successful meeting the requirement of $a_{error} < 0.25\%$, $b_{error} < 0.25\%$, and $\delta < 0.05°$. But as the number of observations is increases, V_n starts performing acceptable results (e.g. V_7 yields 300 occurrences out of 441 scenarios with $\Delta t = 80$ s). Laplace failed in all scenarios(it is not suitable for LEO IOD problems) and Gauss showed its best performance for the smallest time interval $\Delta t = 60$ s. V_n exhibits different performances depending upon the number of observations and time intervals. For comparatively small time intervals $\Delta t = 60$ s, the performance is more affected by the level of the noise, but as the time interval increases to a point $\Delta t = 80$ s, the

results accuracy improves as the measured data are less affected by the level of noise, but for larger time intervals $\Delta t = 100$ s, the performance drops again regardless of the level of the noise involved as the velocity approximation accuracy decreases. So, there is an optimum combination of number of observation and time intervals. For coplanar scenarios, Laplace, Gauss, and V_3 failed. Coplanar cases are sensitive to the level of noise involved in the measurements, so a larger time interval is required compared to the case of non-coplanar. As can be seen from Table XV, the result id achieved with V_8 and $\Delta t = 150$s. As the time interval decreases, the data get more affected by the noise and as it increases, the velocity approximation accuracy drops, so like for the non-coplanar cases, there is an optimum combination of number of observations and time interval. Apart from this qualitative analysis, we also were interested in testing some specific scenarios as quantitative comparison. So, one random case was considered for each non-coplanar and coplanar with the level of noise of $3\sigma = 10''$. The orbital elements of the non-coplanar and coplanar scenarios are presented in Table XVI.

Table XVI. Orbital Elements for a Single Random Scenario

Scenario	a	e	i	Ω	ω	φ
	km	[-]	(deg)	(deg)	(deg)	(deg)
Non-coplanar	7,800.0	0.1	45	345	15	0
Coplanar	7,800.0	0.1	0	0	0	0

Tables XVII, XVIII, and XIX present the semi-major axis, semi-minor axis relative percentage errors (orbit shape error), attitude error matrix principal angle (orbit orientation error), position and velocity relative percentage errors for the non-coplanar single case with $\Delta t = 60, 80, 100$ s.

As can be seen, the best performance is yielded by V_7 with $\Delta t = 60$ s and as

Table XVII. Performance Comparison for One Non-coplanar Single Scenario ($3\sigma = 10''$), $\Delta t = 60$ s

Algorithm	$a_{error}(\%)$	$b_{error}(\%)$	δ (deg)	$r_{error}(\%)$	$V_{error}(\%)$
Laplace	4	3.6	0.2	0.38	1.47
Gauss	0.26	0.25	0.013	0.025	0.1
V_3	0.3	0.27	0.16	0.003	0.36
V_6	0.12	0.11	0.005	0.01	0.046
V_7	0.04	0.039	0.0018	0.0035	0.016

Table XVIII. Performance Comparison for One Non-coplanar Single Scenario ($3\sigma = 10''$), $\Delta t = 80$s

Algorithm	$a_{error}(\%)$	$b_{error}(\%)$	δ (deg)	$r_{error}(\%)$	$V_{error}(\%)$
Laplace	7.5	6.6	0.3	0.6	2.65
Gauss	0.5	0.46	0.025	0.05	0.2
V_3	0.5	0.46	0.2	0.004	0.36
V_6	0.2	0.19	0.008	0.016	0.078
V_7	0.12	0.11	0.005	0.0096	0.048

the time interval increases, the accuracy of V_n drops due to the fact that the velocity approximation accuracy decreases. Tables XX and XXI present the semi-major axis, semi-minor axis relative percentage errors (orbit shape error), angle between the estimated and true angular momentum, position and velocity relative percentage errors for the non-coplanar single case with $\Delta t = 150, 180$ s.

Laplace, Gauss, and V_3 failed for the coplanar and the acceptable results are obtained using V_8 with $\Delta t = 150$ s. As the time interval increases, the estimation accuracy drops as the velocity approximation loses accuracy.

Table XIX. Performance Comparison for One Non-coplanar Single Scenario ($3\sigma = 10''$), $\Delta t = 100$ s

Algorithm	$a_{error}(\%)$	$b_{error}(\%)$	δ (deg)	$r_{error}(\%)$	$V_{error}(\%)$
Laplace	11.9	10.3	0.5	0.8	4
Gauss	0.86	0.78	0.045	0.088	0.32
V_3	0.77	0.7	0.27	0.015	0.65
V_6	0.15	0.14	0.0062	0.012	0.056
V_7	0.28	0.23	0.001	0.02	0.094

Table XX. Performance Comparison for One Coplanar Single Scenario ($3\sigma = 10''$), $\Delta t = 150$ s

Algorithm	$a_{error}(\%)$	$b_{error}(\%)$	θ (deg)	$r_{error}(\%)$	$V_{error}(\%)$
V_7	0.31	0.28	0.001	0.008	0.12
V_8	0.2	0.19	0.001	0.003	0.097

E. Conclusions

A novel technique of initial orbit determination based on the variation of orbital error was developed and tested. The main idea of the method is based on the fact that, for Keplerian orbits, the orbital elements, defining the orbital error, should remain constant at any time. Different Monte Carlo analysis for both non-coplanar and coplanar Low Earth Orbit scenarios were performed as a qualitative analysis with various time intervals between the measurements. Also one single specific scenarios for each non-coplanar and coplanar were tested as a quantitative analysis. The estimated errors were presented in terms of orbit shape, orbit orientation errors, and position and velocity relative percentage error. The results from V_n were compared to those of the classical initial orbit determination methods of Gauss and Laplace. The

Table XXI. Performance Comparison for One Coplanar Single Scenario ($3\sigma = 10''$), $\Delta t = 180$ s

Algorithm	$a_{error}(\%)$	$b_{error}(\%)$	θ (deg)	$r_{error}(\%)$	$V_{error}(\%)$
V_7	0.4	0.36	0.002	0.0078	0.167
V_8	0.37	0.34	0.002	0.0039	0.165

best results were achieved using V_7 and V_8 for non-coplanar and coplanar scenarios respectively. With small time intervals, the measurements are more affected by the noise and as the time interval increases, the estimation accuracy improves to some point and as the time interval continue growing, the performance drops mainly because of the fact that the velocity approximation accuracy decreases. For number of observations more than three, least square scheme was employed rather than Lagrange interpolation functions to approximate the velocity which leaded to less complex derivations/coding and higher accuracy. For the coplanar case, Laplace, Gauss, and V_3 failed whereas V_8 with $\Delta t = 150$ s showed the most acceptable result. The coplanar cases are sensitive to the level of noise involved in the measurements, so to avoid convergence instability, a larger time interval compared to a non-coplanar case should be selected. The method V_n is rather robust with respect to the initial guess as this technique is iterative and works very well with the initial guess ranging from zero to the values close to the true solution. The orbit shape and orientation error residuals used in this analysis had a vector form. Different types of residual/cost functions should be tried and tested.

CHAPTER VI

SPACE-BASED INITIAL ORBIT DETERMINATION

In this chapter, the performance of the developed techniques are tested through two different space-based initial orbit determination scenarios. The first scenario is a Low Earth Orbit-to-Low Earth Orbit (LEO-to-LEO) problem and the satellites Iridium33 and Cosmos 2251 which collided into each other on February 10, 2009 is considered as the case study. The second scenario is a LEO-to-GEO (Geosynchronous) case.

A. Challenges of Space-based IOD versus Ground-based IOD

As seen in the foregoing sections, the initial orbit determination problems under study were all ground-based, with a stationary observing site, whereas in space-based case, the observer is an orbiting object itself. The fact that the known observer has a velocity with a magnitude compared to that of the unknown observed orbiting object, poses a problem. As a result, the measured lines-of-sight are more effected by the noise and this makes the problem of space-based orbit determination more challenging versus the ground-based scenarios. A technique to lessen the effect of the noise on the measured data is presented.

1. Satellite Conjunction

The collision of two satellites on February 10, 2009, Iridium-33 and Cosmos-2251, has generated a renewed interest in collision detection and avoidance. The recent collision occurred 789 km above northern Siberia, a location where no current observation stations exist. Current methods of optical and radar tracking and high-fidelity propagation obviously failed in this case as post collision analysis showed that the collision could have been avoided. This paper presents a novel method of collision

detection and avoidance based on in-orbit orbit determination.

The problem statement for this work is as follows: from a satellite with known orbit parameters, can we estimate the orbit parameters of an unknown object (e.g., satellite) using an on-board optical system–like a star tracker–and then determine if (or where) the satellites collide?

An accurate estimate of the orbit of the approaching object is required to be able to avoid the collision. The known satellite plays the role of an observer trying to track and determine the orbit of the unknown approaching one, the unknown. Methods P_n and J_n were used for the purpose.

Example problems are solved to validate the orbit determination technique being capable of handling a collision avoidance problem. According to ESA-MASTER 2001, the highest spatial density of space debris belongs to the orbits with altitude of almost 1000 km. The examples studied in this paper will have an altitude of the LEO satellites around 1000 km. The problems were also solved with different number of observations and time intervals between the measurements to come up with the optimum number of measurements-time intervals with respect to accuracy and processor running time, as time plays a significant role in a collision avoidance problem.

2. Problem Description

Figure 21 shows a schematic of a potential satellite collision problem. Satellite 1 has a known orbit and is the observer. It is tracking satellite 2, the target, which has an unknown orbit and poses a potential threat to the observer. Once the position and velocity vectors of the target are determined through the initial orbit determination (IOD) technique explained in the next section, the orbital elements of the unknown approaching object can be determined. Points P_1 and P_2 are the respective perigees,

$\mathbf{e}_1$ and $\mathbf{e}_2$ are the eccentricity vectors, $\mathbf{r}_{s1}$ and $\mathbf{r}_{s2}$ are the position vectors, and ν_{s1} and ν_{s2} are the true anomalies of the observer and the target respectively.

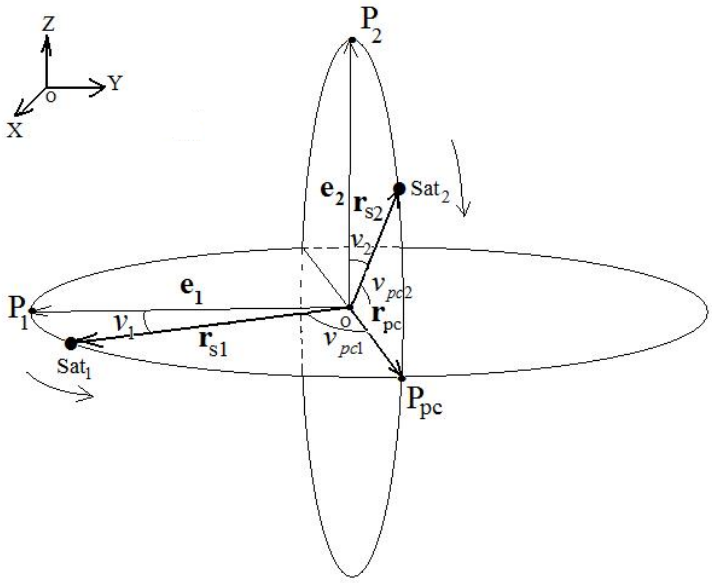

Fig. 21. A Typical Potential Collision Problem

The potential collision point, P_{pc}, can be determined as the intersection of the vector $\mathbf{r}_{pc}$ and one of the orbits. The direction of the vector $\mathbf{r}_{pc}$ is a cross product of the two eccentricity vectors. Next step toward solving the problem is to find the potential collision time t_{pc}. With $\mathbf{r}_{s1}$ and $\mathbf{r}_{pc}$ known, the potential collision true anomaly of the observer ν_{s1} can be calculated as

$$\nu_{pc1} = cos^{-1}\left(\frac{\mathbf{r}_{s1}^T \mathbf{r}_{pc}}{|\mathbf{r}_{s1}||\mathbf{r}_{pc}|}\right) \tag{6.1}$$

and the respective eccentricity anomaly

$$\tan\frac{E_{pc1}}{2} = \left[\frac{1-e}{1+e}\right]^{\frac{1}{2}} \tan\frac{\nu_{pc1}}{2} \tag{6.2}$$

where e is the orbit eccentricity. The mean anomaly also can be found using the

Kepler's equation

$$M_{pc1} = E_{pc1} - e \sin E_{pc1} \tag{6.3}$$

and finally the potential collision time t_{pc} can be determined as

$$t_{pc} = \frac{M_{pc1}}{n_1} \tag{6.4}$$

where n_1 is the mean motion of the observer satellite. Next, the last position vector of the target, $\mathbf{r}_{s2}$, is propagated as determined by the observer. Having done this, the resultant position vector would be $\mathbf{r}_{pc2}$, the potential collision position vector of the approaching object. Note that $\mathbf{r}_{pc1}$ is the same as $\mathbf{r}_{pc}$ whose direction was calculated as the cross product of $\mathbf{e}_1$ and $\mathbf{e}_2$. The last step is now to apply the collision criterion as

$$|\mathbf{r}_{pc} - \mathbf{r}_{pc2}| < \epsilon \Rightarrow COLLISION \tag{6.5}$$

where ϵ is the radius of a ball within which collision occurs. To have a higher accuracy, the observer needs to keep on measuring the line-of-sights from the unknown object as it is approaching the observer to correct the previous data. Also the observer needs to have enough time so in the case of predicted collision the observer is able to perform an avoidance maneuver.

3. Noise Effect Reduction

The noise involved in the measurements (typically up to few arcsecs for conventional star-trackers) plays a significant role in the performance of the IOD methods and has a big impact on the accuracy of the estimated orbit parameters. So a technique to reduce the effect of the noise seems to be vital for the orbit determination problems.

The scheme that was developed in this work is based on the concept of curve-fitting. The measured direction $\hat{\rho}_i, \quad i = 1, 2, ...n$ can be written in a component form as

$$\begin{cases} \hat{\rho}_i^x = \dfrac{1}{\rho_i}(r_i^x - R_i^x) \\ \hat{\rho}_i^y = \dfrac{1}{\rho_i}(r_i^y - R_i^y) \\ \hat{\rho}_i^z = \dfrac{1}{\rho_i}(r_i^z - R_i^z) \end{cases} \tag{6.6}$$

The behavior of the measured directions components $\hat{\rho}_i^x$, $\hat{\rho}_i^y$,and $\hat{\rho}_i^z$ then can be approximated by a fitting curve well representing the behavior of the noise-less data. For the purpose of the current work, a second order polynomial exhibited the best fit. More details will be presented in the Simulation section.

Figure 22 shows a simulated actual orbit (blue), the unfiltered noisy data (green), and the filtered estimate (red). As can be seen from the figure, the filtering process greatly improves the accuracy of the estimates.

4. Simulation and Results

To test the performance of the proposed techniques, three space-based initial orbit determination scenarios were considered. The first one is a LEO-to-LEO case with orbits similar to the Iridium-33 and Cosmos-2251 spacecraft (some tweaking was done to ensure collision for the simulation). The initial orbital elements used for the simulation are shown in Table XXII and the orbits are shown in Figure 23 (the spacecraft representing Iridium is shown in blue while the spacecraft representing Cosmos is shown in red). The second case, is a LEO-to-GEO case in in which a low earth orbit spacecraft is trying to estimate the orbit of a Geosynchronous satellite, and the the last is a GEO-to-GEO case (Geosynchronous observing Geosynchronous).

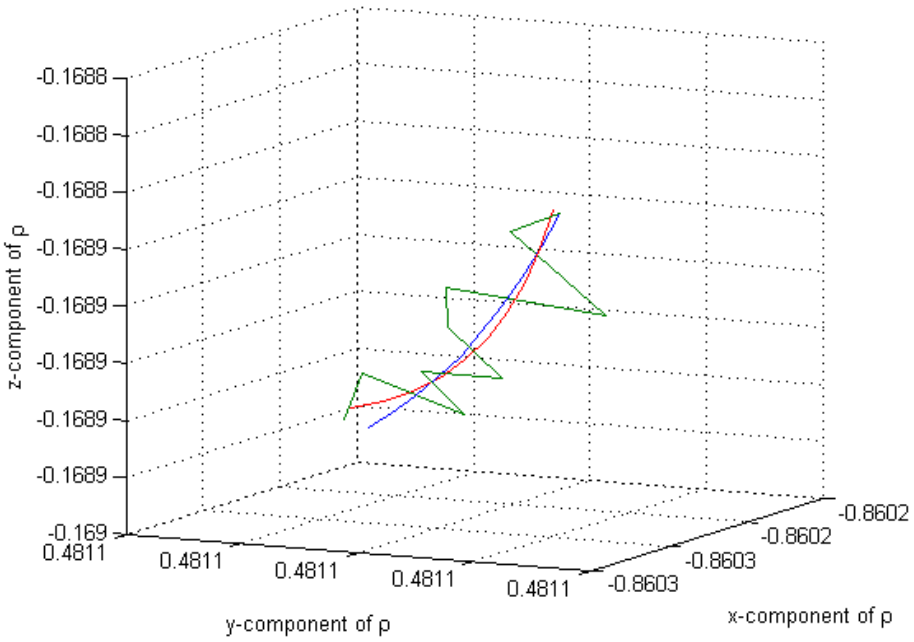

Fig. 22. Measured Directions: True, Noisy, and Filtered

a. LEO-to-LEO (Iridium 33-Cosmos 2251 Scenario)

Due to the spacecraft both being in low Earth orbit (LEO), the maximum possible observation range between the two (without interference from the Earth's limbs) was about 6300 km. Methods J_n and P_n exhibited acceptable performance and methods L_n, V_n, and ML_n did not yield applicable results. The observations are made before the collision for various times of collision t_c ranging from 1200s to 400s.Three different time intervals $\Delta = 20, 40, 60$s are considered for J_n and two time intervals $\Delta t = 80, 100$s for P_n. The two techniques showed their best performances with different number of observations. While J_n required ten observations $N_{obs} = 10$ to show its acceptable performance, P_n used eight. The level of noise involved in the measurements has a standard deviation of $3\sigma = 10$". Since we are dealing with a satellite conjunction detection and avoidance problem, two things should be

Table XXII. Orbital Elements of Satellites for Simulation

Orbital Element	Target Spacecraft Value	Observer Spacecraft Value
a (km)	7187.3	7161.2
e	0.00337	0.00056
i (deg)	74.04	86.38
ω (deg)	136.89	261.48
Ω (deg)	71.16	51.13
M (deg)	223.45	98.85

considered: a) The last observation should be made early enough before the potential conjunction so that the satellite has time to perform an evasive manoeuver, and b) after the initial obit determination is done, the estimated position and velocity should be propagated for the purpose of collision detection, so to evaluate the estimation accuracy of J_n and P_n, the set r_{error} and v_{error} should be considered together. Tables XXIII, XXIV, and XXV show the results of J_n and Tables XXVI and XXVII show those of P_n. The orbital elements of the target satellite (Cosmos) are presented and since the orbit of Cosmos is near circular, the sum of argument of perigee and true anomaly is considered (e.g. $\theta = \omega + \varphi$). Also the estimation error is presented in the form of relative percentage error.

As can be seen, the best (r_{error},v_{error}) sets using J_n are $(0.07\%, 0.71\%), t_c = 600$s, $(0.08\%, 0.65\%), t_c = 400$s, $(0.027\%, 1.28\%), t_c = 1200$s, and $(0.063\%, 0.82\%), t_c = 1000$s, and the best ($r_{error}$,$v_{error}$) sets using P_n are $(0.058\%, 0.77\%), t_c = 1000$s and $(0.086\%, 0.71\%), t_c = 1000$s. Note that in the set where $r_{error}\%$ has the lowest value of 0.027, $v_{error}\%$ has the maximum value of 1.28. Besides, the potential conjunction time t_c is 1200s, while the set (r_{error},v_{error})=$(0.08\%, 0.65\%)$ has a higher position and almost same order velocity error compared to the previous set, but the potential col-

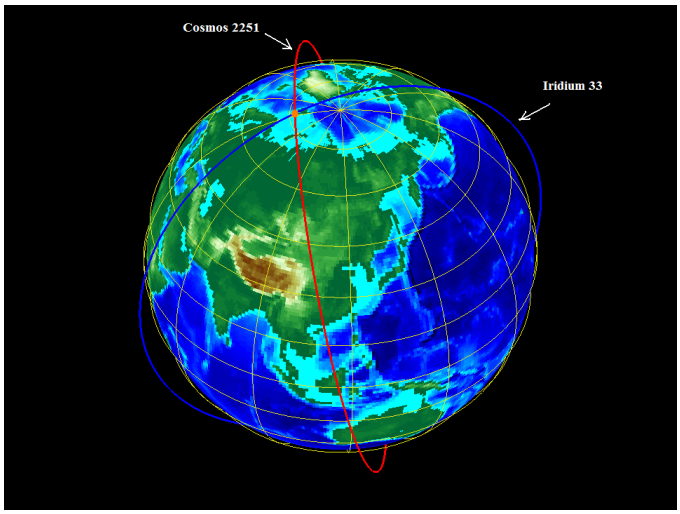

Fig. 23. Orbits of the Simulated Spacecrafts

lision time is 400s. So, the error propagation possibly is not as much as the previous case. Since the subject of error propagation and satellite conjunction detection and avoidance is beyond the scope of this dissertation, the interested reader is referred to [38]. Method P_n typically requires larger time intervals to yield accuracies equal to or better than J_n. The shortest time interval used for P_n was $\Delta = 80$s that is 20s longer than the largest time interval of J_n which is 60s.

b. LEO-to-GEO (Coplanar)

In this scenario, a low earth orbit satellite is observing an unknown geosynchronous orbiting object. To make the problem more challenging, the orbits were considered circular and coplanar. The orbital elements of both satellites can be found in Table XXVIII.

The best results were achieved using methods J_n, L_n, and P_n. Three time intervals $\Delta = 900, 1200, 1800$s were considered with $N_{obs} = 8$, and the noise involved has a standard deviation of $3\sigma = 10$". The errors are presented in terms of shape

Table XXIII. Iridium33 - Cosmos2251 Scenario Using J_n, $N_{obs} = 10$, $\Delta t = 20$s, $3\sigma = 10$”

t_c (s)	$a_{err}(\%)$	$b_{err}(\%)$	$i_{err}(\%)$	$\Omega_{err}(\%)$	$(\omega+\varphi)_{err}(\%)$	$r_{err}(\%)$	$V_{err}(\%)$
1200	0.249	0.249	0.63	1	0.049	0.14	1.5
1000	0.25	0.25	0.28	0.79	0.035	0.11	1
800	0.25	0.25	0.071	0.66	0.03	0.088	0.85
600	0.18	0.18	0.043	0.4	0.018	0.07	0.71
400	0.1	0.1	0.11	0.18	0.0097	0.08	0.65

Table XXIV. Iridium33 - Cosmos2251 Scenario Using J_n, $N_{obs} = 10$, $\Delta t = 40$s, $3\sigma = 10$”

t_c (s)	$a_{err}(\%)$	$b_{err}(\%)$	$i_{err}(\%)$	$\Omega_{err}(\%)$	$(\omega+\varphi)_{err}(\%)$	$r_{err}(\%)$	$V_{err}(\%)$
1200	0.3	0.3	0.37	0.96	0.044	0.027	1.28
1000	0.27	0.27	0.067	0.67	0.03	0.063	0.82
800	0.2	0.2	0.12	0.38	0.02	0.147	0.47
600	0.033	0.033	0.22	0.063	0.004	0.3	0.13

error (semi-major and semi-minor axis) and since the orbits are coplanar, the angle between the angular momentum vectors θ is considered as the orientation error. Tables XXIX, XXX, and XXXI present the results.

As can be seen, all three methods show superb performance and specifically L_n with $\Delta t = 1200$s for shape error and with $\Delta t = 1800$s for orientation and position and velocity errors. One reason could be due to the fact that L_n is capable of using more terms of Lagrange coefficients f and g;hence, more accurate results compared to J_n. Also note that P_n is based on polynomial approximations.

Table XXV. Iridium33 - Cosmos2251 Scenario Using J_n, $N_{obs} = 10$, $\Delta t = 60$s, $3\sigma = 10$"

t_c (s)	$a_{err}(\%)$	$b_{err}(\%)$	$i_{err}(\%)$	$\Omega_{err}(\%)$	$(\omega+\varphi)_{err}(\%)$	$r_{err}(\%)$	$V_{err}(\%)$
1200	0.348	0.348	0.048	0.83	0.04	0.16	1
1000	0.254	0.254	0.237	0.425	0.025	0.32	0.51
800	0.052	0.052	0.426	0.148	0.0078	0.59	0.084

Table XXVI. Iridium33 - Cosmos2251 Scenario Using P_n, $N_{obs} = 8$, $\Delta t = 80$s, $3\sigma = 10$"

t_c (s)	$a_{err}(\%)$	$b_{err}(\%)$	$i_{err}(\%)$	$\Omega_{err}(\%)$	$(\omega+\varphi)_{err}(\%)$	$r_{err}(\%)$	$V_{err}(\%)$
1200	0.31	0.31	0.24	0.86	0.035	0.14	1
1000	0.27	0.27	0.01	0.63	0.026	0.058	0.77

c. GEO-to-GEO

In this scenario, a geosynchronous satellite is trying to determine the orbit of another GEO spacecraft. This scenario is the most challenging one as far as the angles-only initial orbit determination is concerned. This case has observability issue and almost all available IOD methods are not capable of fully handling the problem. The space-based orbit determination cases in which the distance between the observer and target (range) is small, also suffer from observability issues. The results of GEO-to-GEO will not be presented in this dissertation as requested by the Space Engineering Research Center (SERC), Texas A&M University.

5. Conclusion

The performance of the angles-only initial orbit determination algorithms developed in this work were tested for three specific different space-based IOD scenarios, namely LEO-to-LEO (Iridium 33 - Cosmos 2251 case), LEO-to-GEO, and GEO-to-GEO.

Table XXVII. Iridium33 - Cosmos2251 Scenario Using P_n, $N_{obs} = 8$, $\Delta t = 100$s, $3\sigma = 10$"

t_c (s)	$a_{err}(\%)$	$b_{err}(\%)$	$i_{err}(\%)$	$\Omega_{err}(\%)$	$(\omega+\varphi)_{err}(\%)$	$r_{err}(\%)$	$V_{err}(\%)$
1200	0.34	0.34	0.12	0.85	0.033	0.16	1
1000	0.28	0.28	0.11	0.57	0.36	0.086	0.71

Table XXVIII. Orbital Elements of LEO-GEO Scenario (Circular and Coplanar Orbits)

Orbital Element	LEO Satellite	GEO Target
a (km)	10,000.0	42,164.137
e	0	0
i (deg)	0	0
ω (deg)	0	0
Ω (deg)	0	0
φ (deg)	0	1.5

The methods P_n and J_n showed acceptable results for the Iridium 33 - Cosmos 2251 problem. A collision occurred between the satellites Iridium 33 and Cosmos 2251 on Feb.10, 2009 and the main reason behind selecting this case was find out if the conjunction could have been detected and avoided. Different number of observations and time intervals were tested among which J_n with $N_{obs} = 10$, $\Delta = 20$s and potential collision time t_c of 400s seemed to have the highest accuracy for the purpose. Also if the orbit determination is performed too late, the observer satellite may not have enough time to perform an evasive manoeuver, or have to apply a large amount ΔV which may not be feasible due to the energy limitations on board spacecraft. For the LEO-to-GEO case, the methods P_n, J_n, and L_n showed excellent results. The obits were considered circular and coplanar to challenge the proposed algorithms.

Table XXIX. LEO-to-GEO Scenario, (Circular and Coplanar), $N_{obs} = 8$, $\Delta t = 900$s, $3\sigma = 10$”

Method	$a_{err}(\%)$	$b_{err}(\%)$	$\theta(Deg)$	$r_{err}(\%)$	$v_{err}(\%)$
P_n	0.0013	0.0013	0.041	0.0039	0.079
J_n	0.0028	0.0028	0.0077	0.0057	0.041
L_n	0.0013	0.0013	0.0077	0.0048	0.03

Table XXX. LEO-to-GEO Scenario, (Circular and Coplanar), $N_{obs} = 8$, $\Delta t = 1200$s, $3\sigma = 10$”

Method	$a_{err}(\%)$	$b_{err}(\%)$	$\theta(Deg)$	$r_{err}(\%)$	$v_{err}(\%)$
P_n	0.00117	0.00117	0.029	0.0041	0.054
J_n	0.0169	0.0169	0.005	0.0042	0.041
L_n	0.00032	0.00032	0.0056	0.00389	0.0178

The number of observations $N_{obs} = 8$ with different time intervals were used among which the technique L_n with $\Delta t = 1200$s yielded the most accurate orbit shape and with $\Delta t = 1800$s showed the most accurate orientation and position and velocity estimation. And finally, the GEO-to-GEO case which because of the sensitivity of the material, the results were not included.

Table XXXI. LEO-to-GEO Scenario, (Circular and Coplanar), $N_{obs} = 8$, $\Delta t = 1800$s, $3\sigma = 10$”

Method	$a_{err}(\%)$	$b_{err}(\%)$	$\theta(Deg)$	$r_{err}(\%)$	$v_{err}(\%)$
P_n	0.0012	0.0012	0.015	0.0043	0.03
J_n	0.016	0.016	0.0031	0.02	0.19
L_n	0.00075	0.00075	0.003	0.0037	0.012

CHAPTER VII

DESIGNING AN INTERPLANETARY AUTONOMOUS SPACECRAFT NAVIGATION SYSTEM USING VISIBLE PLANETS

In this chapter, the design of an interplanetary autonomous spacecraft navigation system is presented. The first section discuses the challenges of an interplanetary spacecraft navigation problem. Second two explains how to implement the corrections need to be made to the initial orbit determination method to make it suitable for the spacecraft navigation scenario. Then, Extended Kalman Filter is briefly explained and applied as the autonomous navigation system. Finally, the results and conclusion are presented. This chapter is the continuation of [39].

A. Challenges of an Interplanetary Spacecraft Navigation Problem

An interplanetary mission is a voyage through space involving more than one planet. Mariner 2 was the first successful interplanetary spacecraft flying past Venus in 1962. Mars exploration began with Mariner 4 in 1965. Since then, all the planets except Pluto have been visited by interplanetary spacecrafts. In every interplanetary mission, the navigation plays a significant role in the success of the mission. Spacecraft navigation comprises two aspects: (1) knowledge and prediction of spacecraft position and velocity, which is orbit determination, and (2) firing the rocket motor to alter the spacecraft's velocity, which is flight path control. The current work focuses on the first aspect of the spacecraft navigation. Duality exists between the problem of orbit determination from line-of-sight measurements and the problem of an interplanetary autonomous navigation system. Both problems want to estimate an orbit. So basically, in an interplanetary navigation problem, we are dealing with an space-based orbit determination. There are challenges associated with an interplanetary

spacecraft navigation problem which makes it different from a typical space-based orbit determination scenario. So, corrections need to be make to the orbit determination algorithms to make them applicable for the purpose. In the following subsection, the corrections are described.

Corrections

In an Interplanetary spacecraft navigation problem, because of large distances between the orbiting objects and also the high speed of the observer (spacecraft) compared to the ground-based case, two issues rise which need care, namely light-time effect and relativistic aberration effects. These two phenomena are big sources of error in the measured lines-of-sight. So apart from the measurement noise which is dependent on the quality of the star treks, we are dealing with other sources of measurement noise. In the following, the techniques through which the light-time effect and stellar aberration including restricted relativistic aberration effect can be corrected are described.

a. Light-time Correction

Light-time correction is a displacement in the apparent position of a celestial object from its true position (or geometric position) caused by the object's motion during the time it takes its light to reach an observer, see [40],[41] for more on light-time correction. The effect of finite light speed starts playing a role in the accuracy of the solution $\rho_j, \quad j = 1, 2, ..., N_{obs}$ as we are dealing with more distant objects than earth-orbiting satellites, specifically an interplanetary mission. For example, it takes light several minutes to reach a typical spacecraft traveling in space (for instance between Mars and Jupiter) and is observing Earth for navigation. Assume that the observations are made at times $t_k, \ k = 1, 2, \cdots, n$ with the respective measured

directions, $\hat{\rho}_k,\ k = 1, 2, \cdots, n$. Since the spacecraft does not have any knowledge of how far it is from the Sun and correspondingly from the Earth (but it knows the planet it is observing is Earth),so the known position vectors of the planet, $\mathbf{R}_k$, and the measured directions, $\hat{\rho}_k,\ k = 1, 2, \cdots, n$, will be considered the ones at times $t_k,\ k = 1, 2, \cdots, n$ while these belong to the time $t_k - \delta t_k$ where δt_k is the time that takes light to reach the spacecraft.

To fix this problem, a modification in the algorithm needs to be made. The first step would be determining the δt as

$$\delta t_k = \frac{\rho_k^*}{c} \tag{7.1}$$

where c is the speed of light.

The next step would be updating the planet position vector as

$$\mathbf{R}_{updated} = \mathbf{R}(t_k - \delta t_k) \tag{7.2}$$

The position vector can be updated using Eq. (7.1) and Eq. (7.2). This process is repeated until the desired accuracy is achieved.

b. Stellar Aberration Including Restricted (Special) Relativistic Effect

Relativistic aberration is described by Einstein's special theory of relativity, and in other relativistic models such as Newtonian emission theory. It results in aberration of light when the relative motion of observer and light source changes the position of the light source in the field of view of the observer. The effect is independent of the distance between observer and light source.

The aberration of light (also referred to as astronomical aberration or stellar

aberration) is an astronomical phenomenon which produces an apparent motion of celestial objects. At the instant of any observation of an object, the apparent position of the object is displaced from its true position by an amount which depends upon the transverse component of the velocity of the observer, with respect to the vector of the incoming beam of light (i.e., the line actually taken by the light on its path to the observer). Stellar aberration is independent of the distance of a celestial object from the observer, and depends only on the observer's instantaneous transverse velocity with respect to the incoming light beam, at the moment of observation. The light beam from a distant object cannot itself have any transverse velocity component, or it could not (by definition) be seen by the observer, since it would miss the observer. Thus, any transverse velocity of the emitting source plays no part in aberration. Another way to state this is that the emitting object may have a transverse velocity with respect to the observer, but any light beam emitted from it which reaches the observer, cannot, for it must have been previously emitted in such a direction that its transverse component has been "corrected" for. Such a beam must come "straight" to the observer along a line which connects the observer with the position of the object when it emitted the light [42]. In our problem, the light aberration is also an issue which needs to be corrected. Assume that the angle between the spacecraft velocity and the observed direction, $\hat{\rho}_{obs}$, is θ_{obs} and the aberration angle (between the true and observed directions) is ϵ, so the the corrected (true) planet observed direction could be determined as

$$\hat{\rho}_{obs} = \frac{\hat{\mathbf{v}} \sin\epsilon + \hat{\rho}_{true} \sin\theta_{obs}}{\sin\theta_{true}} \tag{7.3}$$

where $\hat{\mathbf{v}}$ is the spacecraft velocity unit vector and θ_{true} is the angle between the velocity and true observation direction. The aberration angle ϵ, at any time, can be

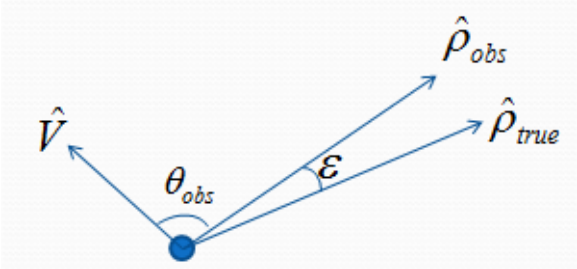

Fig. 24. Light Aberration Caused by the Finite Speed of Light

obtained as

$$\tan\epsilon = \frac{(c/v)\sqrt{(1-(\hat{\rho}_{obs}^T\hat{\mathbf{v}})^2)}}{1-(c/v)(\hat{\rho}_{obs}^T\hat{\mathbf{v}})} = \frac{(v/c)\sin\theta_{obs}}{1-(v/c)\cos\theta_{obs}} \tag{7.4}$$

where c and v are the speed of light and spacecraft velocity magnitude respectively. Note: The combination of light aberration and light-time correction is called *planetary aberration*.

The relativistic aberration is basically the light aberration including the special relativity. According to Einstein's special relativity theory, light directions are affected by the aberration toward inertial velocity vector. The apparent (observed) and true light directions can be related as

$$\cos\theta_{obs} = \frac{\cos\theta_{true} + (v/c)}{1 + (v/c)\ \cos\theta_{true}} \tag{7.5}$$

The apparent angle between the observed planet direction and spacecraft velocity vector is known, and the true direction can be obtained using Eq. (7.5). This ends the last modification we need to apply to the orbit determination (spacecraft navigation) algorithm. Figure (24) illustrates the concept of stellar aberration. See [43],[44] for more on relativistic aberration.

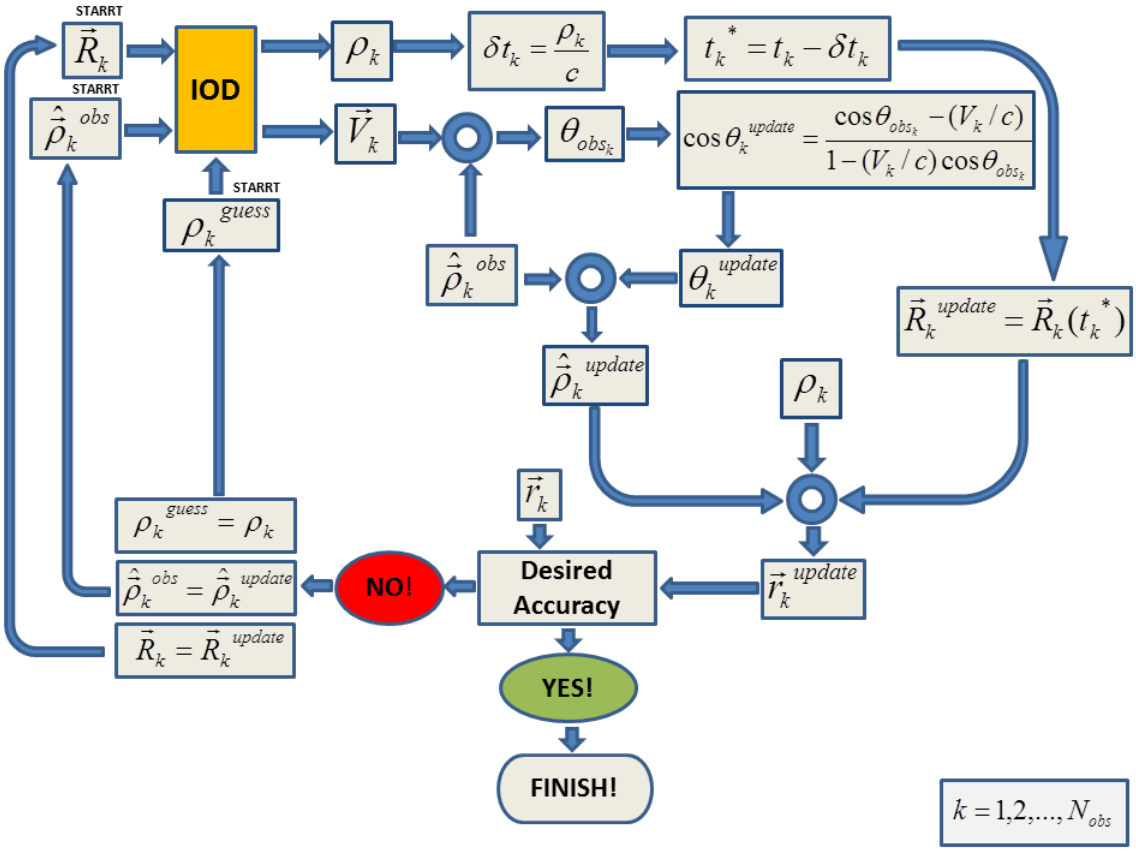

Fig. 25. Light-time and Stellar Aberration Including Restricted Relativistic Effect Correction to the IOD Algorithm

Implementing the Corrections to the IOD Algorithm

The following flowchart Fig.(25) illustrates how the light-time and relativistic aberration corrections are implemented into the initial orbit determination algorithm .

B. Extended Kalman Filter Implementation

Up to now, we've developed some modifications through which an initial orbit determination technique can be applied to an interplanetary orbit determination scenario. To have an autonomous navigation system, we need to perform a sequential state

estimation so we can have the real-time position and velocity of the space craft. To this end, the Extended Kalman Filter (EKF) is employed as the estimation problem under study involves nonlinear model. Considering a continuous-time truth nonlinear model and discrete-time measurement, we have

$$\begin{cases} \dot{\mathbf{x}}(t) = \mathbf{f}(\mathbf{x}(t), \mathbf{u}(t), t) + G(t)\mathbf{w}(t) \\ \tilde{\mathbf{y}}_k = \mathbf{h}(\mathbf{x}_k) + \nu_k \end{cases} \tag{7.6}$$

where $\mathbf{x}$ is the system state vector, $\tilde{\mathbf{y}}$ is the measurement, $\mathbf{f}$ is the system, $\mathbf{u}$ is the input control, and G is the model error. And also, v and w are zero-mean Gaussian white-noise processes meaning that the errors are not correlated forward or backward in time. Their covariances are given by

$$E\{\nu_k \nu_j^T\} = \begin{cases} 0, & k \neq j \\ R_k, & k \neq j \end{cases} \tag{7.7}$$

and

$$E\{\mathbf{w}(t)\mathbf{w}^T(\tau)\} = Q(t)\delta(t-\tau) \tag{7.8}$$

and since ν and $\mathbf{w}$ are uncorrelated

$$E\{\nu_k \mathbf{w}^T(t_k)\} = 0 \tag{7.9}$$

A summary of the continuous-discrete Extended Kalman Filter is given in Table XXXII.

where $\tilde{\mathbf{x}}(t)$ is the state estimate error, K_k is Kalman gain matrix at time t_k, and $P(t) = E\{\tilde{\mathbf{x}}(t)\tilde{\mathbf{x}}^T(t)\}$ is the covariance of the state estimate error.

Now let us apply the Extended Kalman Filter to our problem. The system

Table XXXII. Continuous-discrete Extended Kalman Filter

Model	$\dot{\mathbf{x}}(t) = \mathbf{f}(\mathbf{x}(t), \mathbf{u}(t), t) + G(t)\mathbf{w}(t), \quad \mathbf{w}(t) \sim N(0, Q(t))$ $\tilde{\mathbf{y}}_k = \mathbf{h}(\mathbf{x}_k) + \nu_k, \quad \nu_k \sim N(0, R_k)$
Initialize	$\hat{\mathbf{x}}(t_0) = \hat{\mathbf{x}}_0$ $P_0 = E\{\tilde{\mathbf{x}}(t_0)\tilde{\mathbf{x}}^T(t_0)\}$
Gain	$K_k = P_k^- H_k^T(\hat{\mathbf{x}}_k^-)[H_k(\hat{\mathbf{x}}_k^-)P_k^- H_k^T(\hat{\mathbf{x}}_k^-) + R_k]^{-1}$ $H_k(\hat{\mathbf{x}}_k^-) \equiv \frac{\partial \mathbf{h}}{\partial \mathbf{x}}\|_{\hat{\mathbf{x}}_k^-}$
Update	$\hat{\mathbf{x}}_k^+ = \hat{\mathbf{x}}_k^- + K_k[\tilde{\mathbf{y}}_k - \mathbf{h}(\hat{\mathbf{x}}_k^-)]$ $P_k^+ = [I - K_k H_k(\hat{\mathbf{x}}_k^-)]P_k^-$
Propagation	$\dot{\hat{\mathbf{x}}}(t) = \mathbf{f}(\hat{\mathbf{x}}(t), \mathbf{u}(t), t)$ $\dot{P}(t) = F(\hat{\mathbf{x}}(t), t)P(t) + P(t)F^T(\hat{\mathbf{x}}(t), t) + G(t)Q(t)G^T(t)$ $F(\hat{\mathbf{x}}(t), t) \equiv \frac{\partial \mathbf{f}}{\partial \mathbf{x}}\|_{\hat{\mathbf{x}}(t)}$

under study is well known and the truth model is available. For the space craft traveling in the solar system under the Sun gravitational field, the motion is governed by Keplerian two-body equations. Note that no perturbations (solar pressure and gravity from other celestial bodies) are considered in this formulation, so we have

$$\ddot{\mathbf{r}} = -\frac{\mu_\odot}{r^3}\mathbf{r} \tag{7.10}$$

or in Cartesian form

$$\begin{cases} \ddot{x} = -\dfrac{\mu_\odot}{r^3}x \\ \ddot{y} = -\dfrac{\mu_\odot}{r^3}y \\ \ddot{z} = -\dfrac{\mu_\odot}{r^3}z \end{cases} \tag{7.11}$$

where $\mu_\odot$ is the Sun Gravitational constant and $\mathbf{r}$ is the space craft position vector. Defining the state vector $\mathbf{X}$ as

$$\begin{cases} X_1 = x \\ X_2 = y \\ X_3 = z \\ X_4 = \dot{X}_1 = \dot{x} \\ X_5 = \dot{X}_2 = \dot{y} \\ X_6 = \dot{X}_3 = \dot{z} \end{cases} \tag{7.12}$$

and the system dynamic would be

$$\dot{\mathbf{X}} = \mathbf{f}(\mathbf{X}(t)) = \begin{Bmatrix} \dot{x} \\ \dot{y} \\ \dot{z} \\ -\frac{\mu_\odot}{(x^2+y^2+z^2)^{3/2}}x \\ -\frac{\mu_\odot}{(x^2+y^2+z^2)^{3/2}}y \\ -\frac{\mu_\odot}{(x^2+y^2+z^2)^{3/2}}z \end{Bmatrix} \tag{7.13}$$

The input measurement vector $\tilde{\mathbf{y}}$ contains of azimuth ϕ and elevation θ angles as illustrated in Fig.26.

$$\tilde{\mathbf{y}} = \begin{Bmatrix} \tilde{\theta} \\ \tilde{\phi} \end{Bmatrix} = \begin{Bmatrix} \theta + \nu_\theta \\ \phi + \nu_\phi \end{Bmatrix} \tag{7.14}$$

where ν_θ and ν_ϕ are the measurement noise associated with the elevation and azimuth angles respectively. The elevation and azimuth angles can be computed as

$$\begin{cases} \theta = sin^{-1}[\dfrac{(x-R_x)}{[(x-R_x)^2+(y-R_y)^2+(z-R_z)^2]^{1/2}}] \\ \phi = tan^{-1}[\dfrac{(y-R_y)}{(x-R_x)}] \end{cases} \tag{7.15}$$

For matrix H we have

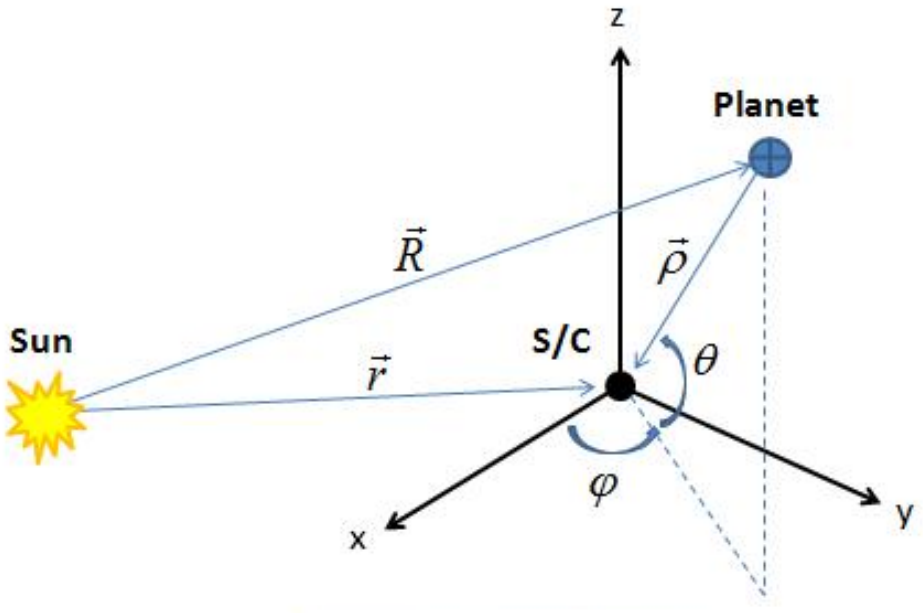

Fig. 26. Azimuth and Elevation Angles as Input Measurements

$$H = \frac{\partial \mathbf{h}}{\partial \mathbf{X}} = \begin{bmatrix} \frac{\partial h_1}{\partial X_1} & \frac{\partial h_1}{\partial X_2} & \frac{\partial h_1}{\partial X_3} & \frac{\partial h_1}{\partial X_4} & \frac{\partial h_1}{\partial X_5} & \frac{\partial h_1}{\partial X_6} \\ \frac{\partial h_2}{\partial X_1} & \frac{\partial h_2}{\partial X_2} & \frac{\partial h_2}{\partial X_3} & \frac{\partial h_2}{\partial X_4} & \frac{\partial h_2}{\partial X_5} & \frac{\partial h_2}{\partial X_6} \end{bmatrix} \tag{7.16}$$

or

$$H = \begin{bmatrix} \frac{\partial \theta}{\partial x} & \frac{\partial \theta}{\partial y} & \frac{\partial \theta}{\partial z} & 0 & 0 & 0 \\ \frac{\partial \phi}{\partial x} & \frac{\partial \phi}{\partial y} & 0 & 0 & 0 & 0 \end{bmatrix} \tag{7.17}$$

and components of matrix H

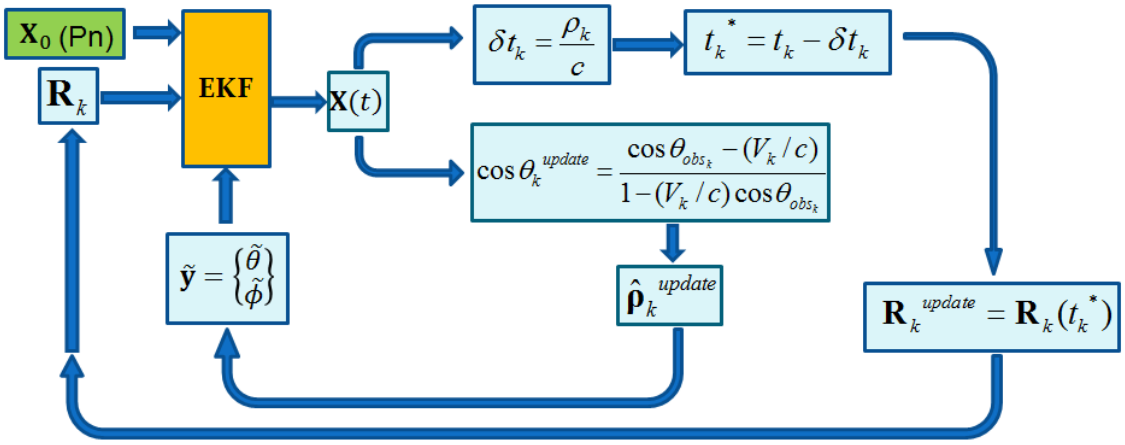

Fig. 27. Light-time and Stellar Aberration Including Restricted Relativistic Effect Correction to EKF

$$
\begin{cases}
\dfrac{\partial\theta}{\partial x} = -\dfrac{(x-R_x)(z-R_z)}{[(x-R_x)^2+(y-R_y)^2+(z-R_z)^2][(x-R_x)^2+(y-R_y)^2]^{1/2}} \\
\dfrac{\partial\theta}{\partial y} = -\dfrac{(y-R_y)(z-R_z)}{[(x-R_x)^2+(y-R_y)^2+(z-R_z)^2][(x-R_x)^2+(y-R_y)^2]^{1/2}} \\
\dfrac{\partial\theta}{\partial z} = -\dfrac{[(x-R_x)^2+(y-R_y)^2]^{1/2}}{(x-R_x)^2+(y-R_y)^2+(z-R_z)^2} \\
\\
\dfrac{\partial\phi}{\partial x} = -\dfrac{y-R_y}{(x-R_x)^2+(y-R_y)^2} \\
\dfrac{\partial\phi}{\partial y} = \dfrac{x-R_x}{(x-R_x)^2+(y-R_y)^2}
\end{cases}
\tag{7.18}
$$

Note that in the heart of the Extended Kalman Filter algorithm, the two corrections of light-time and restricted relativistic light aberration are implemented. Figure (27) illustrates how the light-time and stellar aberration relativistic aberration corrections are implemented into EKF. For more details on extended Kalman filter, see [45].

C. Results

In this section the performance of the Autonomous Interplanetary Spacecraft Navigation System Using Visible Planets is tested. The planet Earth is considered as the known visible sun-orbiting object. A spacecraft is traveling on a trajectory with an initial position of more than two hundred million kilometers from the Sun with a distance of approximately seventy million kilometers from Earth (has almost the same distance from Earth as Mars). The spacecraft is observing Earth for the navigation purposes. The methods P_n, J_n, and L_n showed excellent performance for the interplanetary space-based initial orbit determination part. Modified Laplace ML_n did not yield acceptable accuracy and V_n offered the trivial solution of almost zero estimated ranges which is similar to the original Gooding method from this aspect. Finally method P_n was selected for the IOD part (as the input to the extended Kalman filter) due to the fact that to make the special relativistic aberration correction, the estimated velocities at each t_k, $\quad k = 1, 2, ..., N_{Nobs}$ should be known and method P_n computes those velocities in the heart of its algorithm and they are already available as a part of the output and no need for extra computations as in L_n and J_n. For the initial orbit determination part, the number of observations used was $N_{obs} = 8$ with time interval $\Delta t = 3(10^5)$s (3 days 11 hr 20 min). To make the problem more challenging, the spacecraft orbit was considered coplanar with the sun-earth orbit plane. Also note that the other planets have very small inclination angles. The position and velocity components of the spacecraft and Earth at the initial time t_1 of observation are

$$\mathbf{r}_{s/c}=\begin{Bmatrix}-2\\-0.5\\0\end{Bmatrix}10^8\,\text{km},\quad \mathbf{v}_{s/c}=\begin{Bmatrix}2\\-30\\0\end{Bmatrix}\,\text{km/s},\quad \mathbf{r}_e=\begin{Bmatrix}-1.521\\0\\0\end{Bmatrix}10^8\,\text{km},\quad \mathbf{v}_e=\begin{Bmatrix}0\\-29.29\\0\end{Bmatrix}\,\text{km/s}$$

The noise involved in the measurements has the standard deviation of $3\sigma = 10$". The last (at t_8) estimated position and velocity were used as the output of the IOD algorithm and input to the Extended Kalman Filter. The state vector X_0 (initial conditions for EKF) is defined as $[r_x, \quad r_y, \quad r_z, \quad v_x, \quad v_y, \quad v_z]^T$ and for this problem

$$X_0=\begin{Bmatrix}-183553246.154077\\-129751886.849561\\47.8566691563623\\9.2804459659289\\-26.6655452207945\\0\end{Bmatrix}$$

For the Extended Kalman filter part, 150 observations with time interval $\Delta t = 3(10^3)$s (50 min) were considered. For the navigation purpose,the estimated position and velocity of the spacecraft are desired. No process noise was considered and also we assumed the model has no error(no perturbations due to gravitational fields of other planets and so solar pressure), so the covariance of the process noise q was considered zero, $q = 0$. Also the initial values for P_0 (covariance of the state estimate error) was considered as $P_0 = 2(10^6)I_{6\times6}$. Figures 28 and 29 show the history of position and velocity error and the associated 3-σ bounds and the true and estimated position and velocity respectively. The final estimated position and

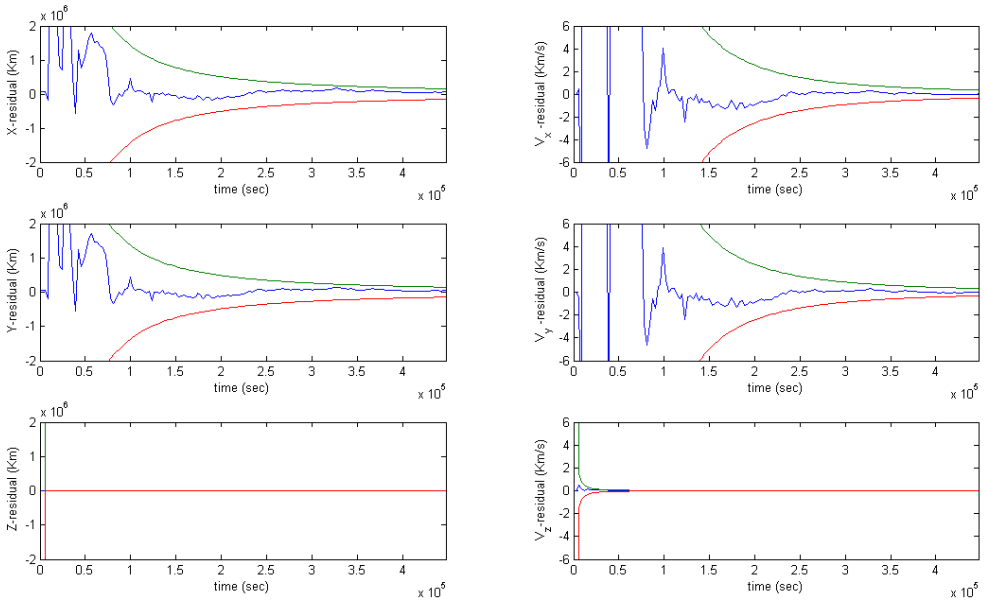

Fig. 28. Estimated Position and Velocity Error with the 3-σ Bounds

velocity relative percentage error are $r_{error} = 0.04\%$ and $V_{error} = 0.15\%$ respectively.

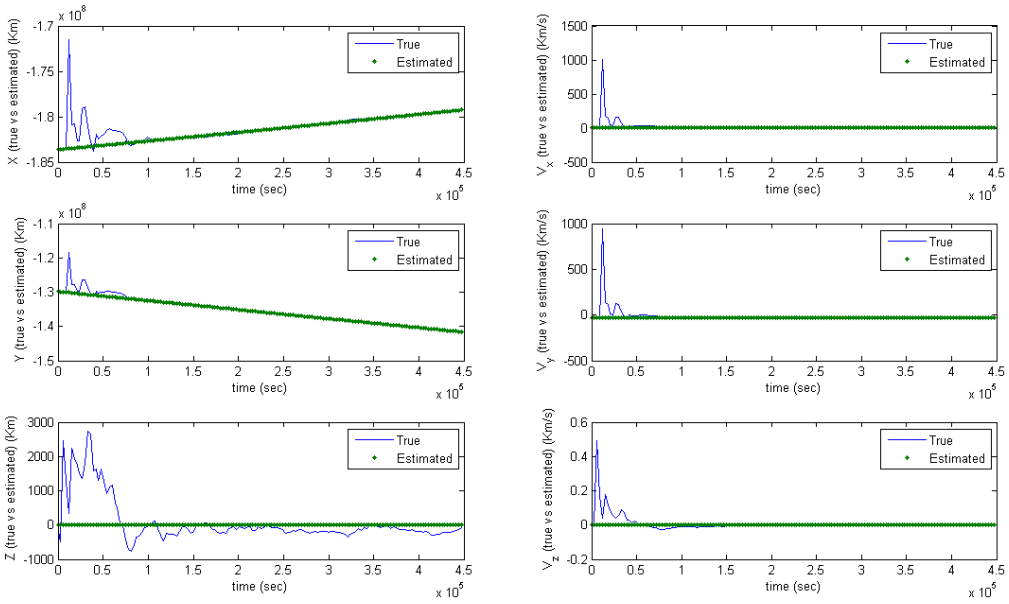

Fig. 29. Estimated and True Position and Velocity Components

D. Conclusion

An interplanetary autonomous spacecraft navigation system using visible planets was designed and tested. Two corrections (light-time and light abberation) were made to the space-based initial orbit determination algorithm to make it applicable for an interplanetary spacecraft navigation problem. The output of the IOD method (position and velocity) was used as the initial condition to Extended Kalman Filter (EKF) for the autonomous estimation of the position and velocity of the spacecraft. Planet Earth was used as the visible planet for the navigation purpose and the spacecraft was traveling on a trajectory with a distance of approximately seventy million kilometers from the planet(almost as the same distance as Mars). Of all the five algorithms developed, P_n, J_n, L_n showed excellent performances for the interplanetary angles-only initial orbit determination, but eventually P_n was chosen for the autonomous navigation purpose as it was more comfortable to work with when implementing the corrections of light-time and light abberation. For the initial orbit determination, eight observations ($N_{obs} = 8$) was used with the time interval of $\Delta t = 3(10^5)$s (3 days 11 hr 20 min). The level of noise used to corrupt the ideal data was considered as $3\sigma = 10$". For the autonomous navigation part, the number of observations of 150 with $\Delta t = 3(10^3)$s (50 min) were fed into the extended Kalman filter.The final estimated position and velocity relative percentage error are $r_{error} = 0.04\%$ and $V_{error} = 0.15\%$ respectively.

CHAPTER VIII

CONCLUSION

An interplanetary autonomous spacecraft navigation system using visible planets was successfully designed and tested. The problem of interplanetary spacecraft navigation is the dual problem of the space-based angles-only Initial Orbit Determination (IOD). The orbit determination methods can be used to solve the dual problem. The classical and majority of newly developed angles-only IOD methods use three lines-of-sight which pose the problem of singularity when used for the coplanar orbit determination cases and also not efficient when employed for the space-based cases. So, new tools were required to be built using which higher orbit estimation accuracy is achieved and also the issue of the singularity can be handled as the planets have near to coplanar orbits. The techniques J_n, L_n, P_n, and ML_n were developed for the purpose. All five methods are capable of using multiple observations which makes them suitable for the coplanar orbit determination problems. Also, using more than three observations improve the estimation accuracy. The proposed algorithms were tested for the ground-based, space-based (LEO-to-LEO and LEO-to-GEO) and interplanetary (spacecraft-to-visible planet) initial orbit determination cases. For the ground-based scenario, all five methods showed excellent performances for both coplanar and non-coplanar cases. For the space-base (LEO-to-LEO, collision scenario of Iridium 33 and Cosmos 2251 was considered as the case study), P_n and J_n showed good performance. For the LEO-to-GEO, P_n,J_n, and L_n yielded excellent results(a coplanar case was considered to make it more challenging). The methods V_n and ML_n showed their best performances for the ground-based orbit determination problems. To use the IOD method for the interplanetary spacecraft navigation problem, two corrections needed to be made namely light-time (due to the large dis-

tance between the observer and observed objects and finite speed of light) and special relativistic light aberration which causes the measured light-of-sight of the observed planet to be compressed towards the velocity vector of the observer(spacecraft). Also, to simulate the real world data, the ideal measured directions (lines-of-sight) were corrupted with zero-mean Gaussian noise. For the interplanetary initial orbit determination scenario, three techniques(P_n,J_n, and L_n) offered very well performances. The output of the IOD method (position and velocity) was used as the initial condition to Extended Kalman Filter (EKF) for the autonomous estimation of the position and velocity of the spacecraft. Planet Earth was used as the visible planet for the navigation purpose and the spacecraft was traveling on a trajectory with a distance of approximately seventy million kilometers from the planet(almost as the same distance as Mars). Out the three methods, P_n was eventually chosen for the autonomous navigation purpose as it was more comfortable to work with when implementing the corrections of light-time and light abberation. For the initial orbit determination, eight observations ($N_{obs} = 8$) was used with the time interval of $\Delta t = 3(10^5)$s (3 days 11 hr 20 min). The level of noise used to corrupt the ideal data was considered as $3\sigma = 10$". For the autonomous navigation part, the number of observations of 150 with $\Delta t = 3(10^3)$s (50 min) were fed into the extended Kalman filter. The estimated position and velocity of the spacecraft had relative percentage errors of 0.04% and 0.15% respectively.

CHAPTER IX

FUTURE WORK

The designed autonomous spacecraft navigation system is tested experimentally and the planet Earth will be considered as the spacecraft traveling in space while observing some other planet (could be Jupiter, Mars, or Venus) for navigation. Since Earth has radius and is rotating, some modifications need to made as the original algorithm considers the spacecraft as a point mass with no dimensions.

All the number of observations and time interval between the measurements were chosen manually by the operator in such a way the estimation accuracy is achieved. A smart scheme which can adaptively select the optimal number of observations and time interval needs necessary. Such a work has already been started by the authors, but still is at the early stages of development.

The method V_n yielded excellent performance for the ground-based initial orbit determination whereas failed for the space-based case. The residual definitions should be revised and different types of residual functions should be tested.

REFERENCES

[1] Green, R.M., *Spherical Astronomy*, Cambridge University Press, New York, 1988.

[2] Beer, A., and Strand, K.A., *Copernicus*, Pergamon Press, Oxford, UK, 1975.

[3] Vallado, D.A., *Fundamental of Astrodynamics and Application*, 3^{rd} Ed., Microcosm Press, Hawthorne, CA, 2007.

[4] Vetter, J.R., "Fifty Years of Orbit Determination: Development of Modern Astrodynamics Methods," *Johns Hopkins APL Technical Digest* , Vol. 27, No. 3, 2007, pp. 239–252.

[5] McClusky, S.C., *Astronomies and Culture in Early Medical Early Europe*, Cambridge University Press, Cambridge, UK, 2000.

[6] Laplace, P.S., "Mémoires de l'Académie Royale des Sciences," Paris, Reprinted in Laplace's Collected Works, Vol. 10, No. 93, pp. 93–146, 1780.

[7] Gauss, C.F., *Theory of the Motion of the Heavenly Bodies Moving about the Sun in Conic Sections*, English Translation, Dover Publication, New York, 1963.

[8] Anderson, J.D., "Theory of Orbit Determination. Part I: Classical Methods," Jet Propulsion Laboratory Technical Report, No. 32-497, Prepared Under Contract No. NAS7-100, NASA, October 1963.

[9] Long, A.C., *Goddard Trajectory Determination System (GTDS) Mathematical Theory*, Goddard Space Flight Center, Greenbelt, MD, 1989.

[10] Herget, P., "Determination of Orbits," *The Astronomical Journal*, Vol. 44, No. 18, 1935, pp.153–161.

[11] Herget, P., *The Computation of Orbits*, Edwards Brothers, Inc., Ann Arbor, MI, 1948.

[12] Escobal, P.R., *Methods of Orbit Determination*, John Wiley and Sons, Inc., New York, 1965.

[13] Gooding, R.H., "A New Procedure for the Solution of the Classical Problem of Minimal Orbit Determination from Three Lines of Sight," *Celestial Mechanics and Dynamical Astronomy*, Vol. 66, No. 4, 1997, pp. 387-423.

[14] Taff, L.G., "On Initial Orbit Determination," *The Astronomical Journal*, Vol. 89, No. 9, 1984, pp.1426–1428.

[15] Gibbs, J.W., *On the Detrmination of Elliptic Orbits from Three Complete Observations*, Kessinger Publishing, Whitefish, Montana, 2008.

[16] Moulton, F.R., *Celestial Mechanics*, MacMillan, New York, 1902.

[17] Bate, R.R., Mueller, D.D., and White, J.E., *Fundamental of Astrodynamics*, Dover Publications, New York, 1971.

[18] Herrick, S., *Astrodynamics*, Van Nostrand Reinhold Co., London, 1971.

[19] Battin, R.H., *An Introduction to the Mathematics and Methods of Astrodynamics*, Education Series, AIAA, New York, 1987.

[20] Henderson, T.A., Mortari, D., and Davis, J., "Modifications to the Gooding Algorithm For Angles-Only Initial Orbit Determination," 2010 AAS/AIAA Space Flight Mechanics Meeting Conference, San Diego, CA, Paper AAS 10-238, Feb. 2010.

[21] Celletti, A., and Pinzari, G., "Four Classical Methods For Determining Planetary Elliptic Elements: A Comparision," *Celestial Mechanics and Dynamical Astronomy*, Vol. 93, No.1–4, 2005, pp.1–52.

[22] Shefer, V.A., "A Method of Intermediate Orbit Determination Based on Four Positions of a Minor Body on the Celestial sphere," *Solar System Research*, Vol. 42, No. 5, 2008, pp. 405-413.

[23] Taff, L.G., and Hall, D.L., "Use of Angles and Angular Rates in Initial Orbit Determination," *Celectial Mechanics*, Vol. 16, No. 4, 1977, pp. 481–488.

[24] Baker, R.M.L., Jr, and Jacoby, N.H., Jr, "Preliminary Orbit Determination Method Having no Coplanar Singularity," *Celestial Mechanics*, Vol. 15, No. 2, 1977, pp.137–160.

[25] Neutsch, W., "A Simple Method of Orbit Determination," *Astronomy and Astrophysics*, Vol. 102, No. 1, 1981, pp. 59–64.

[26] Kristensen, L.K., "Single Lunation N-Observation Orbits," *Celestial Mechanics and Dynamical Astronomy*, Vol. 105, No. 4, 2009, pp. 275–287.

[27] Karimi, R.R. and Mortari, D., "On Laplace's Orbit Determination Method: Some Modifications," 2011 AAS/AIAA Space Flight Mechanics Meeting Conference, New Orleans, LA, Paper AAS 11-121, Feb. 2011.

[28] Karimi, R.R. and Mortari, D., "On Preliminary Orbit Determination: A New Approach," 2009 AAS/AIAA Space Flight Mechanics Meeting Conference, Savannah, GA, Paper AAS 09-106, Feb. 2009.

[29] Karimi, R.R. and Mortari, D., "Initial Orbit Determination Using Multiple Observations," *Celestial Mechanics and Dynamical Astronomy*, Vol. 109, No. 2,

2010, pp.167-180.

[30] Karimi, R.R. and Mortari, D., "Orbit Determination Using Prescribed Orbits," 2010 AAS/AIAA Space Flight Mechanics Meeting Conference, San Diego, CA, Paper AAS 10-236, Feb. 2010.

[31] Karimi, R.R. and Mortari, D., "Orbit Determination Based on Variation of Orbital Error," 2012 AAS/AIAA Space Flight Mechanics Meeting Conference, Charleston, SC, Paper AAS 12-201, Jan. 2012.

[32] Mortari, D., Scuro, R.S., and Bruccoleri, C. "Attitude and Orbit Error in n-Dimensional Spaces," *AAS Journal of the Astronautical Sciences*, Vol. 54, No.3–4, 2006, pp. 467–484.

[33] Taff, L.G., Randall, P.M.S., and Stansfield, S.A., M.I.T. Lincoln Laboratory Technical Report 618, May 1984.

[34] Curtis, H.D., *Orbital Mechanics for Engineering Students*, Elsevier Butterworth-Heinemann, Oxford, UK, 2005.

[35] Turner, J.D., "Automated Generation of High-Order Partial Derivative Models," *AIAA Journal*, Vol. 41, No. 8, 2003, pp. 1590–1598.

[36] Prussing, J.E. and Conway, B.A., *Orbital Mechanics*, Oxford University Press, New York, 1993.

[37] Karimi, R.R., and Mortari, D., "An Adaptive Scheme on Optimal Number of Observations and Time Intervals For An Iinitail Orbit Determination Problem," 2010 AAS/AIAA Space Flight Mechanics Meeting Conference, San Diego, CA, Paper AAS 10-152, Feb. 2010.

[38] Karimi, R.R., Henderson, T.A., and Mortari, D., "Satellite Collision Detection and Avoidance using Star Trackers," 2009 AAS/AIAA Astrodynamics Specialist Conference, Pittsburgh, Pennsylvania, Paper AAS 09-302, Aug. 2009.

[39] Karimi, R.R. and Mortari, D., "Designing an Interplanetary Autonomous Spacecraft Navigation System Using Visible Planets," 2009 AAS/AIAA Space Flight Mechanics Meeting Conference, Savannah, GA, Paper AAS 09-160, Feb. 2009.

[40] Seidelmann, P.K., *Explanatory Supplement to the Astronomical Almanac*, University Science Books, Mill Valley, CA, 1992.

[41] Berry, A., *A Short History of Astronomy*, Dover Publications, Mineola, NY, 1961.

[42] Hirschfeld, A., *Parallax: The Race to Measure the Cosmos*, Henry Holt, New York, 2001.

[43] Liebscher, D.E., and Brosche, P., "Aberration and Relativity," *Astronomische Nachrrichten*, Vol. 319, No. 5, 1998, pp.309–318.

[44] Gjurchinovski, A., "Aberration of Light in a Uniformly Moving Optical Medium," *American Journal of Physics*, Vol. 72, No. 7, 2004, pp. 934–940.

[45] Crassidis, J.L., and Junkins, J.L., *Optimal Estimation of Dynamic Systems*, 2^{nd} Ed., CRC Press, Boca Raton, FL, 2011.

APPENDIX A

JACOBIAN MATRIX CONSTRUCTION

This appendix provides the procedure/algorithm used to build the Jacobian matrix:

$$
\begin{aligned}
\text{for } i \;=\; & 1, \ldots, (N_{\text{obs}} - 2) \\
& c = \frac{1}{2} + \frac{\mu}{4|\mathbf{r}_{i+1}|^3}\Delta t^2 \\
& \frac{\partial c}{\partial \rho_{i+1}} = -\frac{3\mu}{4|\mathbf{r}_{i+1}|^5}\left(\hat{\boldsymbol{\rho}}_{i+1}^{\mathrm{T}}\mathbf{r}_{i+1}\right)\Delta t^2 \\
& J[(3i-2):3i, i] = c\,\hat{\boldsymbol{\rho}}_i \\
& J[(3i-2):3i, i+1] = \frac{\partial c}{\partial \rho_{i+1}}\left(\mathbf{r}_i + \mathbf{r}_{i+2}\right) - \hat{\boldsymbol{\rho}}_{i+1} \\
& J[(3i-2):3i, i+2] = c\,\hat{\boldsymbol{\rho}}_{i+2} \\
& \text{end}
\end{aligned}
$$

where N_{obs} is the number of observations, Δt is the time interval between the measurements, and J is Jacobian, a $3(N_{\text{obs}} - 2) \times N_{\text{obs}}$ matrix. Also, $\mathbf{r}_i$, $\hat{\boldsymbol{\rho}}_i$, and ρ_i, are the i^{th} satellite position vectors, the measured line-of-sight directions, and the ranges, respectively.

VITA

Reza Raymond Karimi graduated from Tehran Azad University with a B.S. degree and from Tarbiat Modares University with a M.S. degree in Mechanical Engineering. Reza migrated to the United Stated a year after his graduation and resided in Texas. He attended Texas A&M University pursuing his PhD in Aerospace Engineering and graduated in May 2012. His areas of interests are Orbital Dynamics with a focus on orbit determination and spacecraft navigation, nonlinear adaptive control, real-time trajectory generation, and aircraft design. Reza will continue his research as a postdoc and is seeking a research job in industry. He is the winner of Lowy award for the best aircraft design, 2008 and outstanding graduate teaching assistance award, 2007. He can be reached at rezaraymond@tamu.edu or in care of Dr. Daniele Mortari at the Aerospace Engineering Department of Texas A&M University, College Station, 77843-3141.